Distribution Agreement

In presenting this thesis or dissertation as a partial fulfillment of the requirements for an advanced degree from Emory University, I hereby grant to Emory University and its agents the non-exclusive license to archive, make accessible, and display my thesis or dissertation in whole or in part in all forms of media, now or hereafter known, including display on the world wide web. I understand that I may select some access restrictions as part of the online submission of this thesis or dissertation. I retain all ownership rights to the copyright of the thesis or dissertation. I also retain the right to use in future works (such as articles or books) all or part of this thesis or dissertation.

Signature:

_____ _____

Miranda Jade McDaniel Date

Investigating the Role of the Pre-M1 Helix and Other Highly Conserved Regions in NMDA Receptor Function

By

Miranda Jade McDaniel
Doctor of Philosophy

Graduate Division of Biological and Biomedical Science
Molecular and Systems Pharmacology

Stephen F. Traynelis, Ph.D.
Advisor

Criss Hartzell, Ph.D.
Committee Member

John Hepler, Ph.D.
Committee Member

Nael McCarty, Ph.D.
Committee Member

Accepted:

Lisa A. Tedesco, Ph.D.
Dean of the James T. Laney School of Graduate Studies

Date

Investigating the Role of the Pre-M1 Helix and Other Highly Conserved Regions in NMDA Receptor Function

By

Miranda Jade McDaniel
B.S., Georgia Institute of Technology, 2014

Advisor: Stephen F. Traynelis, Ph.D.

An abstract of a dissertation submitted to the Faculty of the James T. Laney School of Graduate Studies of Emory University in partial fulfillment of the requirements for the degree of Doctor of Philosophy in Graduate Division of Biological and Biomedical Science Molecular and Systems Pharmacology
2019

Abstract

Investigating the Role of the Pre-M1 Helix and Other Highly Conserved Regions in NMDA Receptor Function

By: Miranda Jade McDaniel

NMDA receptors (NMDARs) are calcium-permeable ion channels with a critical role in the slow-component of fast excitatory neurotransmission. Typically comprised of two glycine-binding GluN1 subunits and two glutamate-binding GluN2 subunits, these receptors respond to the synaptic release of glutamate to facilitate the opening of the cation-selective pore. The GluN2 subunits can be one of four subtypes (A-D), while the GluN1 subunits can be one of eight splice variants. Moreover, each NMDAR subunit contains four semi-autonomous domains—an amino terminal domain (ATD), an agonist-binding domain (ABD), a transmembrane domain (TMD), and a carboxy terminal domain (CTD)— connected through a series of flexible linkers. In the healthy brain, NMDARs are critical for neuronal development, learning and memory, synaptic plasticity, and several other important processes. Pathologically, they have been associated with such neurological disorders as Parkinson's disease, Alzheimer's disease, and schizophrenia. As we learn more about their role in brain physiology and pathology, it becomes increasingly important to develop a more comprehensive understanding of NMDAR function. In this dissertation, I explore the functional role of three highly conserved regions of the NMDAR: the pre-M1 helix, the GluN2 glutamate binding site, and the GluN1 exon 5 motif. Guided by genetic regulation and variation, I introduced purposeful mutations within these regions and report the effect of these substitutions on a multitude of channel properties. I show that these regions are likely under such strict genetic protection as a consequence of their considerable influence on receptor function. Moreover, I present a structure-based model to investigate how independent subunits contribute to the activation of NMDARs. Finally, I show that deactivation rate correlates with both proton sensitivity and glutamate egress time. Together, the results presented in this dissertation shed light on the role of specific highly conserved regions— and the amino acids therein—in the function of the NMDAR ion channel. Moreover, this study emphasizes the value of using genetics to guide the rational design of investigative scientific inquiry.

Investigating the Role of the Pre-M1 Helix and Other Highly Conserved Regions in NMDA Receptor Function

By

Miranda Jade McDaniel
B.S., Georgia Institute of Technology, 2014

Advisor: Stephen F. Traynelis, Ph.D.

A dissertation submitted to the Faculty of the James T. Laney School of Graduate Studies of Emory University in partial fulfillment of the requirements for the degree of Doctor of Philosophy in Graduate Division of Biological and Biomedical Science Molecular and Systems Pharmacology
2019

Acknowledgements

My completion of this degree would not have been made possible without the support and guidance I received from several important individuals in my life. I would like to take a brief moment to acknowledge and thank these people for the invaluable role they played throughout my graduate career. I would first like to thank my parents, Danny and Trina McDaniel, who have provided me with endless and unconditional love and support throughout this journey. I would also like to thank my sister, Christa McDaniel, who has been both an absolute inspiration and a wonderful friend. And I would like to thank Hirofumi Kusumoto, who has provided me with motivation, encouragement, love, and laughter every day. I must also thank my classmates and lab mates who shared in my experiences and provided a listening ear as often as necessary and the numerous faculty members who provided me with advice, guidance, and mentorship throughout my time here at Emory. Lastly, I have to thank my research advisor, Dr. Stephen Traynelis, for his expertise, training, ideas, and instruction.

Table of Contents

List of Figures

List of Tables

List of Abbreviations

ABD	agonist-binding domain
AMPA	α-amino-3-hydroxy-5-methyl-4-isoxazolepropionate
ATD	amino-terminal domain
CNS	central nervous system
CTD	carboxy-terminal domain
HEK	human embryonic kidney cells
EC_{50}	half-maximal effective concentration
iGluR	ionotropic glutamate receptor
M1	first transmembrane helix
M3	third transmembrane helix
M4	fourth transmembrane helix
MD	molecular dynamics
MOT	mean open time
MST	mean shut time
MTSEA	methanethiosulfonate ethylammonium
NMDA	N-methyl-D-aspartate
P_{open}	open probability
RAMD	random acceleration molecular dynamics
RMSD	root-mean-square deviation
τ	tau, time constant
TMD	transmembrane domain

Chapter 1: Introduction

Neurotransmission and Cognition

From sea squirts and pond snails to African elephants and human beings, the nervous system is responsible for transmitting signals throughout the body. Our ability to recognize and respond to various stimuli allows us to regulate internal functions, adapt to changing conditions, and initiate action. Even marine-dwelling sponges, which lack a true nervous system, are able to recognize and respond to stimuli through the coordination of several proteins that assemble in a manner reminiscent to that of the evolved nervous system (Leys, 2015). Waves of calcium provide sponges with the ability to sense and respond to external triggers or changes in water quality (Leys, 2015). Despite their lack of complexity relative to the vast neural architecture of higher order animals, many scientists believe that sponges belong at the very roots of the ancestral tree. Even without a true nervous system, these filter feeders contain several neural precursors, a "neural toolkit", found in more evolutionarily complex organisms (Miller, 2009).

The primary distinction between organisms with and without nervous systems is the presence of neurons, specialized cells designed to send and receive signals to and from other nerve cells through a complex, highly regulated network. The signals passed between neurons take the form of electrochemical waves or neurotransmitters, endowing neurons with both directionality and electrical excitability. Generally, neurons receive signals at their dendrites, thin structures that branch from the nucleus-containing cell body forming a "dendritic tree". When the dendrites receive a signal, an electrochemical wave is sent down a long threadlike extension of the nerve cell called an axon. When these electrical impulses, called action potentials, reach the end of the axon, synaptic transmission is initiated. The neuron is provoked to release its neurotransmitters into the synaptic cleft where they can activate, inhibit, or otherwise modulate

their target postsynaptic neurons. With increasing complexity, the cellular signaling within these neural circuits has allowed for more diverse neuronal functions including learning, behavior, movement, perception, and comprehension.

With evolution came diversification, allowing for the vast library of genes that we now know can be expressed by a single neuron. However, while the complex brain developed more neural circuits, sophisticated structures, and functional capabilities, it retained some of the simpler structures required for its basic functions. For example, several synaptic proteins and ion channels can be traced all the way back to single-celled ancestors (Christensen et al., 1997; Ryan and Grant, 2009). Single-celled organisms make use of electrical excitability to respond to stimuli and systematically initiate action (Galizia and Lledo, 2013). Additionally, several non-animal eukaryotes and even some prokaryotes are able to communicate through the use of chemical transmitters. In higher order species, these relatively rudimentary processes of electrical and chemical signaling allow for communication between neurons during the process of neurotransmission.

During neurotransmission, information is passed between neurons through the use of neurotransmitters. These signaling molecules can range from amino acids and monoamines to peptides and purines, each allowing for unique communication between and classification of neurons. Once a neurotransmitter is released from the axon terminal of the presynaptic neuron into the synaptic cleft, it is available to bind to and activate the receptors on the dendrites of the postsynaptic neuron. This event ignites a cascade of phenomena within the postsynaptic neuron, ultimately leading to its excitation or inhibition.

Excitatory Neurotransmission Involves Ionotropic and Metabotropic Glutamate Receptors

During excitatory neurotransmission, the binding of neurotransmitters to transmembrane receptors of the postsynaptic neuron initiates depolarization (Meldrum, 2000). Specifically, the activation of ligand-gated ion channels facilitates the flow of positively charged ions into the cell, shifting the potential within the neuron away from its more negative resting membrane potential and towards its threshold potential. This temporary depolarization, referred to as an excitatory postsynaptic potential, makes the postsynaptic neuron more likely to fire an action potential. As the neuron receives simultaneous excitatory and inhibitory signals, spatial and temporal summation continues to drive the potential closer and closer to the threshold voltage. Should the potential reach threshold and initiate an action potential, the neuron can release its own neurotransmitters from its axons, thereby perpetuating the neuronal signal.

The principal excitatory neurotransmitter in the mammalian brain is glutamate (Meldrum, 2000). Glutamate is thought to be at a concentration of ~100 mmol/L within the vesicles of presynaptic terminals (Meldrum, 2000). Upon activation of voltage-dependent calcium channels, the glutamate-filled vesicles dock to the membrane and release their contents into the synaptic cleft. Glutamate must then traverse the synapse, which ranges in width from 200 to 500 Å (Eccles and Jaeger, 1958). Glutamate then reaches the postsynaptic membrane in less than 10 μs and diffuses throughout the cleft in 50 to 100 μs (Eccles and Jaeger, 1958). At concentrations exceeding a millimolar and a decay of 1.2 ms, glutamate in the synapse is available to bind to and activate receptors of the postsynaptic neuron (Clements et al., 1992). The family of receptors that are activated by glutamate can be divided into two distinct classes. The first class, metabotropic glutamate receptors, are G-protein-coupled receptors. These receptors convey glutamate signaling to the postsynaptic neuron by initiating intracellular biochemical cascades

(Willard and Koochekpour, 2013). The downstream pathways that are activated by GPCRs are dependent on the identity of the G-protein, with Gi/o leading to reduced adenylyl cyclase activity and decreased cAMP, Gs leading to increased adenylyl cyclase activity and increased cAMP, and Gq leading to the activation of PLC, resulting in increased intracellular calcium and PKC activity. The Gq-coupled mGluRs are primarily found at the postsynaptic terminal (Shigemoto et al., 1994). They have been implicated in synaptic plasticity— both long-term potentiation and long-term depression (Mannaioni et al., 2001; Swanson et al., 2005)—by increasing intracellular calcium concentrations through interactions with ionotropic receptors (Rose and Konnerth, 2001). These ionotropic glutamate receptors (iGluR), the second class of glutamate-activated receptors, are ion channels that are responsible for mediating the vast majority of excitatory neurotransmission throughout the brain (Dingledine et al., 1999).

Ionotropic Glutamate Receptors are Involved in Fast Excitatory Neurotransmission

Ion channels, specifically iGluRs, are one of the families of neuron proteins that have been conserved throughout evolution. Although first discovered in vertebrates, putative iGluRs have been identified in several invertebrate species and even the model plant *Arabidopsis thaliana* (Chiu et al., 1999; Lam et al., 1998). The first glutamate receptor identified in prokaryotes, GluR0, shares structural homology with the eukaryotic iGluRs and potassium channels (Chen et al., 1999; Mayer et al., 2001). As a result, NMDA receptors and the other members of the ionotropic glutamate receptor family are considered to be the result of a fusion between bacterial periplasmic binding proteins (PBP) and potassium channels. Specifically, the NMDAR ABD is considered to have evolved from the periplasmic binding proteins based on a significant amount of sequence and structural similarity (Nakanishi et al., 1990; Price et al.,

2012). The TMD domain, comprised of three transmembrane helices and a short re-entrant loop, resembles the structure of tetrameric potassium channels (e.g. KcsA), with inverted topology (MacKinnon, 2003). Finally, a group of genes found in some unicellular organisms—the bacterial periplasmic amino-acid-binding proteins— share identity with some functional regions of the eukaryotic iGluRs (Meldrum, 2000). Overall, the evolutionary map of iGluRs suggests that the excitatory signaling crucial to our healthy brain function evolved from a primitive signaling mechanism. Additionally, the conservation of ion channels along the evolutionary timeline emphasizes their importance in cell signaling and communication.

In general, ion channels are transmembrane proteins that allow the passage of ions from one side of the membrane to the other down their electrochemical gradients. As opposed to simple aqueous pores, ion channels are gated, meaning that they are not continuously open. For ion channels to open, they must first undergo conformational changes induced by ligand binding (ligand-gated channels) or a change in voltage (voltage-gated channels). These structural changes allow for the aqueous pore to become accessible to ions. By controlling the flow of ions, these channels are responsible for establishing the resting membrane potential, generating action potentials, and regulating cell volume (Alberts et al., 2002).

There are three pharmacologically defined classes of iGluRs, which can be subdivided into the NMDA and non-NMDA receptors. The non-NMDA receptors include kainate receptors and AMPA receptors, so named due to their selective responses to kainate and α-amino-3-hydroxy-5-methyl-4-isoxazolepropionate (AMPA), respectively (Bettler and Mulle, 1995; Frerking and Nicoll, 2000). Kainate receptors are encoded by five distinct genes (*GRIK1-5*), while AMPA receptors are encoded by four distinct genes (*GRIA1-4*). Both kainate and AMPA receptors are permeable to sodium and potassium ions, and their calcium permeability is

dependent upon RNA editing that alters an uncharged glutamine (Q) to a positively charged arginine (R) inside the channel pore (Burnashev et al., 1992a; Burnashev et al., 1992b; Dingledine et al., 1999; Egebjerg and Heinemann, 1993; Lomeli et al., 1994). Kainate and AMPA receptors display accelerated deactivation rates thought to be a result of their low-affinity binding sites for glutamate (Dingledine et al., 1999; Lomeli et al., 1994). Additionally, these receptors desensitize rapidly and profoundly on the millisecond timescale (Mosbacher et al., 1994; Sun et al., 2002). Although both kainate and AMPA receptors lose the ability to conduct current upon continuous exposure to glutamate, AMPA receptors recover from desensitization with time constants approximately 10-fold faster than kainate receptors (Dingledine et al., 1999; Mosbacher et al., 1994) and have been studied more extensively for their role in development and synaptic plasticity (Carroll et al., 2001; Henley and Wilkinson, 2016; Song and Huganir, 2002). Overall, the non-NMDA receptors are thought to make up the fast component of excitatory neurotransmission because the gating of these receptors by glutamate is incredibly fast relative to that of NMDA receptors.

NMDA Receptors

NMDA receptors selectively respond to n-methyl-D-aspartate and are thought to make up the slow component of fast excitatory neurotransmission (Collingridge et al., 1988; Forsythe and Westbrook, 1988; Lester et al., 1990). The concentration of glutamate that gives a half maximal response (EC_{50}) at NMDA receptors ranges from 0.4 to 1.8 μM depending on the receptor composition (Dingledine et al., 1999). As a result, the peak synaptic glutamate concentrations, which have been estimated to reach up to 1.1 mM, are always considered to be high enough to fully activate these receptors, (Clements, 1996; Clements et al., 1992). NMDA receptors activate

slowly with a rise time between 10 and 50 ms and deactivate with a much slower time course than most of their non-NMDA counterparts and that of glutamate in the synaptic cleft (1.2 ms) (Clements et al., 1992; Lester et al., 1990; Wyllie et al., 1998).

NMDA Receptor Deactivation is Defined by Four Receptor Properties

An important feature of NMDA receptors is their diversity in gating kinetics, which defines the time course of synaptic currents (Lester et al., 1990). The time course of deactivation of nearly all NMDA receptors can be described by multiple exponential components (Dingledine et al., 1999; Ogden et al., 2017). These multiple components may reflect complex channel behavior with each component resulting from a distinct conformational change within the receptor (Dingledine et al., 1999). The deactivation time course is predominantly a feature of four main receptor properties. Firstly, the deactivation rate is a function of agonist dissociation. If agonist affinity for a receptor is high, the deactivation time course of the receptor will be prolonged because the agonist will remain bound to the receptor for a longer period of time, allowing the channel to remain open longer. Secondly, the deactivation time course is influenced by the rate at which the channel undergoes conformational channels to return to its closed state. Previous single-channel studies have shown that the deactivation time course of macroscopic currents of NMDA receptors is dependent on channel burst length, which has been shown to depend on a series of rate constants that describe NMDA receptor gating and differ according to the type of GluN2 subunit present in the receptor (Vance et al., 2011; Wyllie et al., 1998). Thirdly, the amount of time that the receptor spends in its open state will directly influence the rate at which the receptor can deactivate following agonist removal. And fourthly, deactivation is influenced by desensitization of the receptor. In the desensitized state, the receptor has agonist

bound, but the ion channel is closed (Sun et al., 2002; Zhang et al., 2008). The receptor must undergo a conformational change to exit the desensitized state before glutamate can be released from its binding site (Gibb et al., 2018; Sun et al., 2002).

Additionally, the desensitization of NMDA receptors in the continued presence of agonist is slow and complex, involving rearrangement of the dimer interface (Sun et al., 2002). As such, in the continued presence of glutamate, NMDA receptors continue to conduct a substantial amount of current relative to the non-NMDA receptors. Modest desensitization of the NDMA receptor is an intrinsic mechanism for ion-channel activity regulation. By visiting a non-conducting conformational state in the continued presence of agonist, the neuron is at least partially protected from overactivation by prolonged glutamate exposure and potential excitotoxity. Additionally, decreased ion flux will ultimately lead to smaller intracellular calcium transients and a shift in the balance between long-term potentiation and long-term depression (Tong et al., 1995). More broadly, because NMDA receptors heavily contribute to the time course of synaptic neurotransmission, the kinetics of desensitization can influence the size, time course, and frequency of transmitted signals (Jones and Westbrook, 1996). Because calcium has important signaling roles in the postsynaptic terminal, shifting the concentration of calcium by desensitization changes the activity of proteins such as actin and calmodulin. Calcium-induced actin depolymerization (Bouhamdan et al., 2006; Rosenmund and Westbrook, 1993) and calcium-dependent calmodulin (Ehlers et al., 1996) have been shown to reduce NMDAR channel activity.

The activity of NMDA receptors is also affected by the activity of local mGluRs. NMDA receptors have been shown to be potentiated by Group I mGluRs in spinal cord motoneurons (Ugolini et al., 1997) and rat hippocampal slices (Fitzjohna et al., 1996), and an inhibitory

mGluR agonist has been shown to attenuate NMDA neurotoxicity (Buisson and Choi, 1995). Finally, NMDARs are slowed by voltage dependence. At resting membrane potential, NMDA receptors are blocked by Mg^{2+} (Coan and Collingridge, 1985). As such, the NMDA receptor acts as a coincidence receptor whereby, without a depolarization event, it is unable to pass ions even if bound by ligand. AMPA receptors are kinetically poised to relieve the NMDA receptor Mg^{2+}-block by supplying a rapid depolarization due to their prompt activation and brief open time. Once this block is relieved, NMDA receptors are permeable to sodium, potassium, and calcium (Jahr and Stevens, 1993; McBain and Mayer, 1994). These general properties of the NMDA receptor are what make them so important for neuronal function. As coincidence detectors regulated by several direct and indirect interactions with endogenous proteins, the NMDA receptor coordinates the activity of several events taking place within a single postsynaptic terminal.

The NMDA Receptor is Involved in Brain Physiology and Pathology

The intricate interplay between AMPA and NMDA receptors in the brain is critical for brain development (Ewald and Cline, 2009) and synaptic plasticity (Asztély and Gustafsson, 1996; Liu et al., 2004; Maren and Baudry, 1995; Takeuchi et al., 2014). Synaptic plasticity is defined as the ability of synapses to strengthen (long-term potentiation) and weaken (long-term depression) in response to patterns of synaptic activity. It is this process, whereby synaptic efficacy is altered as a result of prior experience, that has been deemed the neural correlate of learning and memory (Hebb, 1962). Following AMPA receptor-mediated depolarization and subsequent NMDA receptor activation following relief of magnesium block, there is a substantial increase in intracellular calcium within the postsynaptic neuron (Cain, 1997). During

long-term potentiation, calcium in the postsynaptic neuron activates calcium-dependent protein kinases, such as Ca^{2+}/calmodulin-dependent protein kinase II (CaMKII), which are responsible for altering the phosphorylation state of AMPA receptors. With phosphorylation, AMPA receptors experience increased conductance and rapid insertion into the postsynaptic membrane (Lu et al., 2001; Malenka and Bear, 2004). Because a greater number of more highly conductive receptors are present at the synapse to receive inputs, subsequent stimuli result in a heightened response in the postsynaptic terminal relative to that of the initial response. That is, the excitability of the neuron is increased leading to an overall increase in synaptic strength. Over time, with repeating patterns of activity, this persistent strengthening leads to a long-lasting increase in signal transmission between the two neurons. The inverse of this process, LTD, involves the endocytosis of AMPA receptors following dephosphorylation by serine/threonine-protein phosphatase 2B (PP2B) (Lüscher and Malenka, 2012). When the concentration of excitatory ionotropic receptors at the synapse is reduced in this way, the subsequent responses to neurotransmitter release will be much smaller. That is, the synaptic strength will have decreased.

While NMDA receptor-mediated calcium influx is critically important for normal brain function, aberrant NMDA receptor function has been associated with several neurological disorders. Firstly, over-activation of NMDA receptors has been linked to excitotoxicity as a result of calcium overload within the neuron (Choi, 1992; Choi, 1994). When calcium ions enter the cell, a number of enzymes are activated, some of which can result in the damage of several important cellular structures if the concentration of calcium is too high or the duration of its presence too long (Choi, 1992; Choi, 1994). Additionally, excess calcium in the cytosol can induce opening of the mitochondrial permeability transition pore. When this pore opens, mitochondria can swell and release reactive oxygen species (ROS) leading to apoptosis

(Stavrovskaya and Kristal, 2005). This ROS-induced cell death and disruption in the production of ATP can ultimately lead to elimination of biologically important electrochemical gradients that drive neuron signaling (Stavrovskaya and Kristal, 2005). NMDA receptor hyperfunction, or overactivation, has been linked to the development of Alzheimer's disease (Hynd et al., 2004), Huntington's disease (Zeron et al., 2002), epilepsy (Lemke et al., 2014; Rice and DeLorenzo, 1998; Yuan et al., 2015b), and intellectual disabilities (XiangWei et al., 2018). Alternatively, hypofunction, or underactivation, of NMDA receptors has been associated with schizophrenia (Coyle, 2006; Olney et al., 1999) and memory impairment (Newcomer et al., 1999). Finally, several *de novo* mutations and rare variants identified in NMDA receptors have been associated with diverse neurodevelopmental conditions ranging from developmental delays to seizures (Swanger et al., 2016). Genetic variation, or the lack thereof, within the different subunits of the NMDA receptor can shed light onto how different NMDA receptor subunits contribute to channel function.

The Properties of the Tetrameric NMDA Receptors Are Dependent on Subunit Composition

NMDA receptors are tetrameric proteins formed from the assembly of four distinct subunits. Most commonly, NMDA receptors are comprised of two GluN1 subunits and two GluN2 subunits arranged in a 1-2-1-2 fashion endowing the receptors with a 2-fold axis of symmetry in its extracellular region and a 4-fold axis of symmetry within the pore (Karakas and Furukawa, 2014; Lee et al., 2014). The subunits make extensive contact with each other, allowing for unique and important allosteric communication that influences channel function. As such, it is important to gain a better understanding of how the subunits in the tetramer could interact with each other. Furthermore, as different subunits endow the receptor with distinct

spatial, pharmacological, and kinetic properties (Cull-Candy et al., 2001; Paoletti and Neyton, 2007), unique functional properties are further influenced by the domains that make up each subunit. All NMDA receptors subunits contain an amino-terminal domain (ATD), an agonist-binding domain (ABD), a transmembrane domain (TMD), and a carboxy-terminal domain (CTD) (**Figure 1.1**). Understanding the mechanisms by which NMDA receptor structure influences function has long been a goal in the field.

The GluN1 subunit is ubiquitously expressed in the central nervous system (CNS), serves as the obligatory subunit of the NMDA receptor, and is responsible for binding co-agonist glycine (Dingledine et al., 1999). It is encoded by a single gene (*GRIN1*), but can be alternatively spliced to produce eight different isoforms (Durand et al., 1992; Hollmann et al., 1993; Nakanishi et al., 1992; Sugihara et al., 1992). Exon 5 encodes a 21 amino acid sequence in the ATD, while exon 21 and exon 22 encode sequences in the CTD with lengths of 37 amino acids and 38 amino acids, respectively. The GluN1 splice variants show distinct regional and developmental profiles, and the presence or absence of particular exons can influence receptor function and pharmacology (Laurie and Seeburg, 1994; Paupard et al., 1997; Zhong et al., 1995). The functional roles of exons 21 and 22 have not been entirely elucidated, but they are thought to influence surface trafficking and anchoring of receptors at the synapse due to their interactions with intracellular regulatory, scaffolding, and trafficking proteins (Hansen et al., 2018; Mu et al., 2003; Scott et al., 2001; Wenthold et al., 2003). Alternatively, much more is known about the function of exon 5 due to its more accessible location within the ATD and its measurable functional effects.

The exon 5 sequence is conserved throughout vertebrate GluN1 subunits, suggesting this region likely plays an important, evolutionarily-conserved role in healthy neurological function

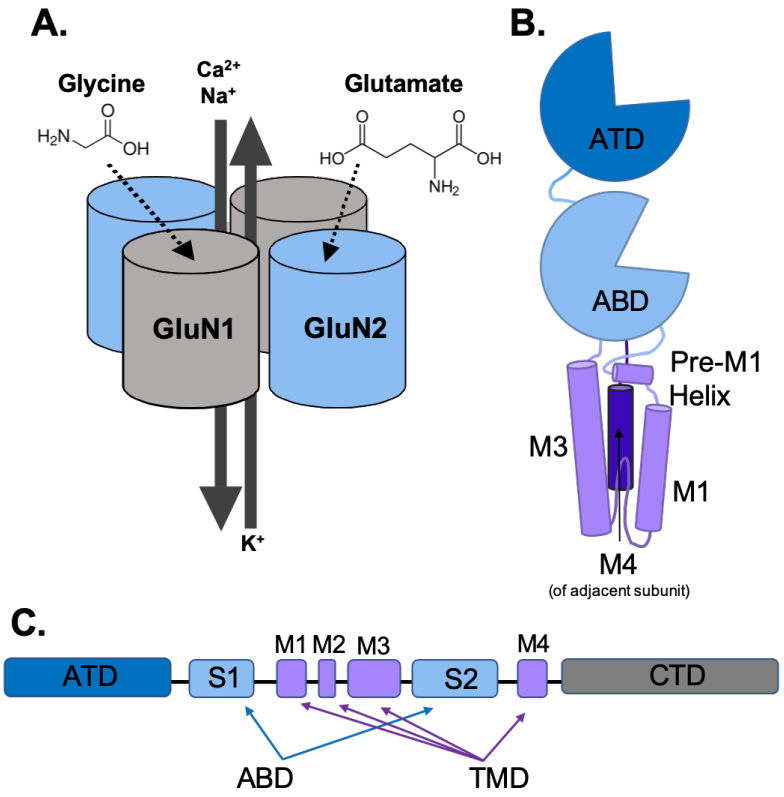

Figure 1.1: Subunit and Domain Architecture of the NMDA Receptor
A) Simple schematic illustrating the tetrameric assembly of the GluN subunits. Two glycine-binding GluN1 subunits (gray) and two glutamate-binding GluN2 subunits (blue) assemble to form a Na^+, Ca^{2+}, and K^+ permeable channel. **B)** Schematic illustrating the domain architecture within a single subunit of the NMDA receptor. Each subunit contains an extracellular-most ATD (dark blue), a clamshell-like ABD (light blue) and pore-forming transmembrane domains (purple). The pre-M1 helix and M3 helix of one subunit are in close proximity to the pre-M4 linker of the adjacent subunit. **C)** Linear representation of the domain structure of an NMDA receptor subunit. The ABD (light blue) is comprised of two segments, S1 and S2, which are separated by the M1 and M3 transmembrane helices and the M2 re-entrant loop (purple).

(Hansen et al., 2018; Regan et al., 2018). GluN1 subunits containing amino acids encoded by exon 5 have been shown to display reduced agonist potency and an accelerated deactivation time course following the removal of glutamate (Cull-Candy et al., 2001; Rumbaugh et al., 2000; Traynelis et al., 1998; Traynelis et al., 1995; Vance et al., 2012). Together, these functional consequences suggest that the residues encoded by exon 5 might alter the interactions between the ATD of GluN1 and the ABD of GluN1 and GluN2. Additionally, the ATD of the NMDA receptor contains the binding site of subunit-selective antagonists (i.e. ifenprodil at GluN2B) (Perin-Dureau et al., 2002), polyamines (Durand et al., 1993), and extracellular zinc (Paoletti et al., 2000) and is thought to contribute to proton sensitivity (Herin and Aizenman, 2004; Karakas et al., 2009; Perin-Dureau et al., 2002; Williams, 2001). The presence of exon 5 encoded amino acids has been shown to reduce inhibition by allosteric modulators and zinc (Traynelis et al., 1998), diminish potentiation by extracellular polyamines (Hansen et al., 2018), and relieve proton inhibition (Traynelis et al., 1995). As a consequence of its effect on pH sensitivity, it has been proposed that exon 5 might contribute to enhanced excitotoxity during ischemia-induced acidosis. If proton inhibition of the NMDA receptor is reduced by the presence of exon 5, then it is likely that a decrease in pH resulting from injury, stroke, or seizure could lead to enhanced NMDA receptor activity and, therefore, damage to the neurons in that region (Kaku et al., 1993; Rumbaugh et al., 2000; Traynelis et al., 1995).

Despite its role in both brain physiology and pathology, the mechanism by which exon 5 encoded amino acids exert their control over receptor function has remained elusive as a result of limited structural analysis. It has been shown that during receptor activation the GluN1 ATD undergoes large structural rearrangements (twisting ~39°) that could introduce new intra- and intersubunit interactions, that altering the GluN1 ATD hinge flexibility affects receptor function,

and that locking closed the GluN1 ATD "clamshell" decreases receptor activity and pharmacology (Esmenjaud et al., 2019; Zhu et al., 2013). Additionally, it has been shown that the conformation of the GluN1 ATD is influenced by the identity of the GluN2 subunit with which it is assembled (Sirrieh et al., 2015). Together, these data emphasize the functionally important allostery that exists between NMDA receptor subunits, which might help to explain the functional consequences of the exon 5 encoded amino acids. If the presence of the exon 5 cassette interferes with ATD-mediated allosteric interactions, then it is likely to result in significant changes to channel function.

Allosteric regulation of NMDAR activity also occurs beneath the lipid membrane through interactions with the CTD. The CTD offers the most diversity in terms of amino acid sequence and is known to be implicated in the modulation of NMDAR function by intracellular ions, post-translational modifications, and protein interactions. The CTD of glutamate receptors have been shown to interact with PDZ (i.e. PSD95, shank1), cytoskeletal (i.e. actin), scaffolding (i.e. RACK1), adaptor (i.e. AP2), anchoring, structural, signaling, and other proteins (Traynelis et al., 2010). NMDAR interactions with PSD95 (Kornau et al., 1995) and actin (Allison et al., 1998) facilitate receptor trafficking and localization at the cell membrane. The GluN1 subunit contains an ER retention signal (RRR) similar to the RXT motif in ATP-sensitive calcium channels. When PDZ proteins bind to the ER retention sequence, the receptors are able to effectively traffic to the surface of the membrane (Standley et al., 2000) and anchor at the post-synaptic density (Sans et al., 2003). Additionally, GluN2A and GluN2B contain a PDZ binding domain in their C-termini, which also regulate surface expression and anchoring even in the absence of the RRR ER retention signal (Horak et al., 2014). Rack1 binds to the GluN2B subunit and inhibits phosphorylation, thereby decreasing NMDAR-mediating currents (Yaka et al.,

2002). Association of the NMDA receptor with the AP2 complex facilitates receptor downregulation and recycling (Carroll and Zukin, 2002). Interestingly, the CTD has been shown to influence activity of extracellularly-acting positive and negative allosteric modulators (Sapkota et al., 2019). However, despite its numerous roles in the regulation of the receptor, deletion of the CTD from GluN1 or GluN2 subunits does not abolish the function of the receptor, but can alter desensitization, expression, distribution, and other properties (Ehlers et al., 1998; Köhr and Seeburg, 1996; Krupp et al., 1996; Vissel et al., 2001).

While the GluN1 subunit is critically important to channel function and provides splice-dependent functional diversity, it is the identity of the GluN2 subunit that endows the receptor with unique spatial, pharmacological, and functional properties. NMDA receptor GluN2 subunits have a high degree of sequence identity within their ABD (63%) and TMD (73%) domains, but share only 19% sequence identity within their ATD domains (Paoletti, 2011). Each of the four GluN2 subunits is encoded by a single gene: *GRIN2A, GRIN2B, GRIN2C, and GRIN2D* encoding for GluN2A, GluN2B, GluN2C, and GluN2D, respectively. Temporal and spatial expression patterns of the GluN2 subunits change drastically throughout development (Akazawa et al., 1994; Monyer et al., 1994). For example, the GluN2A subunit expression gradually increases after birth and is abundantly expressed throughout the CNS in adulthood. Widespread GluN2B subunit expression peaks shortly after birth, but progressively becomes restricted to forebrain areas into adulthood. The expression of GluN2C is confined primarily to the cerebellum and the olfactory bulb and appears much later in development relative to the GluN2A and 2B subunits. And finally, the high levels of GluN2D expression strictly within the diencephalon and brainstem regions during the prenatal period experience a drastic decrease following birth (Monyer et al., 1994; Paoletti, 2011; Watanabe et al., 1992). The properties of

NMDA receptor-mediated synaptic currents vary as a consequence of this developmental switch in GluN2 expression and the differences in functional characteristics of individual GluN2 subunits.

Due to their widespread and abundant expression in the adult brain, the function of GluN2A-containing NMDA receptors is of particular interest. GluN2A receptors have the lowest glutamate and glycine potencies with EC_{50} values of around 3.3 μM and 1.1 μM, respectively (Chen et al., 2008; Erreger et al., 2007; Traynelis et al., 2010). Additionally, GluN2A NMDA receptors deactivate the most rapidly with a deactivation time constant (τ) of 40 ms and have the highest open probability around 0.5 (Paoletti et al., 2013). GluN2A-containing receptors are particularly sensitive to zinc ions with an IC_{50} value in the low nanomolar range and are selectively modulated by the antagonist TCN-201 (Edman et al., 2012; Paoletti et al., 2013). Single channel analysis of GluN2A-containing receptors revealed two conductance levels, a main conducting state of 50 pS and a sub-conducting state of 38 pS, a mean open time between 3 and 5 ms, and 18% calcium permeability (Paoletti, 2011). These specific and defined properties allow the GluN2A receptor to participate in neuronal communication so as to uniquely contribute to synaptic time course in the adult brain. Should these specific properties be altered due to a mutation, there is a much greater chance of developing one of the aforementioned neurological disorders.

However, these single channel properties are not entirely unique to GluN2A-containing receptors. The conductance levels, mean open time, and calcium permeability of GluN2A-containing receptors are similar to those of GluN2B-containing receptors (Paoletti et al., 2013). The macroscopic properties of GluN2B-containing receptors are, however, notably different from those of GluN2A. Glutamate and glycine potency at GluN2B-containing receptors are

higher with EC_{50} values of around 2 μM and 0.4 μM, respectively (Chen et al., 2008; Erreger et al., 2007; Traynelis et al., 2010). These receptors also deactivate much more slowly with a τ around 300 ms and have an open probability between 0.1 and 0.2 (Erreger et al., 2005; Paoletti et al., 2013). GluN2B-containing receptors are also modulated by ifenprodil, Ro 25-6981, and CP-101,606 with IC_{50} values of 0.15 μM, 0.009 μM, and 0.039 μM, respectively (Ogden and Traynelis, 2011; Paoletti, 2011; Perin-Dureau et al., 2002). As with the GluN2A subunit, the unique properties of the GluN2B subunit allow it to play the role it does in the brain. Because GluN2B expression is highest early in life, the functional properties of these receptors need to be strictly maintained for normal neurodevelopment. Again, if the specific properties of the GluN2B subunit were to deviate from "normal" due to a mutation, there is a greater chance of a neurological disorder.

Just as the GluN2A- and GluN2B-containing receptors share several functional properties, so too do the GluN2C- and GluN2D-containing receptors. These receptors display two conductance levels, a main conducting state of 37 pS and a sub-conducting state of 18 pS (Paoletti, 2011). Additionally, these receptors have a mean open time between 0.5 and 1 ms and an open probability around 0.01. GluN2C-containing receptors have a glutamate EC_{50} of 1μM, a glycine EC_{50} of 0.3 μM, and a deactivation time course of 300 ms. Alternatively, GluN2D-containing receptors have a glutamate EC_{50} of 0.4 μM, a glycine EC_{50} of 0.1 μM, and a deactivation time course of 2000 ms (Paoletti, 2011). Both GluN2C and GluN2D can be potentiated by the positive allosteric modulator CIQ and inhibited by noncompetitive antagonists QNZ46 and DQP-1105 (Ogden and Traynelis, 2011; Wyllie et al., 2013; Zhu and Paoletti, 2015). These modulators show no preference between the GluN2C and GluN2D subunits, but have no observable effect at GluN2A or GluN2B (Ogden and Traynelis, 2011; Wyllie et al., 2013; Zhu

and Paoletti, 2015). Overall, the GluN2A and GluN2B subunits confer greater receptor activity with a more transient profile, while the GluN2C and GluN2D subunits impart receptors with lower activity for a longer duration.

Triheteromeric NMDA Receptors Have Unique Functional Properties

While much is known about NMDA receptors with a diheteromeric composition of two GluN1 subunits and two identical GluN2 subunits, NMDA receptors are also capable of forming functional triheteromeric receptors. Triheteromeric NMDA receptors are typically comprised of two GluN1 subunits and two different GluN2 subunits and are thought to make up the majority of native NMDA receptors (Hansen et al., 2014; Luo et al., 1997). Historically, functional analysis of these recombinant receptors was limited by an inability to differentiate them from co-expressed diheteromers. For example, when GluN1 is simply co-expressed with GluN2A and GluN2B in HEK cells, the population of receptors at the cell surface will be some combination of GluN1/GluN2A, GluN1/GluN2B, and GluN1/GluN2A/GluN2B receptors. In 2014, however, an approach to selectively dictate receptor stoichiometry and expression by exploiting the dual retention sequence of GABA-B receptors was introduced. The $GABA_{B1}$ subunit contains a retention signal (RXR motif) in its CTD that retains the subunit in the endoplasmic reticulum unless the retention signal is masked through a coiled-coil interaction with the CTD retention signal of the $GABA_{B2}$ subunit (Margeta-Mitrovic et al., 2000). Two different C-terminal peptide tags (C1 and C2) composed of the leucine zipper motifs and the ER retention motifs from $GABA_{B1}$ and $GABA_{B2}$ were engineered. By attaching each NMDA receptor subunit with a CTD peptide tag, subunits remain trapped in the endoplasmic reticulum unless their retention sequence is masked by a coiled-coil interaction with the appropriate binding partner (Hansen et al., 2014;

Stroebel et al., 2014). That is, only when the C1 tag of one subunit forms a coiled-coil interaction with the C2 tag of another subunit will the receptor be expressed at the cell surface. With this innovation, characterization of triheteromeric receptors became possible.

The first triheteromeric receptor to be investigated was the GluN1/GluN2A/GluN2B receptor. Interestingly, this receptor displayed properties that appeared to be distinct from those of either the GluN2A or GluN2B diheteromeric receptors. Specifically, GluN2A-specific inhibitor TCN-201 was able to inhibit the triheteromeric receptor, but with much less potency and efficacy than measured for the GluN2A diheteromeric receptor (Hansen et al., 2014). This same trend was observed for GluN2B-specific inhibitor ifenprodil which showed reduced potency and efficacy at the GluN1/GluN2A/GluN2B receptor (Hansen et al., 2014). Kinetically, GluN1/GluN2A and GluN1/GluN2B deactivate with drastically different time courses (tens-of-millisecond for GluN2A vs. hundreds-of-millisec for GluN2B) (Paoletti et al., 2013). The triheteromeric receptor deactivated with a time course that was significantly different from those of both GluN2A and GluN2B (Hansen et al., 2014). Specifically, although the GluN1/GluN2A/GluN2B deactivation time constant was intermediate (57 ms), it was of a similar magnitude to that of GluN1/GluN2A (32 ms) than that of GluN1/GluN2B (314 ms) (Hansen et al., 2014). Together, these results suggest that the GluN1/GluN2A/GluN2B receptors have distinct pharmacological and kinetic profiles that appear to be dominated by the GluN2A subunit.

NMDA Receptor Gating

The influence of GluN2A on these functional properties is likely a result of asymmetrical contributions of each subunit to overall allosteric interactions, conformational states, and

activation mechanism. In a process referred to as gating, a series of conformational changes promote channel opening in response to agonist binding. Agonists glycine (GluN1) and glutamate (GluN2) bind to the ABD formed by two discontinuous segments of the polypeptide referred to as S1 and S2 (Swanger et al., 2016). Crystallographic data suggests that the bi-lobed ABDs initiate activation by adopting a closed-cleft conformation due to atomic contacts between the agonist and the D1 upper and D2 lower lobes of the clamshell (Armstrong and Gouaux, 2000; Furukawa et al., 2005; Inanobe et al., 2005; Jin et al., 2003; Karakas and Furukawa, 2014; Lee et al., 2014; Mayer, 2011; Sun et al., 2002; Vance et al., 2011). Alternatively, when agonist-induced clamshell closure is prevented or agonist binding is disrupted, the receptor is unable to gate. For example, a mutation identified in a patient with developmental delay, E413G, is located in the GluN2B ABD and reduces glutamate potency by 50-fold (Adams et al., 2014). Based on the proximity of this mutation to the binding site of glutamate, it was hypothesized that it would some way interfere with agonist association and dissociation. Visual analysis of the GluN2B subunit structure with E413G modeled suggested that this mutation would increase solvent access to the ABD, which was confirmed by molecular modeling (Wells et al., 2018). As a consequence of disrupted agonist binding, the normal clamshell closure that is required for the channel to open will also be altered, leading to aberrant receptor function.

The Pre-M1 Helix Controls Channel Gating

Generally, in response to agonist binding, the pore-forming M3 transmembrane helices reorient away from the central axis of the pore allowing for the passage of cations. The M3 helices form pseudo four-fold symmetrical interactions and are thought to make up the physical gate of the receptor (Karakas and Furukawa, 2014; Lee et al., 2014). The bundle crossing of the

M3 helices is positioned similarly to that of the shut gate of the antagonist bound AMPA receptor (Karakas and Furukawa, 2014; Lee et al., 2014; Sobolevsky et al., 2009). The narrowest constriction is defined by residues within a highly conserved segment of amino acids (SYTANLAAF) crucial to ion channel gating, near the extracellular boundary of the M3 helices (Jones et al., 2002). In AMPA receptors, the gating mechanism involves a "kinking" of the M3 helices within the SYTANLAAF sequence (Twomey and Sobolevsky, 2017; Twomey et al., 2017). This sequence is shared among all members of the iGluR family, including the NMDA receptor. Because NMDA and AMPA receptors share pseudo 4-fold symmetry within the pore and the SYTANLAAF motif, it is thought that this "kinking" motion might also occur for NMDARs (Karakas and Furukawa, 2014; Lee et al., 2014; Tajima et al., 2016). It has been hypothesized that the linkers tethering the ABD to the TMD are responsible for facilitating communication between these two domains (Gibb et al., 2018; Karakas and Furukawa, 2014; Lee et al., 2014; Schorge et al., 2005; Sobolevsky et al., 2009; Talukder et al., 2010; Talukder and Wollmuth, 2011). Thus far, the flexible and dynamic nature of the ABD-TMD linkers has prevented high resolution structure of this region, and the structure of the fully open NMDA receptor pore remains elusive. Lower resolution analyses have revealed novel structural features within these linkers that are uniquely positioned to transduce agonist binding into channel opening (Karakas and Furukawa, 2014; Lee et al., 2014; Sobolevsky et al., 2009).

Specifically, the linker between the ABD and the first transmembrane (M1) helix (the S1-M1 linker) contains a short, two-turn pre-M1 helix that is thought to be a key contributor to the gating mechanism. The pre-M1 helix is perpendicular to the channel pore, downstream of the ABD, and is in van der Waals contact with the extracellular end of the M3 helical bundle (Karakas et al., 2015; Sobolevsky et al., 2009; Tajima et al., 2016). As such, it is thought that

agonist-induced closure of the bi-lobed ABD leads to a reorientation of the M3 helices by altering the position of the ABD-TMD linkers and, therefore, the pre-M1 helices (Furukawa and Gouaux, 2003; Furukawa et al., 2005; Hansen et al., 2018; Inanobe et al., 2005; Vance et al., 2011). This hypothesis is supported by data showing that cysteine substitutions within the ABD-TMD linker and the pre-M1 helix are sufficient to alter NMDAR responses, and MTS covalent modification of cysteine-substituted residues in this region altered receptor leak currents (Beck et al., 1999; Chang and Kuo, 2008; Sobolevsky et al., 2007). If contact between the pre-M1 helix and the M3 helix is essential for stabilizing a closed channel state, then agonist-induced reorientation of the pre-M1 helix or its residue side chains may constitute a required, rate-limiting pre-gating step that must be traversed before the channel can open (Gibb et al., 2018; Krupp et al., 1998; Regalado et al., 2001).

NMDAR Gating is Thought to Involve a Triad Between the TMD and Linkers

Several models have been developed to elucidate NMDA receptor activation mechanisms. Some models can accurately describe the macroscopic properties, namely the slow rise and decay time course, of synaptic currents (Lester and Jahr, 1992), while others can account for the more complex properties identified from single channel data (Auerbach and Zhou, 2005; Banke and Traynelis, 2003; Popescu and Auerbach, 2004; Schorge et al., 2005). More recently, a model has been developed to analyze the functional properties of receptors based on the single subunit contributions to the gating mechanism. This model, which relies on atomic-level structural data and functionally-characterized human mutations, can be used to model receptors that contain two different GluN1 or GluN2 subunits, two different GluN1 splice variants, or one copy of a disease-associated *de novo* mutation (Gibb et al., 2018). Moreover, this

model could be used to identify the role of the pre-M1 helix in gating by revealing changes in transition rates in response to a single copy or two copies of a functionally consequential pre-M1 human mutation.

One such human mutation, GluN2A-P552R, was identified in a patient displaying seizure disorders and intellectual disability (De Ligt et al., 2012). This residue, along with a few others in the pre-M1 helix, is conserved across all GluN subunits (Ogden et al., 2017) suggesting a conserved role in channel function. Characterization of this mutation revealed that GluN1/GluN2A receptors with one or two GluN2A-P552R subunits exhibit prolonged glutamate response time course, but only those with two mutant subunits exhibit a slow rise time (Ogden et al., 2017). This finding suggests that structural rearrangement of one GluN2A pre-M1 helix in response to agonist binding is sufficient for rapid, wild-type-like activation. Alternatively, two copies of GluN1-P557R did not produce the same slow rise time as that seen for the GluN2A subunit (Ogden et al., 2017), suggesting that the pre-M1 helices of different subunits make nonequivalent contributions to channel gating.

The idea that the pre-M1 helices of GluN1 and GluN2 have different roles in channel gating is further supported by the proposal that the pre-M1 helix is part of a triad comprised of the M3 pore-forming helix and the pre-M4 linker of the adjacent subunit (Chen et al., 2017; Ogden et al., 2017). Specifically, two distinct triads exist in each tetrameric assembly: GluN1-pre-M1/GluN1-M3/GluN2-pre-M4 and GluN2-pre-M1/GluN2-M3/GluN1-pre-M4. As a consequence, despite the high degree of sequence similarity, there might arise structural differences in each triad as a result of different amino acids within the GluN1 or GluN2 pre-M1 and pre-M4 regions. That is, global receptor asymmetry and disparate amino acid environments may contribute to subunit specific pre-M1 contributions to the gating mechanism.

Kazi et al. (2014) conducted a study to investigate the mechanical coupling of the NMDA receptor that allows for agonist binding to be transduced into pore opening. Their computational and thermodynamic analyses suggested that the agonist bound ABD pulls on the pore lining elements such that mutations inserted into the linker regions destabilized pore opening (Kazi et al., 2014). Moreover, this group reported that the pulling energy required for pore opening was more prominent in the GluN2 subunit than the GluN1 subunit. Specifically, they report that the glycine-bound GluN1 and glutamate-bound GluN2 subunits pull on M3 with about equivalent energy to open the pore, but that the GluN2 subunit transduces more energy during earlier transitions. This energy imbalance between the GluN1 and GluN2 subunits appears to be consistent with the presence of the gating triad.

A study by Yelshanskaya et al. (2017) also showed that mutations within the extracellular collar region of the AMPA receptor resulted in significant effects on gating. Their molecular dynamics simulations suggested that opening of the ion channel requires the helical bundle to move apart to open the pore. To enter the open state, the M3 helices are proposed to change in orientation with respect to the pre-M1, M1, and M4 helices in a way that is disrupted by the introduction of mutations in these regions. With the energetic information, these findings support the hypothesis that the channel opens through interactions between the S1-M1 linker, the M3 helix, and the pre-M4 linker.

The pre-M4 linker is positioned at the extracellular end of the ion channel pore between the S2 segment of the ABD and the M4 transmembrane helix (Karakas and Furukawa, 2014; Lee et al., 2014; Tajima et al., 2016). Structural analysis of the NMDA receptor open state has revealed that the pre-M4 helix unwinds and the S2-M4 linker moves toward the central pore axis (Twomey and Sobolevsky, 2017; Twomey et al., 2017). Additionally, it has been shown that

MTS covalent modification of cysteine-substituted residues in the S2-M4 linker altered receptor leak currents (Talukder et al., 2010), and constraining movement in this region by disulfide cross-linking resulted in impaired pore opening (Talukder and Wollmuth, 2011). Together, these results suggest that the S2-M4 linker is critical to the gating mechanism and, moreover, that conformational freedom of this linker is required for normal receptor function.

The hypothesis, then, is that the NMDA receptor bi-lobed ABDs initiate activation by adopting a closed-cleft conformation due to atomic contacts between the agonist and the D1 upper and D2 lower lobes of the clamshell (Armstrong and Gouaux, 2000; Furukawa et al., 2005; Inanobe et al., 2005; Jin et al., 2003; Karakas and Furukawa, 2014; Lee et al., 2014; Mayer, 2011; Sun et al., 2002; Vance et al., 2011). This motion within the ABD pulls on the ABD-TMD linkers: the S1-M1 linker containing the pre-M1 helix, the M3-S2 linker, and the S2-M4 linker (**Figure 1.2**). The S1-M1 and M3-S2 linkers are thought to pull the extracellular ends of the M3 helices apart resulting in bending away from the central axis of the pore (Wollmuth and Sobolevsky, 2004) ultimately leading to channel opening. Additionally, the intersubunit triads suggest that the S2-M4 helix of the adjacent subunit also interacts with the M3 helix and S1-M1 linker, such that the conformational changes facilitating channel opening in one subunit may be influenced by the conformational state of the adjacent subunit (Chen et al., 2017; Gibb et al., 2018; Ogden et al., 2017).

Pre-M1 Helices are Highly Conserved

Several amino acids that make up the pre-M1 helix can be found in ionotropic glutamate receptors across several species. Specifically, a large degree of sequence similarity in the pre-M1 helix has been identified between the GluN1 subunit of humans and mice, the GluA1 receptor of

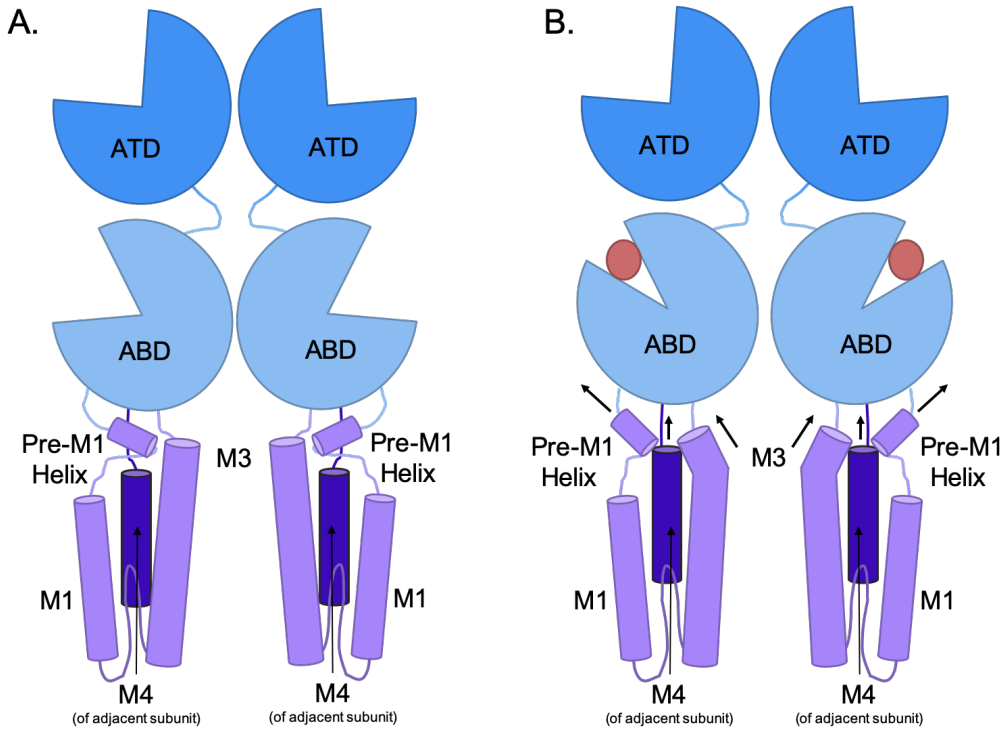

Figure 1.2: A Basic Model of the Gating Mechanism as Mediated by the ABD-TMD Linkers
Each subunit contains an extracellular-most ATD (dark blue), a clamshell-like ABD (light blue) and pore-forming transmembrane domains (purple). The pre-M1 helix and M3 helix of one subunit are in close proximity to the pre-M4 linker of the adjacent subunit. **A)** A simple model of two subunits of the NMDA receptor in the unbound, closed channel state. In the unbound state, the extracellular end of the M3 helices are oriented toward the interior (central axis) of the channel pore. **B)** In the agonist (red) bound state, the ABD clamshell closes ~20° and the S1-M1 linker pulls outward and upward, while the M3 helix and M4 helix are being pulled directly by their associated linkers connected to the ABD.

humans and zebrafish, and the GluK2 receptors of C. elegans and a species of ant (Alsaloum et al., 2016). The pre-M1 helix of the GluN1 subunit is different from the GluN2 subunits, however, with the exception of two conserved residues, GluN1-Phe554 and GluN1-Pro558. Among the GluN2 subunits, the pre-M1 helix is conserved with the exception of the last two residues on the M1 end of the sequence, which differs between GluN2A/2B and GluN2C/2D (Ogden et al., 2017). With these similarities and differences in mind, it is possible to speculate on the role of the pre-M1 helix. Firstly, this collective information would suggest that the conserved pre-M1 helix, particularly that of the GluN1 subunit, is functionally important for general ion channel function. Alternatively, the difference between the highly-conserved GluN1 and GluN2 might suggest that this region of the receptor in the GluN2 subunits plays a different role than the GluN1 subunit in channel function. Specifically, it is likely that the sequence of the GluN2 subunits offers functional control over channel gating that is unique to the NMDA receptor and may explain some of the functional differences between NMDA receptors and other iGluRs.

In a population of over 140,000 healthy individuals, the GluN2A and GluN2B pre-M1 helices are devoid of missense mutations (gnomad.broadinstitute.org)(Ogden et al., 2017). This trend would suggest that the pre-M1 helix of these subunits is under purifying selection such that mutations would likely lead to an observable neuropathologic phenotype. Missense tolerance ratio (MTR) summarizes available human standing variation data within genes to encapsulate population level genetic variation. Analysis of the MTR of a subset of epilepsy-associated genes identified several that display at least some invariance in specific regions. Specifically, the KCNQ2 gene, which encodes for a potassium channel, and the SCN1A, SCN2A, and SCN8A genes, which encode for sodium channels, and the GRIN2A gene displayed regions of absolute selection against mutations (Traynelis et al., 2017).

In addition, the NMDAR pre-M1 helix is a locus for disease-associated *de novo* mutations (**Figure 1.3**). In addition to the previously discussed GluN2A-P552R mutation, several other GluN2A pre-M1 mutations (A548T, A548P, E551K, and S554T) have been identified in patients displaying phenotypes ranging from language and movement disorders to epilepsy and intellectual disability (CFERV Database: http://functionalvariants.emory.edu/database/index.html). The mutations included in the CFERV database are those that have been identified in patients presenting with one or more neurological phenotypes. However, just because embryonic lethal mutations are not included in the database does not mean that they do not occur. It has been shown that abnormal GluN subunits—mutations GluN1-N598Q and GluN1-N598R (Single et al., 2000) or GluN1 and GluN2B knock-outs (Forrest et al., 1994; Moy et al., 2006; Sprengel and Single, 1999; Tsien et al., 1996)—are embryonic lethal in mice. While these deleterious mutations are not specific to the pre-M1 helix, it is possible that, because of the importance of the gating triad in the function of the NMDA receptor, mutations in this region could be consequential enough to lead to absolute incompatibility with life. Additionally, because of the expression shift in GluN2A and GluN2B, it is likely that these potentially deleterious mutations are more likely to be found in the GluN2B subunit. Finally, the GluN2D subunit has fewer missense variants, despite having similar intolerance to mutations as GluN2A (XiangWei et al., 2018). This would suggest that mutations also occur in the GluN2D subunit, but they are incompatible with life.

The GluN1 and GluN2B subunits also present disease-associated mutations in their pre-M1 helices including mutations at their Pro553 homologous residues (GluN1-P557R and GluN2B-P553L). One particular mutation, GluN1-L551P, was identified in a 9-year old female patient with bilateral polymicrogyria, intellectual disability, developmental delay, and epilepsy

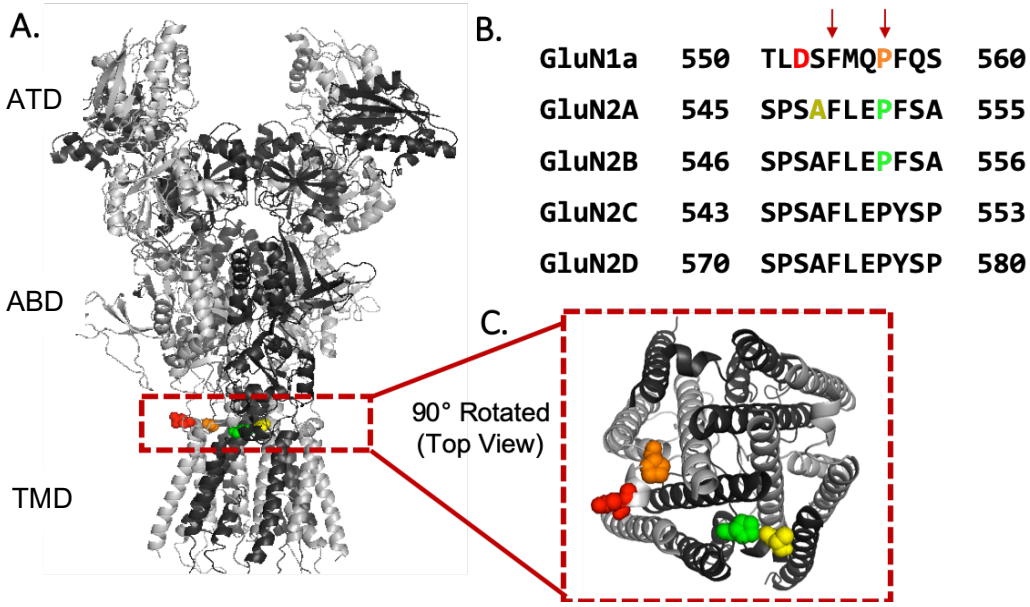

Figure 1.3: The Pre-M1 Helix is a Hub for Disease-Associated *De Novo* Mutations
A) Homology model of a GluN1/GluN2A NMDA receptor. GluN1 subunits are shown in gray, and GluN2A subunits are shown in black. The figure highlights the pre-M1 helices (red dashed box) just above the TMD. **B)** Sequence alignment of the GluN subunits shows residues that have been identified as sites of disease-associated human mutations. These residues include GluN1-Asp551 (red), GluN1-Pro557 (orange), GluN2A-Ala548 (yellow), and GluN2A-Pro552 and GluN2B-Pro553 (green). Red arrows designate residues that are conserved across the GluN subunits. **C)** View of the channel pore from above shows the location of the pre-M1 disease-associated mutations. Residue colors correspond to the amino acids in (B).

(Fry et al., 2018). This residue is not conserved in the other GluN subunits, but it is highly conserved across several species (Ohba et al., 2015). When GluN1-L551P was investigated for its effect on hydrogen bonds between the glycine ligand and the glycine-binding residues of GluN1, it was predicted that the number of bonds would increase from four for wild-type to nine, suggesting that the mutation could contribute to altered kinetics of co-agonist binding. Additionally, modelling the effects of GluN1-L551P on the position of other regions of the GluN1 subunit revealed a 6.5 Å change in the structure of the extracellular gating region of the M3 helix (Fry et al., 2018). Overall, genetic analysis of the pre-M1 helix emphasizes the importance of this region for normal receptor function and begins to shed light on how mutations in this region might contribute to neurodivergent phenotypes.

Summary

As we learn more about the role of NMDA receptors in development and disease, it becomes increasingly important to develop a more comprehensive understanding of their mechanistic function. With the recent advances in structural biology, the establishment of more selective allosteric modulators, and a deeper dive into genetic variation, we are more capable than ever to take strides toward elucidating the mechanism of NMDA receptor function. In this thesis, I explore the functional role of three highly conserved regions of the NMDA receptor: the pre-M1 helix, the GluN2 glutamate binding site, and the GluN1 exon 5 motif. Guided by genetic regulation and variation, I introduced purposeful mutations within these regions and measured the effect on a multitude of channel properties. I show that these regions are likely under such strict genetic regulation as a consequence of their considerable influence on receptor function. Moreover, I present a structure-based model to investigate how independent subunits contribute

to the activation of NMDA receptors as suggested by the GluN2A-P552R human mutation. Finally, I show that deactivation rate correlates with both proton sensitivity and glutamate egress time. Together, the results presented in this thesis shed light on the role of specific highly-conserved structural regions— and the amino acids therein—in the function of the NMDA receptor ion channel. Moreover, this study emphasizes the value of using genetics to guide the rational design of investigative scientific inquiry.

Chapter 2: Materials and Methods

DNA Constructs

For experiments in HEK293 cells, cDNAs for recombinant rat NMDA receptor subunits GluN1-1a (GenBank accession number U08261 for GluN1 lacking exon 5 but containing exon 21 and 22), GluN2A (GenBank accession number D13211), GluN2B (GenBank accession number U11419), and GluN2D (GenBank accession number L31611) were subcloned into a mammalian expression vector (pcI-neo). cDNA for the green fluorescent protein variant maxGFP (formerly Amaxa, currently Lonza) was subcloned in the vector pmaxGFP. For experiments using *Xenopus laevis* oocytes, cDNA for GluN1-1a was subcloned in the pGEMHE vector and cDNAs for GluN2A, GluN2B, and GluN2D were in the pCI-neo vector (Liman et al., 1992). All plasmids contained a gene for ampicillin resistance, except for pmaxGFP, which contained a kanamycin resistance gene.

Site-Directed Mutagenesis

Site-directed mutagenesis was accomplished using Quikchange reactions carried out in a total volume of 50 µL composed of 39 µL ultrapure water (Milli-Q), 5 µL 10x cloned Pfu reaction buffer (Agilent Technologies), deoxyribonucleoside triphosphates (dNTPs, 10 mM each; Promega catalog no. U1511), 2 µL forward and reverse primers (10 µM each), 1 µL DNA template (about 0.2 µg/µL) and 1 µL PfuTurbo DNA polymerase (2.5 U/µL; Agilent Technologies catalog no. 600254). All reagents were thawed and mixed prior to use. Samples were briefly spun down using a minicentrifuge then placed on ice during assembly of the reaction. Reactions were prepared at room temperature and the PfuTurbo DNA polymerase was added last. Reactions were thoroughly mixed by vigorously inverting the tubes 3-5 times and

then placed in a thermal cycler (MJ Research PTC 200). Thermal cycling for the reactions consisted of 1 min at 95 °C followed by 14 cycles of 30 sec at 95 °C, 1 min at 55 °C, and 15 min at 68 °C. When the reactions completed, they were kept at 4 °C (4-8 hours) until 1.5 µL DpnI was added to each. The reactions were mixed and incubated at 37 °C for 3 hours. Reactions were then maintained at 4 °C (0-4 hours) until being used for transforming E. coli.

cDNA Preparation

For transformation of cDNA, chemically-competent Stellar™ *E. coli* (Takara) were thawed on ice while Super Optimal broth with Catabolite repression (SOC) media (Invitrogen catalog no. 15544-034) was warmed to 37 °C in a water bath. 1 µL cDNA (~ 1 ng, for retransformations) or 3.5 µL DNA (~3 ng, for Quikchange reactions) was added to 50 µL of *E. coli*, mixed, and incubated on ice for 10-15 min. Samples were then placed in a 42 °C water bath for 45-60 sec, placed on ice for 20 sec, and moved to the bench top, where 250 µL of preheated SOC media was immediately added. Cells were incubated for 45-60 min at 37 °C while an agar plate containing appropriate ampicillin was warmed upside down in a 37 °C. For retransformations, 10 µL *E. coli* was spread on the agar plates. For Quikchange reactions, all of the E. coli (about 300 µL) was plated. Plates were left at room temperature for 5-15 min and then incubated at 37 °C overnight.

For minipreparations of cDNA, individual colonies from transformations were inoculated into 14 mL round-bottom tubes containing 2 mL 2x YT media with antibiotic. Tubes were incubated at 37 °C for 12-16 hours with constant shaking. Samples were transferred to 2 mL microcentrifuge tubes and centrifuged at 13000 rpm for 3 min. DNA was then isolated and purified from E. coli using a QIAprep Spin Miniprep Kit (QIAGEN catalog no. 27104)

according to the manufacturer's protocol, eluting the DNA with 50 µL elution buffer. DNA sequences were verified before further use (Eurofins Genomics) and DNA concentration was determined using the Thermo Scientific NanoDrop Lite Spectrophotometer.

cRNA Preparation

[cRNA preparation performed by Kevin Ogden]

DNA constructs were linearized by restriction enzymes selected to cut the DNA at least 200 base pairs downstream from the stop codon of the cDNA insert. The digestion reaction consisted of 20 µL 10x NEBuffer specific to the restriction enzyme, 20 µL 10x BSA if required by the enzyme, 5 µg DNA (or 20 µL of DNA from a miniprep), 5 µL restriction enzyme, and the volume of Milli-Q water needed to bring the final volume to 200 µL. Reactions were then vortexed, spun down, and incubated at 37 °C for 3 hours. The QIAquick PCR Purification kit (QIAGEN) was used to purify the linearized template DNA according to the manufacturer's protocol. The linearized cDNA was purified using ethanol precipitation by adding 10 µL 3 M sodium acetate to the eluted DNA and mixing, adding 250 µL 100% ethanol and mixing, and then incubating in the freezer at -80 °C for 30 min. Precipitated DNA was centrifuged at 14000 rpm for 30 min at 4 °C. The supernatant was removed, and the pellet was washed with 200 µL 70% ethanol then re-centrifuged at 14000 rpm at 4 °C for 30 min. The supernatant was again removed, and the DNA pellet was incubated at 37 °C for 3-5 min to dry. The pellet was resuspended in 10.5 µL nuclease-free TE buffer by pipetting for 2-3 min. The quality and quantity of the DNA and the completeness of the linearization was assessed by running 0.5 µL DNA on a 0.8% agarose gel at 100 V for 40-45 min and visualizing the DNA bands by SYBR® Safe Stain.

cRNA was synthesized in vitro using the mMESSAGE mMACHINE Kit (Ambion) according to the manufacturer's protocol. All reagents, with the exception of the RNA polymerase mix, were completely thawed at room temperature and vortexed. All reagents were then placed on ice before assembly. The transcription reaction was prepared in a sterile 1.5 mL microcentrifuge tube at room temperature. Reagents were added to the tube in the following order: 10 µL 2x NTP/CAP, the required amount of nuclease-free water to bring up to 21 µL volume, 2 µL 10x reaction buffer, 3-6 µL linear DNA template (about 1 µg DNA), 1 µL GTP, and 2 µL RNA polymerase mix. GTP was included in the reaction to improve the yield of longer transcripts. The reaction was mixed by gentle flicking and then centrifuged briefly before being incubated for 1.5-2 hours at 37 °C. The template DNA was digested by addition of 1 µL TURBO DNase followed by incubation at 37 °C for 15 min. The cRNA was precipitated by adding 30 µL LiCl Precipitation Solution and 30 µL nuclease-free water, mixing, and chilling at -20 °C for at least 1 hour. The mixture was centrifuged at 14000 rpm at 4 °C for 15 min to pellet the RNA. The pellet was washed once with 0.5 mL 70% ethanol and re-centrifuged to maximize removal of unincorporated nucleotides. After removal of the supernatant, the pellet was dried for 5 min at 37 °C and resuspended in 20 µL nuclease-free water. The quality of the cRNA transcript was assessed by agarose gel electrophoresis. 1 µL cRNA product, 5 µL nuclease-free water, and 6 µL Gel Loading Buffer II (Ambion) were mixed and heated for 1-3 min at 95 °C. cRNA samples were then loaded in a 0.8% agarose gel and run at 85 V for 40 min. 1 µL 0.5-10 Kb RNA ladder (Invitrogen catalog no. 15623200) together with 5 µL nuclease-free water and 6 µL Gel Loading Buffer II was run along with the cRNA samples.

Two electrode voltage clamp recordings from Xenopus oocytes

Defolliculated stage V-VI *Xenopus laevis* oocytes were obtained from EcoCyte Bioscience (Austin, TX), or *Xenopus laevis* stage VI oocytes were prepared from commercially available ovaries (Xenopus 1 Inc.). The ovary was digested with Collagenase Type 4 (Worthington-Biochem) solution (850 μg/ml, 15 ml for a half ovary) in calcium-free Barth's solution, which contained (in mM) 88 NaCl, 2.4 $NaHCO_3$, 1 KCl, 0.33 $Ca(NO_3)_2$, 0.41 $CaCl_2$, 0.82 $MgSO_4$, 10 HEPES (pH 7.4 with NaOH) supplemented with 100 μg/ml gentamycin and 40 μg/ml streptomycin. The ovary was incubated with enzyme for 2 hours at room temperature (23°C) with gentle rocking. The oocytes were rinsed on the mixer with calcium-free Barth's solution five times (35–40 ml of fresh solution each time) for 10 min each time and rinsed with normal Barth's solution (35–40 ml of fresh solution) four times for 10 min each time. The sorted oocytes were kept in 15°C incubator until use.

Individual oocytes were defolliculated and injected with GluN1 and GluN2A cRNA at a 1:2 ratio (5-10 ng total in 50 nl RNAase-free water), as previously described (Hansen et al., 2013; Ogden et al., 2013) using a Nanoject II automated microinjection pipet (Drummond Scientific catalog no. 3-000-204). Following injection, oocytes were maintained for 2-7 days at 15 °C in Barth's culture medium containing (in mM) 88 NaCl, 2.4 $NaHCO_3$, 1 KCl, 0.33 $Ca(NO_3)_2$, 0.41 $CaCl_2$, 0.82 $MgSO_4$, 5 HEPES (pH 7.4), and supplemented with 0.1 mg/mL gentamicin sulfate, and 1 μg/mL streptomycin. Oocytes were placed in a recording chamber and continuously perfused with a solution containing (in mM) 90 NaCl, 1 KCl, 10 HEPES, 0.5-1 $BaCl_2$, 0.01 EDTA (pH 7.4) at about 5 mL/min. Responses were measured at room temperature (21-23°C) for 0.10 - 100 μM glutamate in 100 μM glycine, and 0.03 - 30 μM glycine in 100 μM glutamate perfused by gravity. Solution exchange was regulated by an 8-port automated valve

(Digital Modular Valve Positioner, Hamilton Company) controlled by EasyOocyte http://easyoocyte.io, http://www.pharm.emory.edu/straynelis/downloads/index.html). Microelectrodes were fabricated from borosilicate glass (World Precision Instruments TW150F-4), filled with 0.3-3 M KCl, and currents were recorded under two-electrode voltage clamp at a holding potential of -40 mV (Warner Instruments OC-725C). Currents were low pass filtered at 10 Hz and digitized at 20 Hz using EasyOoctye acquisition software (http://easyoocyte.io, http://www.pharm.emory.edu/straynelis/downloads/index.html).

MTSEA Assay

Channel open probability was calculated from the degree of methanethiosulfonate ethylammonium (MTSEA) potentiation. MTSEA reacts with and modifies sulfydryl cysteine residues engineered at the region of interest. When the MTSEA reagent is applied, if the substituted cysteine is accessible, the reagent irreversibly modifies the amino acid and leading to measurable changes to receptor function. Oocytes expressing GluN1/GluN2A and GluN1/GluN2D were prepared as described above. Currents were evoked by application of 100 μM glutamate and glycine during the continuous perfusion of a solution containing (in mM) 90 NaCl, 1 KCl, 10 HEPES, 0.5-1 $BaCl_2$, 0.01 EDTA (pH 7.4). In the continued presence of agonists, 200 μM MTSEA made fresh daily from powder was applied and degree of potentiation relative to the control was determined. The following equation (Yuan et al., 2005) was used to determine open probability as a function of potentiation:

$$P_{Open} = (\gamma_{MTSEA}/\gamma_{Control}) \times (1/\text{Potentiation})$$

Potentiation is the current after MTSEA treatment divided by the current before treatment. The control and MTSEA γ were estimated from GluN1/GluN2A receptors.

HEK Cell Culture

Human embryonic kidney (HEK) cells (ATCC CRL-1573) were grown in 60 mm tissue culture dishes incubated at 37°C with 5% carbon dioxide. The cells were maintained in 4 mL Dulbecco's Modified Eagle Medium (DMEM) with GlutaMAX I (Gibco catalog no. 10569) supplemented with 10% dialyzed fetal bovine serum (Gibco catalog no. 26400), 10 U/mL penicillin, and 10 µg/mL streptomycin. Cells were split every 1-3 days when they reached 90-95% confluency by rinsing with calcium-free Hank's Balanced Salt Solution (Gibco catalog n. 14175), incubating at 37°C for 1-2 min with 0.5 mL 0.05% trypsin-EDTA (Gibco catalog no. 25300), and adding 1 mL media. After cells were separated by gently pipetting up and down several times, they were seeded into new 60 mm dishes at ratios of 1:5, 1:10, or 1:20.

B-Lactamase Trafficking Assay

HEK cells were seeded in 96-well plates (~50,000 cells/well) and transiently transfected with cDNA encoding ß -lac-GluN1 and GluN2A using Fugene6 (Promega). Cells treated with only Fugene6 were used to determine background absorbance, and cells without GluN2 served as a negative control for surface ß -lactamase activity. NMDAR antagonists (200 µM APV and 200 µM 7-CKA) were added at the time of transfection to reduce the potential for excitotoxicity. Six wells were transfected for each condition; surface and total activities were measured in 3 wells each. After 24 hr, cells were washed with Hank's Balanced Salt Solution (HBSS) supplemented with 10 mM HEPES. Following wash, the three wells for measuring surface activity were treated with 100 mL of a 100 mM nitrocefin (Millipore) solution in HBSS with HEPES was added. In the three wells for measuring total activity, the cells were lysed by a 30 min incubation in 50 mL

water prior to the addition of 50 mL of 200mM nitrocefin. Cell-impermeable nitrocefin is hydrolyzed by ß -lactamase only when the enzyme is expressed at the surface of the cell. When nitrocefin is cleaved, its absorbance changes from 390 nm to 486 nm (Lam et al., 2013). The plate was held at a constant 30°C and the absorbance at 468 nm was measured every min for 30 min using a microplate reader. The rate at which the absorbance increased was determined from the slope of a linear fit. The rate of nitrocefin hydrolysis by β-lactamase (the slope of the curve in the linear range) is directly proportional to the amount of surface expression of the receptor.

Whole cell current recordings from transfected HEK cells

HEK-293 cells (ATCC CRL-1573) were plated onto glass coverslips coated with poly-D-lysine (100 µg/mL) and transiently transfected using the calcium phosphate precipitation method (Chen and Okayama, 1987) with plasmid cDNAs encoding GluN1, wild type or mutant GluN2A, and GFP at a ratio of 1:1:1 (0.2 mg/mL total cDNA). 200 µM D,L-APV and 200 µM 7-chlorokynuernic acid were added to the tissue culture media to reduce activation of the NMDARs by ambient glutamate, thereby reducing excitotoxic cell death. Cells were transferred to a recording chamber 18-24 hours post-transfection and continuously perfused at 2 mL/min with solution containing (in mM) 150 NaCl, 3 KCl, 10 HEPES, 0.01 EDTA, 0.5 $CaCl_2$, and 11 D-mannitol (pH 7.4). Patch electrodes were made from thin-walled filamented borosilicate glass (World Precision Instruments catalog no. TW150F-4) pulled using a Flaming/Brown horizontal puller (Sutter Instrument P-1000) and fire-polished to a final resistance of 3-4 MΩ. The pipettes were filled with a filtered solution comprised of (in mM) 110 D-gluconic acid, 110 CsOH, 30 CsCl, 5 HEPES, 4 NaCl, 0.5 $CaCl_2$, 2 $MgCl_2$, 5 BAPTA, 2 Na-ATP, 0.3 Na-GTP (pH 7.35); the osmolality was 300-310 mOsmol/kg. The membrane potential of HEK cells was held at -60 mV

using an Axopatch 200B patch-clamp amplifier (Molecular Devices). NMDAR current responses were recorded during application of 1 mM glutamate and 30 μM glycine. Current recordings were filtered at 8 kHz (-3 dB, 8 pole Bessel filter) and digitized at 20 kHz using a Digidata 1440A data acquisition system (Molecular Devices) controlled by Clampex 10.3 (Molecular Devices). Rise time for each response was determined as the time measured between 10% and 90% of the peak current. Current response time courses were averaged in Clampfit 10.6 (Molecular Devices), and the deactivation time course was fitted using ChanneLab by the sum of multiple exponential functions:

$$\text{Current (time)} = \text{Amp}_{\text{Fast}}\, e(-\text{time}/\tau_{\text{Fast}}) + \text{Amp}_{\text{Slow}}\, e(-\text{time}/\tau_{\text{Slow}}),$$

where τ_{Fast} is the fast deactivation time constant, τ_{Slow} is the slow deactivation time constant, Amp_{Fast} is the amplitude of the fast deactivation component, Amp_{Slow} is the amplitude of the slow deactivation component, and the peak response at the initiation of deactivation occurs at time=0. Weighted deactivation time constants (τ_w) were determined by the following equation:

$$\tau_w = ([\text{Amp}_{\text{Fast}}/(\text{Amp}_{\text{Fast}} + \text{Amp}_{\text{Slow}})] \times \tau_{\text{Fast}}) + ([\text{Amp}_{\text{Slow}}/(\text{Amp}_{\text{Fast}} + \text{Amp}_{\text{Slow}})] \times \tau_{\text{slow}})$$

To determine the macroscopic current time course, outside-out patches were excised and placed in front of the rapid agonist application system. Responses were recorded to 1 second application of 3 μM or 1 mM glutamate in the continued presence of 100 μM glycine. Recording pipettes were fire-polished to a final resistance of 8.5–11 M. The internal (pipette) solution contained (in mM) 110 D-gluconic acid, 110 CsOH, 30 CsCl, 5 HEPES, 4 NaCl, 0.5 $CaCl_2$, 2 $MgCl_2$, 5 BAPTA, 2 Na-ATP, and 0.3 Na-GTP (pH 7.35), and the osmolality was adjusted to 300–310 mosmol kg−1 using CsCl or water. The external solution contained (in mM) 150 NaCl, 3 KCl, 10 HEPES, 30 D-mannitol, 0.5 $CaCl_2$, and 0.01 EDTA at pH 8.0. At the end of the experiment,

the patch was destroyed by applying pressure and the glutamate solution was diluted by 25% to determine the liquid junction potential between the electrode solution and the bath solution. Waveforms were averaged across patches and normalized to the peak response to maximally effective concentrations of

glutamate and glycine.

Homology Modeling, Molecular Dynamics, and Energy Change Calculations

[Performed in collaboration with Pieter Burger and Steven Kell (Department of Chemistry, Emory University)]

A human GluN1/GluN2A dihetero-tetrameric homology model was constructed from a glutamate/glycine-bound, exon5-lacking GluN1-1a/GluN2B crystal structure (PDBid: 4PE5, 3.96Å resolution) (Karakas et al., 2015), an exon5-containing GluN1-1b/GluN2B crystal structure in the non-active conformation (PDBid: 5FXH, 5Å resolution) (Tajima et al., 2016), and the TMD of the GluA2 crystal structure (PDBid: 5L1B, 4.0Å resolution) (Yelshanskaya et al., 2016). The alignment of the target and template sequences was performed using Multiple Sequence Comparison by Log-Expectation (MUSCLE) (Edgar, 2004). Five homology models were generated using Modeller v9.19 (Šali and Blundell, 1993) from which the lowest energy model was selected and subjected to quality analysis using the PDBsum generator (Laskowski et al., 2018). All titratable residues were assigned their dominant protonation state at pH 7.0 (Schrödinger Release 2018-4; Protein Preparation Wizard; Epik version 3.7; Impact version 7.2; Prime version 4.5, Schrödinger, LLC, New York, NY, 2017), and energy minimization was performed to relieve unfavorable interactions. Hydrogen atoms were minimalized followed by a restrained minimization using imperf (Schrödinger Release 2019-1: Schrödinger Suite 2019-1

Protein Preparation Wizard; Epik, Schrödinger, LLC, New York, NY, 2016; Impact, Schrödinger, LLC, New York, NY, 2016; Prime, Schrödinger, LLC, New York, NY, 2019.) with a convergence of the root-mean-square deviation (RMSD) of heavy atoms to 0.3Å. Using a separate copy of this wild-type model, GluN2A-Phe553 was mutated to alanine for use in a second MD simulation.

The ATD of each structure was truncated (at GluN1-Met394 and GluN2A-Leu424) to accelerate the molecular dynamics simulations. For both the wild-type GluN1/GluN2A and GluN1/GluN2A-F553A models, the optimized and truncated receptor was inserted into an equilibrated 1-palmitoyl-2-oleoyl-sn-glycerol-3-phosphocholine (POPC) lipid bilayer. Solvation of the protein structure was done using the simple point charge (SPC) water model; the orthorhombic solvation box included a 10Å buffer between the protein and periodic boundary on all 3 axes. The overall system was neutralized by the addition of 10 Na^+ ions, and the final salt (NaCl) concentration was set to 150 mM. The system was treated using the OPLS3e force field within the Desmond module of Schrodinger software package (Desmond Molecular Dynamics System, D. E. Shaw Research, New York, NY, 2017). Following the Desmond membrane protein relaxation protocol, two independent 300 ns production runs– one for each receptor (wild-type GluN1/GluN2A and GluN1/GluN2A-F553A)— were performed at a constant temperature of 310 K and pressure of 1.013 bar. Time-step calculations were performed every 2 fsec, and frames were captured every 100 psec. Analysis of the molecular dynamics trajectory was performed in Desmond and Visual Molecular Dynamics (VMD) (Humphrey et al., 1996).

For each of the two trajectories, frames were extracted from a period of 235 nanosec spanning the equilibrated portion of the simulation at 1 nanosecond intervals. These frames were clustered using the 'cluster' function within VMD with an RMSD-based distance function. The

effect on protein stability and affinity of the pre-M1 region for its surrounding contact residues upon the introduction of mutations was calculated using the BioLuminate module within the Schrödinger Biologics Suite (Schrödinger Release 2018-4: BioLuminate, Schrödinger, LLC, New York, NY, 2018).

Fitting of Structure-Based Mechanisms to Macroscopic Current Responses

We evaluated the compatibility of gating models with optimized rate constants from maximum likelihood fitting with macroscopic and synaptic current time course. We used ChanneLab to generate macroscopic waveforms by assuming glutamate binding and unbinding can only occur from GluN2 subunits that have not undergone a pre-gating step. We also added desensitized states only from receptors where both subunits within a dimer had undergone pre-gating steps (Furukawa et al., 2005; Sun et al., 2002). A model that included agonist binding was subsequently fitted simultaneously to two average macroscopic response waveforms recorded from excised outside-out patches as described above using a non-linear least squares algorithm (ChanneLab). We fixed the gating rates in the model to those determined from single channel maximum likelihood fitting and allowed the agonist association and dissociation rates in addition to rates governing entry into and exit from the desensitized states to vary (Erreger et al., 2005). We performed a sensitivity analysis by determining the sum of squares for normalized waveforms simulated with the agonist binding and desensitization rates varied over a range that encompassed the fitted values while all other rates were held constant.

Statistical Analysis

Statistical analysis was conducted using OriginPro 9 or GraphPad Prism 7. Measurements are given as mean ± SEM, with the exception of EC50 values, which are reported as mean with the 95% confidence intervals determined from the log(EC50). For glutamate and glycine potency, no overlap in confidence intervals was considered significant. For deactivation time course, data were analyzed using a one-way ANOVA with Tukey's post hoc test. Significance was set at $p < 0.05$ compared with wild-type and the number of observations was selected to give a power > 0.95 for a minimum detectable difference of 50% for weighted tau. When multiple parameters were compared from the same recording, we corrected for family-wise error.

Chapter 3: NMDA Receptor Channel Gating Control by the Pre-M1 Helix*

*Chapter 3 has been submitted to the Journal of General Physiology for publication:

McDaniel MJ., Ogden KK, Kell SK, Burger PB, Liotta D, Traynelis SF (2019) NMDA Receptor Channel Gating Control by the Pre-M1 Helix. *Journal of general physiolology* (Final Revisions)

Abstract

The NMDA receptor is an ionotropic glutamate receptor formed from the tetrameric assembly of GluN1 and GluN2 subunits. Within the flexible linker between the agonist binding domain (ABD) and the M1 helix of the pore-forming transmembrane helical bundle lies a two-turn, extracellular pre-M1 helix positioned parallel to the plasma membrane and in van der Waals contact with the M3 helix thought to constitute the channel gate. The pre-M1 helix is tethered to the bi-lobed ABD where agonist-induced conformational changes initiate activation. Additionally, it is locus for *de novo* mutations associated with neurological disorders, is near other disease-associated *de novo* sites within the transmembrane domain, and is a structural determinant of subunit-selective modulators. To investigate the role of the pre-M1 helix in channel gating, we performed scanning mutagenesis across the GluN2A pre-M1 helix and recorded whole-cell macroscopic and single channel currents from HEK cell-attached patches. We identified two residues at which mutations perturb channel open probability (P_{Open}), mean open time (MOT), and the glutamate deactivation time course. Molecular dynamics simulations suggest that one particular pre-M1 residue—Phe553— may participate in a subunit-specific network of adjacent aromatic amino acids. Based on these results, we were able to hypothesize about the role of the pre-M1 helix in other NMDAR subunits based on sequence and structure homology. Our results emphasize the role of the pre-M1 helix in channel gating, implicate the surrounding amino acid environment in this mechanism, and suggest unique subunit-specific contributions of pre-M1 helices to GluN1 and GluN2 gating.

Introduction

N-methyl-D-aspartate receptors (NMDARs) are a subfamily of ionotropic glutamate receptors whose calcium-permeable channels mediate the slow component of fast excitatory neurotransmission (Clements, 1996; Jahr and Stevens, 1993; Lester et al., 1990). These receptors, though necessary for synaptic plasticity, learning, and memory, have been implicated in the etiology of several neurological disorders, including epilepsy, intellectual disabilities, and schizophrenia (Coyle, 2006; Lemke et al., 2014; Liu et al., 2004; Olney et al., 1999; Rice and DeLorenzo, 1998; Traynelis et al., 2010; XiangWei et al., 2018; Yuan et al., 2015b). NMDARs are formed from the tetramerization of two glycine-binding GluN1 subunits and two glutamate-binding GluN2 subunits. Each subunit contains four semi-autonomous domains: the amino terminal domain (ATD), the agonist binding domain (ABD), the transmembrane domain (TMD), and the carboxy-terminal domain (CTD).

During a process referred to as gating, agonist binding to the ABD promotes channel opening within the TMD. Despite decades of work, the exact mechanisms of this process remain elusive. Crystallographic data suggests that the bi-lobed ABDs initiate activation by adopting a closed-cleft conformation due to atomic contacts between the agonist, the D1 upper lobe, and the D2 lower lobe (Armstrong and Gouaux, 2000; Furukawa et al., 2005; Inanobe et al., 2005; Jin et al., 2003; Karakas and Furukawa, 2014; Lee et al., 2014; Mayer, 2011; Sun et al., 2002; Vance et al., 2011). Although there is a lack of detailed hypotheses that relate NMDA receptor function to conformational changes or specific regions of the receptor, analysis of the gating mechanism of AMPA receptors may shed light on that of the NMDA receptor. Gating of the AMPA receptor (AMPAR) involves a “kinking” of two non-adjacent, pore-forming M3 transmembrane helices away from the central axis of the pore (Twomey and Sobolevsky, 2017; Twomey et al., 2017).

The AMPAR M3 helices contain a highly conserved amino acid sequence (SYTANLAAF), which can be found in all members of the ionotropic glutamate receptor family, including NMDARs. Finally, NMDARs exhibit similar asymmetry to the AMPA receptor in that the receptors have an overall 2-fold symmetry with pseudo 4-fold symmetry within the pore (Karakas and Furukawa, 2014; Lee et al., 2014; Tajima et al., 2016). Together, these similarities suggest that this "kinking" motion might also occur for NMDARs.

Although the mechanism of NMDAR gating remains poorly understood, it has been hypothesized that the linker tethering the ABD to the TMD is responsible for facilitating communication between these two domains (Gibb et al., 2018; Karakas and Furukawa, 2014; Lee et al., 2014; Schorge et al., 2005; Sobolevsky et al., 2009; Talukder et al., 2010; Talukder and Wollmuth, 2011). Thus far, the flexible and dynamic nature of the ABD-TMD linker has prevented a high resolution structure of this region, and the structure of the fully open receptor pore remains elusive (Tajima et al., 2016). Lower resolution analyses have revealed novel structural features within the linker that are uniquely positioned to transduce agonist binding into channel opening (Karakas and Furukawa, 2014; Lee et al., 2014; Sobolevsky et al., 2009).

Specifically, the linker between the ABD and the first transmembrane helix (M1) contains a short, two-turn pre-M1 helix that is thought to be a key contributor to the gating mechanism. The pre-M1 helix, previously described as a "cuff" helix, is hypothesized to participate in channel gating based on its orientation perpendicular to the channel pore, its position downstream of the ABD, and its van der Waals contact with the extracellular end of the M3 helical bundle (Karakas et al., 2015; Sobolevsky et al., 2009; Tajima et al., 2016). It stands to reason that agonist-induced closure of the bi-lobed ABD alters the position of the ABD-TMD linkers, leading to a reorientation of both the pre-M1 helices and the M3 helices of the GluN1

and GluN2 subunits (Furukawa and Gouaux, 2003; Furukawa et al., 2005; Hansen et al., 2013; Inanobe et al., 2005; Vance et al., 2011). In support of this hypothesis, it has been shown that cysteine substitutions within this linker region are sufficient to alter NMDAR responses, and MTS covalent modification of cysteine-substituted residues in this region altered receptor leak currents (Beck et al., 1999; Chang and Kuo, 2008; Sobolevsky et al., 2007). Therefore, if contact between the pre-M1 helix and the M3 helix is essential for stabilizing a closed channel state, then agonist-induced reorientation of the pre-M1 helix or its residue side chains may constitute a required, rate-limiting pre-gating step that must be traversed before the channel can open (Gibb et al., 2018).

The probable involvement of the pre-M1 helix in the gating mechanism is emphasized by human genetics. In a population of over 140,000 healthy individuals (gnomad.broadinstitute.org), the GluN2A and GluN2B pre-M1 helices are devoid of missense variants, suggesting strong selection against variation in this region. By contrast, the pre-M1 helices of these subunits harbor multiple *de novo* mutations in patients with epilepsy, intellectual disabilities, or developmental delays (Ogden et al., 2017; Swanger et al., 2016; XiangWei et al., 2018). Within the GluN2A and GluN2B subunits, functional analysis of these disease-associated mutations revealed changes to NMDAR kinetics, further implicating the pre-M1 helix in the gating mechanism (Gibb et al., 2018; Ogden et al., 2017).

It has been proposed that the pre-M1 helix is one-third of a triad also comprising the M3 pore-forming helix and the pre-M4 helix of the adjacent subunit (Chen et al., 2017; Gibb et al., 2018; Ogden et al., 2017). These regions all reside with ~5 Angstroms, with modelled side chains appearing close enough to touch or hydrogen bond (Chen et al., 2017; Gibb et al., 2018; Ogden et al., 2017). Moreover, two distinct triads exist in the tetrameric assembly: GluN1-pre-

M1/GluN1-M3/GluN2-pre-M4 and GluN2-pre-M1/GluN2-M3/GluN1-pre-M4. As such, there might arise structural differences in each triad as a result of the different sequences for the GluN1 or GluN2 pre-M1 and pre-M4 helices. That is, global receptor asymmetry and disparate amino acid environments may contribute to subunit specific contributions to the gating mechanism.

Functional data suggests that the GluN2A pre-M1 helix plays a larger role in gating than its GluN1 counterpart. Analysis of the GluN2A-P552R mutation showed a significant delay in receptor activation and deactivation, a finding which could not be recapitulated by the GluN1 equivalent mutation GluN1-P557R (Ogden et al., 2017). Additionally, data has shown that alanine mutations within the pre-M1 helix of the GluN2D subunit significantly alter receptor open probability (Ogden and Traynelis, 2013). Because open probability is a property of the NMDA receptor that differs greatly between GluN2A/2B and GluN2C/2D, we might expect that residues within the pre-M1 helix, specifically those that differ between the two groups, might account for these differences. As such, we explored the GluN2A pre-M1 helix for its role in gating to better understand both its mechanistic function and how this differs from that of the pre-M1 helix in other subunits. We conducted site-directed mutagenesis coupled with two-electrode voltage clamp, single channel, and whole-cell patch clamp recordings to directly monitor changes in receptor pharmacology, response time course, and microscopic properties. We also ran molecular dynamics (MD) simulations of the receptor in the presence of agonist to investigate atomic interactions between the pre-M1 helix and surrounding residues. Our results identified GluN2A-F553 as a significant contributor to receptor gating and suggest that local intra- and inter-subunit amino acid side chain interactions may be important for subunit-specific pre-M1 contributions to this mechanism.

Results

Sobolevsky et al. (2009) first proposed the idea that the pre-M1 helix could play a role in gating by acting as a cuff, based on the observation that it is in contact with the gate of the channel—the M3 helical bundle that occludes the pore in the closed state of a crystal structure of homomeric GluA2 **(Figure 3.1)**. Additionally, human *de novo* mutations are concentrated in this region (Ogden et al., 2017), suggesting that these residues play a central role in NMDAR gating that cannot be carried out by other amino acids. To assess whether the residues of the pre-M1 helix play a role in controlling kinetically distinct pre-gating steps that reflect conformational changes that precede receptor opening, we designed a set of experiments guided by both functional studies of clinically relevant human mutations and limited structural data. We performed scanning mutagenesis of six residues constituting two turns of the GluN2A pre-M1 helix in which we substituted each residue for alanine and recorded the resultant macroscopic current response time course and single channel unitary currents to identify the contributions of individual residues to overall receptor function.

Effects of Pre-M1 Mutations on Agonist Potency and Response Time Course

We expressed wild-type and mutant GluN2A subunits with the wild-type GluN1 subunit in *Xenopus* oocytes and determined the concentration-response relationship for glutamate and glycine. Of the mutants, GluN2A-F553A produced the largest effect on glutamate potency, showing a greater than 10-fold decrease in the EC_{50} from 3.5 to 0.34 μM. The other mutations tested showed minimal effects on glutamate EC_{50}, with L550A, E551A, P552A, F553Y, and A555P changing glutamate potency by 2-fold or less **(Figure 3.2A, Table 3.1)**. These results

A.

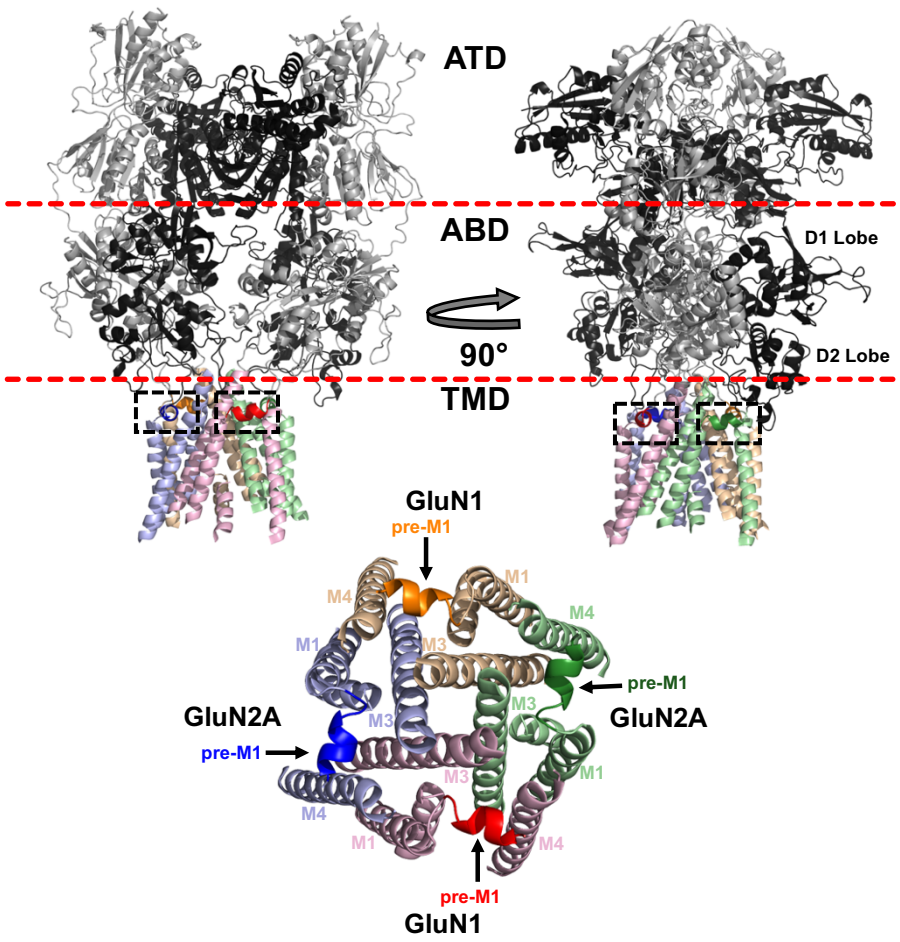

B.

	Pre-M1	M1	M3	Pre-M4
GluN1	(550) TLDSFMQPFQSTLW-LLV	(639)	FAMIISSYTANLAAF	(803) NAPATLTFENMAGVF
GluN2A	(545) SPSAFLEPFSASVWVMMF	(637)	FAVIFLASYTANLAAF	(807) VMSSQLDIDNMAGVF
GluN2B	(546) SPSAFLEPFSADVWVMMF	(638)	FAVIFLASYTANLAAF	(808) VMSSQLDIDNMAGVF
GluN2C	(543) SPSAFLEPYSPAVWVMMF	(635)	FAVIFLASYTANLAAF	(805) VMSSKLDIDNMAGVF
GluN2D	(573) SPSAFLEPYSPAVWVMMF	(665)	FAVIFLASYTANLAAF	(835) VMSSKLDIDNMAGVF

Figure 3.1: Several aromatic residues around the pre-M1 helix are largely conserved across GluN subunits

A) Homology model of a GluN1/GluN2A NMDA receptor. GluN1 subunits are shown in gray, and GluN2A subunits are shown in black. The figure highlights the pre-M1 helices (black boxes) of GluN1 (orange and red helices) and GluN2A (blue and green helices) subunits. Top-down view illustrates the pre-M1 helices forming a "cuff" around the closed channel. **B)** Sequence alignment of the pre-M1, M1, M3, and pre-M4 regions across human NMDA receptor subunits. The positions of aromatic residues of interest are shown in red. Highlighted residues designate those which were mutated in our experiments and gray boxes designate helical regions.

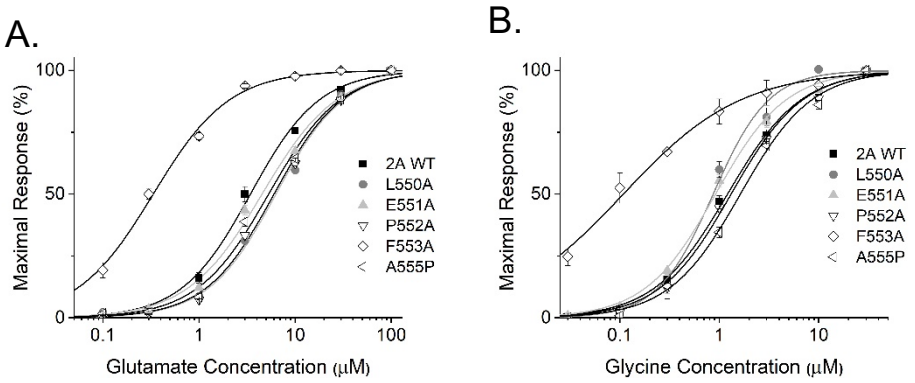

Figure 3.2: Mutations in the GluN2 pre-M1 helix shift glutamate and glycine potency
Steady-state concentration-response curves for glutamate in the presence of 100 μM glycine **(A)** and glycine in the presence of 100 μM glutamate **(B)**. The Hill equation was fitted to the composite data for GluN2A wild-type and GluN2A-L550A, GluN2A-E551A, GluN2A-P552A, GluN2A-F553A, and GluN2A-A555P expressed with wild-type GluN1. GluN2A-F553A shifted glutamate potency ~11-fold (EC_{50} from 3.6 μM to 0.34 μM) and glycine potency ~18-fold (EC_{50} from 1.4 μM to 0.077 μM). Fitted EC_{50} values for all mutants can be found in Table 2.

Table 3.1: Summary of agonist EC50 values

	Glutamate EC_{50} (μM)	N	Glycine EC_{50} (μM)	N
GluN2A WT	3.5 (2.9-4.2)	20	1.2 (0.99-1.5)	12
GluN2A-L550A	6.6 (6.0-7.3)*	17	0.84 (0.60-1.2)	11
GluN2A-E551A	4.8 (4.1-5.5)	18	0.93 (0.77-1.1)	12
GluN2A-P552A	6.4 (5.6-7.3)*	16	1.3 (1.1-1.6)	11
GluN2A-F553A	0.34 (0.30-0.38)*	19	0.12 (0.058-0.23)*	6
GluN2A-A555P	5.4 (4.7-6.1)*	18	1.6 (1.4-1.9)	11
GluN2A-F553Y	3.6 (3.1-4.1)	16	0.85 (0.68-1.1)	12
GluN2D WT	0.24 (0.20-0.30)	14	0.12 (0.091-0.15)	9
GluN2D-Y578F	0.43 (0.34-0.55)*	11	0.19 (0.14-0.25)	10

All data are from GluN1 co-expressed with GluN2A or GluN2D; the concentration response curve for each recording was fitted by the Hill equation, $Response(\%)=100/(1+(EC_{50}/concentration)^{H})$ where EC_{50} is the concentration of agonist that produces a half maximal response and *H* is the Hill slope, which remained largely unchanged among mutants (1.2 ± 0.1). Data are mean EC_{50} with the 95% confidence interval determined from the log EC_{50} given in parentheses (two significant figures). N is the number of oocytes recorded.
* Indicates non-overlapping confidence intervals between mutant and wild-type receptor

were mirrored by the findings for glycine potency, whereby GluN2A-F553A increased the glycine potency approximately 18-fold, shifting EC_{50} from 1.4 to 0.077 μM. Other pre-M1 mutations shifted potency by less than 2-fold (**Figure 3.2B, Table 3.1**). These results, where removing the aromatic side chain of Phe553 drastically alters receptor response to agonist, suggest that this residue in particular may dictate the pre-M1 helix effects on channel gating.

If a conformational change in any part of the pre-M1 helix in response to agonist binding comprises a rate limiting step that precedes pore dilation, then it might be expected that mutations in this region would alter the NMDAR activation or deactivation time course following rapid application and removal of glutamate. In order to test this idea, mutant and wild-type GluN2A subunits were co-expressed with the wild-type GluN1 subunit in HEK cells and whole-cell patch clamp recordings were conducted. HEK cells were maintained in solution with saturating glycine and response time course following brief co-application of maximally effective glutamate plus glycine was measured for each GluN2A mutant. None of the mutants tested showed a significant difference in rise time compared to the wild-type GluN2A receptor. However, analysis of the deactivation time course following 1 second application and rapid removal of glutamate revealed that GluN2A-F553A prolonged deactivation by 9- fold from 46 to 417 ms, whereas GluN2A-L550A accelerated deactivation by 3.5-fold from 46 to 13 ms. The other GluN2A mutations produced only modest effects on deactivation time course (**Figure 3.3, Table 3.2)**. Additionally, GluN2A-L550A and GluN2A-F553A drastically reduced peak amplitude, while the other mutations had no observable effect.

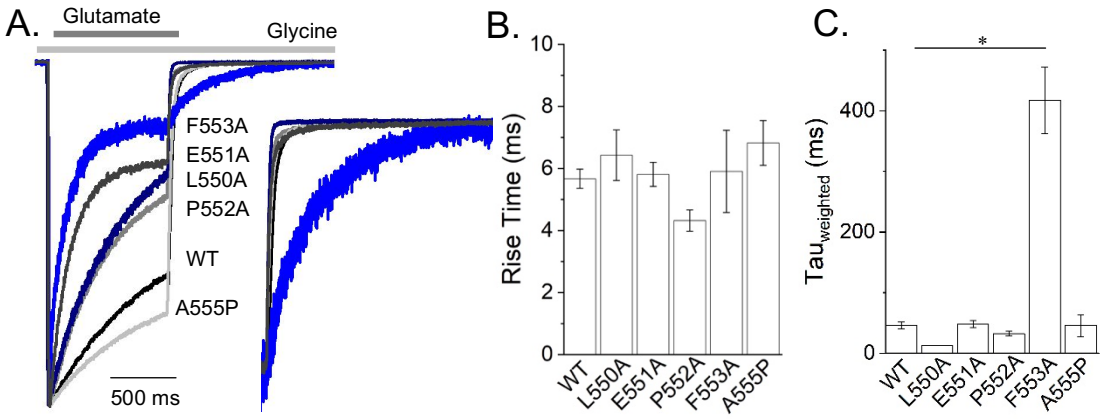

Figure 3.3: GluN2A-F553A significantly prolongs the glutamate deactivation time course
A) Representative current response time course from whole-cell patch clamp recordings of wild-type and mutant GluN2A-containing receptors activated by a 1 second pulse of 1 mM glutamate in the continuous presence of 30 µM glycine. The response time courses are normalized to the peak current levels to allow comparison of the desensitization time course. Inset shows current time course normalized to steady state level on the same time base to allow comparison of the deactivation time course. **B, C)** Average 10-90% rise times (B) and average weighted τ values (C) for wild-type and mutant GluN1/GluN2A receptors. Rise times did not differ significantly for any of the mutant subunits when compared to wild-type GluN2A. GluN2A-F553A prolonged deactivation by approximately 9-fold from 46 ms to 417 ms. Significant difference from wild-type denoted by an asterisk ($p < 0.05$ compared with WT 2A, one-way ANOVA, Tukey *post hoc*). A summary of fitted values can be found in Table 3.2.

Table 3.2: Summary of deactivation time course for GluN2A mutations

	Rise Time (ms)	Tau Fast (ms)	Tau Slow (ms)	% Tau Fast	$Tau_{weighted}$ (ms)	% Desens	Amplitude (peak, pA/pF)	N
GluN2A WT	5.7 ± 0.3	24 ± 2	180 ± 22	84 ± 3	46 ± 6	54 ± 5	190 ± 22	25
GluN2A-L550A	6.4 ± 0.8	11 ± 0.7	66 ± 24	93 ± 3	13 ± 0.4	30 ± 3	28 ± 2.6	12
GluN2A-E551A	5.8 ± 0.4	26 ± 3	220 ± 34	86 ± 3	48 ± 6	54 ± 5	220 ± 52	16
GluN2A-P552A	4.3 ± 0.3	16 ± 2	170 ± 15	87 ± 4	32 ± 4	31 ± 5	160 ± 14	12
GluN2A-F553A	5.9 ± 1	64 ± 16	790 ± 160	43 ± 6	420 ± 55 *	18 ± 2	12 ± 1.5	9
GluN2A-A555P	6.8 ± 0.7	24 ± 2	190 ± 18	87 ± 4	46 ± 18	74 ± 7	170 ± 24	13
GluN2A-F553Y	5.5 ± 0.7	25 ± 2	230 ± 75	94 ± 2	37 ± 6	64 ± 5	79 ± 11	12

All data are from GluN1 co-expressed with GluN2A. Data are mean ± SEM and given to two significant figures.
* $p<0.05$ compared with WT GluN2A, one-way ANOVA, Tukey *post hoc.* Analysis performed on rise time and weighted τ, and corrected for familywise error.

Pre-M1 Mutations Alter NMDA Receptor Single Channel Properties

In order to assess the effects of pre-M1 mutations on channel properties, we recorded single ion channel currents in response to maximally effective concentrations of glutamate and glycine from cell-attached patches that contained one active channel (Colquhoun and Hawkes, 1990). Alanine substitutions at several positions caused a wide range of changes in the duration of prolonged shut periods, suggesting an impact on channel gating **(Figure 3.4A-F, Table 3.3)**. Single channel activity was idealized into a sequence of openings and closings. The shut time histogram was fitted using the sum of 4 or 5 exponential components, and the slowest components used to identify a T_{crit} with which we could differentiate bursts from long closed states likely to reflect desensitization. This approach allowed for a more accurate interpretation of burst channel data without the potential for confounding results arising from mutation-specific effects on desensitization. When selecting bursts of channel openings based on a critical shut time (Jackson et al., 1983; Magleby and Pallotta, 1983) most of the alanine-substituted channels showed intra-burst open probabilities that were similar to wild type GluN2A. By contrast, GluN2A-L550A and GluN2A-F553A, which reside on the same side of the helix, decreased open probability nearly 10-fold. Evaluation of mean open time for each mutation revealed that GluN2A-L550A and GluN2A-F553A reduced mean open time from 1.49 ms for the wild-type GluN2A receptor to 0.53 ms and 0.20 ms, respectively. Evaluation of mean shut times (MST) showed that both GluN2A-L550A and GluN2A-F553A increased mean shut time, with GluN2A-L550A producing the largest shift from 29 ms to 900 ms. These results suggest that multiple residues on one side of the short pre-M1 helix impact channel gating and implicate this region as critical for the gating control mechanism.

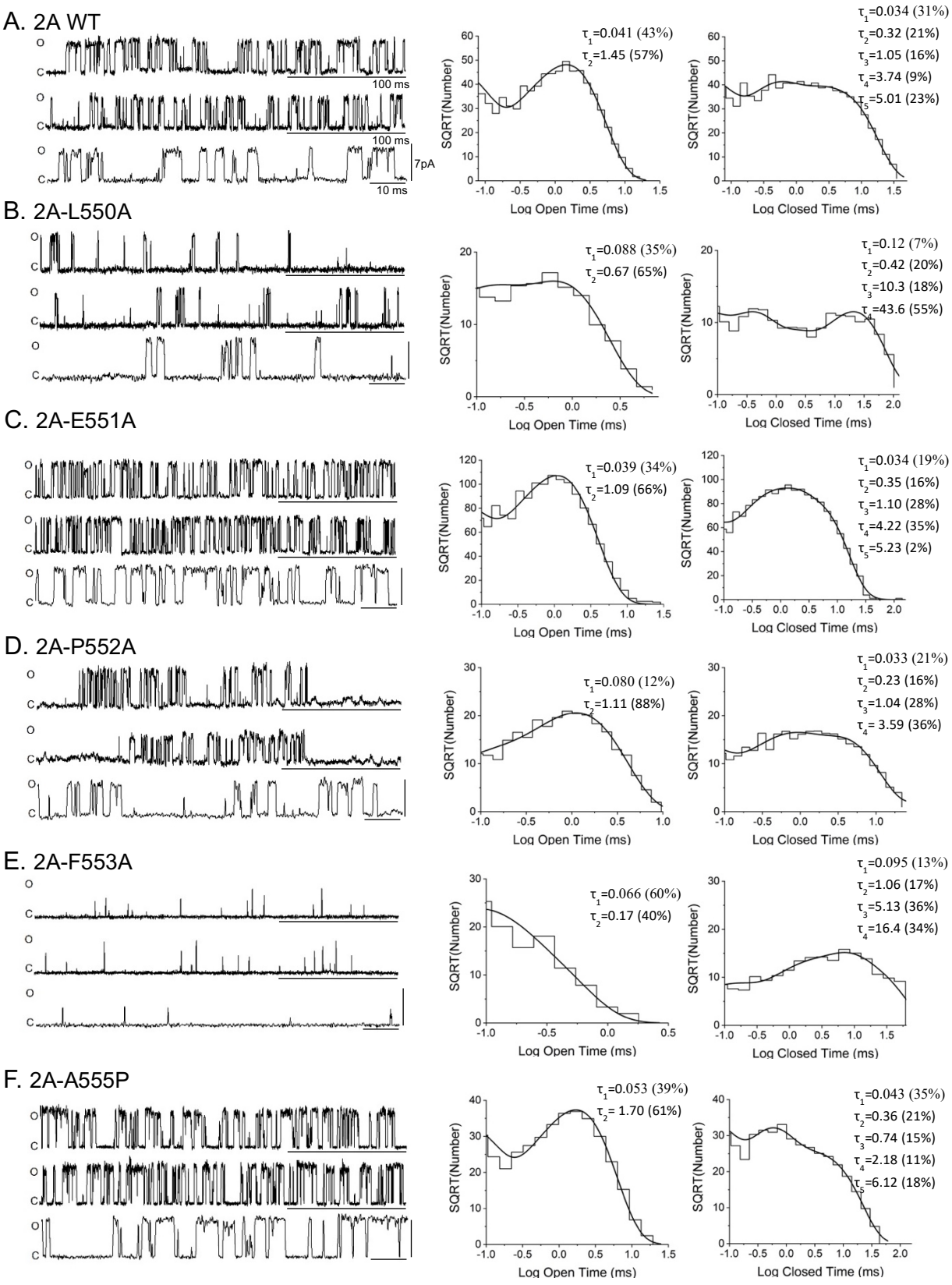
A. 2A WT
100 ms
100 ms
7pA
10 ms
τ1=0.041 (43%)
τ2=1.45 (57%)
τ1=0.034 (31%)
τ2=0.32 (21%)
τ3=1.05 (16%)
τ4=3.74 (9%)
τ5=5.01 (23%)
SQRT(Number)
Log Open Time (ms)
Log Closed Time (ms)
B. 2A-L550A
τ1=0.088 (35%)
τ2=0.67 (65%)
τ1=0.12 (7%)
τ2=0.42 (20%)
τ3=10.3 (18%)
τ4=43.6 (55%)
C. 2A-E551A
τ1=0.039 (34%)
τ2=1.09 (66%)
τ1=0.034 (19%)
τ2=0.35 (16%)
τ3=1.10 (28%)
τ4=4.22 (35%)
τ5=5.23 (2%)
D. 2A-P552A
τ1=0.080 (12%)
τ2=1.11 (88%)
τ1=0.033 (21%)
τ2=0.23 (16%)
τ3=1.04 (28%)
τ4= 3.59 (36%)
E. 2A-F553A
τ1=0.066 (60%)
τ2=0.17 (40%)
τ1=0.095 (13%)
τ2=1.06 (17%)
τ3=5.13 (36%)
τ4=16.4 (34%)
F. 2A-A555P
τ1=0.053 (39%)
τ2= 1.70 (61%)
τ1=0.043 (35%)
τ2=0.36 (21%)
τ3=0.74 (15%)
τ4=2.18 (11%)
τ5=6.12 (18%)

Figure 3.4: GluN2A-L550A and GluN2A-F553A significantly alter single channel properties
A-F) Representative single channel unitary currents from cell-attached patches that contained one active wild-type or mutant GluN1/GluN2A NMDAR activated by 1 mM glutamate and 50 μM glycine. All currents are displayed on the same scale. Representative histograms are shown on a square root-log scale; open time histograms were fitted (maximum likelihood) with two exponential functions and shut time histograms were fitted with four or five exponential functions. Single channels were recorded by Kevin Ogden.

Table 3.3: Summary of single channel data for GluN2A mutations

	Events	Burst P_{open}	Burst Mean Open Time (ms)	Burst Mean Shut Time (ms)	Shut Time Tcrit (ms)	N
GluN2A WT	315,130	0.34 ± 0.008	1.5 ± 0.1	2.9 ± 0.2	31 ± 2	6
GluN2A-L550A	6,519	0.033 ± 0.006*	0.66 ± 0.05*	22 ± 3	155 ± 13	7
GluN2A-E551A	307,463	0.38 ± 0.04	1.3 ± 0.1	2.3 ±0.3	24 ± 2	3
GluN2A-P552A	17,623	0.34 ± 0.02	1.3 ± 0.06	2.5 ± 0.2	25 ± 3	7
GluN2A-F553A	3,484	0.020 ± 0.005*	0.21 ± 0.007*	12 ± 3	59 ± 6	3
GluN2A-A555P	74,905	0.39 ± 0.06	1.7 ± 0.1	2.8 ± 0.5	38 ± 9	3
GluN2A-F553Y	67,723	0.23 ± 0.02*	1.4 ± 0.15	4.6 ± 0.07	48 ± 5	3

All data are from GluN1 co-expressed with GluN2A. Data expressed as mean ± SEM and given to two significant figures.
*$p<0.05$ compared with WT GluN2A, one-way ANOVA, Tukey *post hoc*, corrected for family-wise error for P_{open} and Burst Mean Open Time.

Table 3.4: Open dwell time analysis for GluN2A mutations

	Tau_1 (ms)	$Area_1$ (%)	Tau_2 (ms)	$Area_2$ (%)	N
GluN2A WT	0.053 ± 0.005	41 ± 4	1.6 ± 0.14	59 ± 4	6
GluN2A-L550A	0.081 ± 0.015	47 ± 4	0.68 ± 0.060	53 ± 5	6
GluN2A-E551A	0.045 ± 0.003	26 ± 5	1.3 ± 0.11	75 ± 5	3
GluN2A-P552A	0.059 ± 0.007	29 ± 5	1.2 ± 0.042	72 ± 5	6
GluN2A-F553A	0.050 ± 0.009	58 ± 3	0.16 ± 0.007	42 ± 3	3
GluN2A-A555P	0.053 ± 0.006	35 ± 8	1.6 ± 0.080	65 ± 8	3
GluN2A-F553Y	0.048 ± 0.007	52 ± 3	1.5 ± 0.23	48 ± 3	3

Open time distributions were fitted (maximum likelihood) by two exponential components. Fitted parameters are expressed as mean ± SEM and given to two significant figures. N is the number of patches.

Table 3.5: Closed dwell time analysis for GluN2A mutations

	Tau_1 (ms)	$Area_1$ (%)	Tau_2 (ms)	$Area_2$ (%)	Tau_3 (ms)	$Area_3$ (%)	Tau_4 (ms)	$Area_4$ (%)	Tau_5 (ms)	$Area_5$ (%)	N
GluN2A WT	0.037 ± 0.002	27 ± 2	0.31 ± 0.029	20 ± 1	1.1 ± 0.18	17 ± 12	2.3 ± 0.32	8 ± 3	5.1 ± 0.22	28 ± 2	6
GluN2A-L550A	0.088 ± 0.012	21 ± 3	–	–	0.70 ± 0.21	18 ± 2	9.5 ± 1.6	19 ± 5	36 ± 3.7	41 ± 5	7
GluN2A-E551A	0.035 ± 0.0002	21 ± 2	0.33 ± 0.010	15 ± 1	1.1 ± 0.033	31 ± 5	3.8 ± 0.31	22 ± 8	4.2 ± 0.58	11 ± 5	3
GluN2A-P552A	0.041 ± 0.004	25 ± 4	0.36 ± 0.071	22 ± 3	1.4 ± 0.18	24 ± 9	4.7 ± 0.33	29 ± 4	–	–	6
GluN2A-F553A	0.058 ± 0.018	11 ± 1	–	–	1.1 ± 0.054	16 ± 2	7.5 ± 2.6	36 ± 5	14 ± 1.8	37 ± 7	3
GluN2A-A555P	0.049 ± 0.007	27 ± 4	0.54 ± 0.16	25 ± 2	1.1 ± 0.26	21 ± 8	3.8 ± 0.86	20 ± 8	9.6 ± 3.4	11 ± 7	3
GluN2A-F553Y	0.034 ± 0.0003	31 ± 4	0.30 ± 0.021	17 ± 1	2.5 ± 0.67	13 ± 3	5.4 ± 1.2	5 ± 1	12 ± 4.7	16 ± 9	3

Closed time distributions were fitted (maximum likelihood) by 4-5 exponential components. Fitted parameters are expressed as mean ± SEM and given to two significant figures. N is the number of patches.

The Pre-M1 Helix Imparts Distinguishing Properties to GluN2C and GluN2D

While several residues of the pre-M1 helix are highly conserved across GluN2 subunits, the phenylalanine residue in position 553 is conserved in GluN1, GluN2A, and GluN2B, but corresponds to a tyrosine in GluN2C and GluN2D. Because the aromaticity of the phenylalanine in this position appears to be critical for receptor function, and this residue is the only difference between these subunits in this region, we questioned whether it could be responsible for their differences in open probability. To address this, we recorded single channel currents from GluN2A-F553Y, the GluN2C/D equivalent residue of GluN2A-Phe553 (Dravid et al., 2008; Vance et al., 2012). The GluN2A-F553Y receptors showed a slight reduction in glycine EC_{50} but showed no detectable difference from wild-type for glutamate EC_{50} (**Figure 3.5A-B**) or receptor response time course (**Figure 3.5C**) during brief application of a maximally effective concentration of glutamate in saturating glycine. Single channel analysis of GluN2A-F553Y revealed a 30% decrease in open probability compared to GluN2A wild-type (**Figure 3.5D, Table 3.3**), suggesting that the tyrosine at this pre-M1 site in GluN2C and GluN2D could contribute to the lower open probability of GluN2C- and GluN2D-containing receptors, perhaps through potential hydrogen bond capability of tyrosine compared to phenylalanine.

MTSEA modification of GluN1-A652C has been shown to lock NMDARs in an open state. Based on the assumption that open probability approaches 1 following covalent modification, we used the reciprocal relationship between the degree of potentiation and open probability to calculate the open probability (See Methods). Introduction of the GluN2A-F553Y mutation was shown to significantly reduce the open probability 55% from 0.22 to 0.12 (**Table 3.6**). To support our hypothesis that this specific residue could account for differences in open probability between GluN2A and GluN2D receptors, we measured the changes in agonist

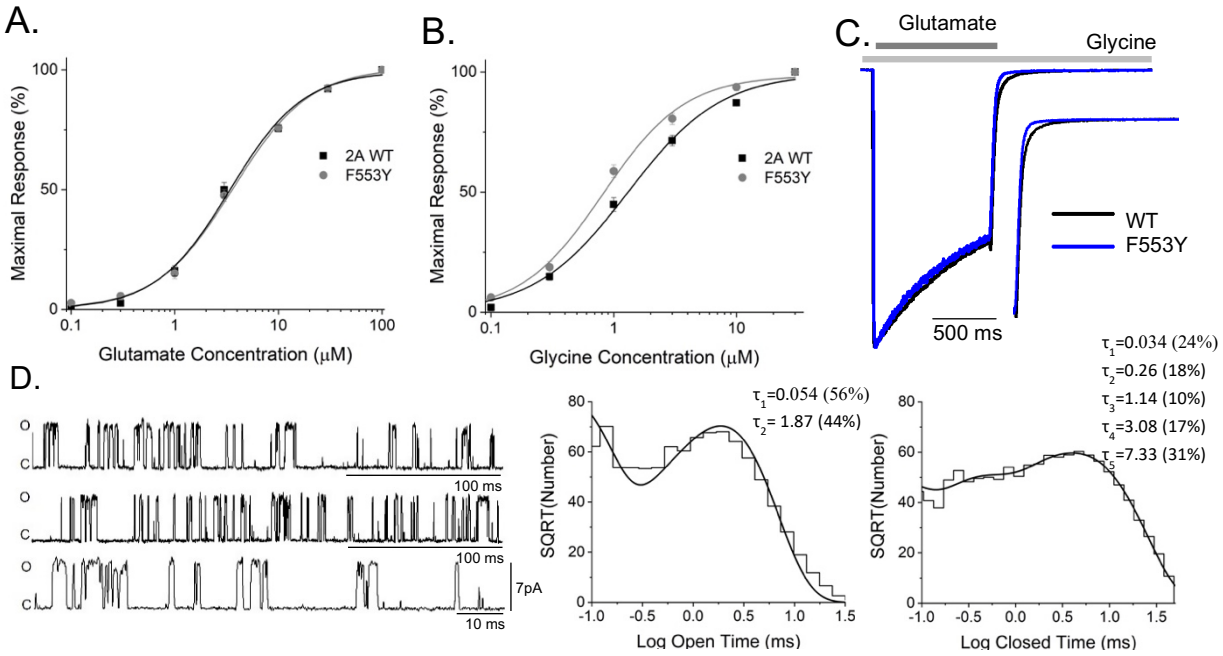

Figure 3.5: Substitution of GluN2A Phe553 with Tyr reduces the open probability
A and B) Steady-state concentration-response curves for glutamate in the presence of 100 μM glycine (A) and glycine in the presence of 100 μM glutamate (B) for wild-type GluN2A and GluN2A-F553Y. **C)** Representative current responses from whole-cell patch clamp recordings of wild-type GluN2A and GluN2A-F553Y activated by a 1 second pulse of 1 mM glutamate in the continued presence of 30 μM glycine. Inset shows current response time course normalized to steady state to show deactivation. **D)** Representative single channel unitary currents recorded from cell-attached patches containing one active GluN1/GluN2A-F553Y receptor activated by 1 mM glutamate and 50 μM glycine. Representative histograms for the open time are shown on a log-square root scale and were fitted (maximum likelihood) with two exponential functions; shut time histograms were fitted with five exponential functions. Single channels were recorded by Kevin Ogden.

Table 3.6: Oocyte MTSEA calculated open probability

	Calculated P_{open}	N
GluN2A WT	0.22 ± 0.007	8
GluN2A-F553Y	0.12 ± 0.008*	10
GluN2D WT	0.0055 ± 0.0007	12
GluN2D-Y578F	0.0086 ± 0.0005*	12

All data are from GluN1 co-expressed with GluN2A or GluN2D. Open probability was calculated according to the equation given in the methods. N is the number of oocytes recorded. Value are reported as mean ± SEM.
* $p<0.05$ compared with WT, unpaired t-test.

potency and open probability of GluN2D-Y578F, the reciprocal substitution to GluN2A-F553Y. Both glutamate and glycine potency were reduced for the mutant receptor with glutamate EC_{50} shifting from 0.24 to 0.43 μM and glycine EC_{50} shifting from 0.12 to 0.19 μM (**Table 3.1**). Additionally, GluN2D-Y578F increased the open probability 33% from 0.0055 to 0.0086 (**Table 3.6**). Together, these results support our hypothesis that the disparate residue identity at this position between GluN2A/GluN2B and GluN2C/GluN2D contributes in part to the difference in open probability between these subunits.

Subunit-Specific Pre-M1 Helix Interactions

A homology model of a GluN1/GluN2A diheteromeric structure was used to interpret the results presented thus far. Recently, several GluN1/GluN2A structures were resolved using X-ray and cryo-EM techniques (Jalali-Yazdi et al., 2018; Zhang et al., 2018), however none of these structures were available at the start of this study and were therefore not included. Three template structures were used in modeling of the GluN1a/GluN2A NMDA receptor. Two of the templates were that of the closely related GluN1/GluN2B NMDAR— PDB entries 4PE5 and 5FXH. PDB entry 4PE5 is an X-ray structure resolved at resolution of 3.96Å and was selected because it has a well-resolved ABD and ATD. However, there are two limitations of this structure: 1) the linker region between ABD and the TMD is not resolved and, 2) the TMD region only has the backbone residues resolved with no density for the side chains. The second template, PDB entry 5FXH a cryo-EM structure resolved at 5Å, was selected because it has a resolved linker region between the ABD and TMD. This template is
limited in that only the backbone residues are resolved, but it allowed us to build in the linker region. The third template used, an X-ray PDB entry 5L1B (resolution 4.0Å) is an AMPA receptor structure from which the ATD and ABD were removed in the model building process.

This template was selected to build in missing residues of GluN2B structures in the TMD. The TMDs of GluN1/GluN2B and AMPA show a 3.5Å RMSD when aligned on the backbone structures and shares a 30.3% (GluN1) and 27.6% (GluN2) sequence identity within this region. The GluN1 template structures share 92.2 and 94.5% sequence identity with GluN1a target sequence used to build the GluN1a/GluN2A. The GluN2B template structures share a 64.0 and 69.1% sequence identity with the GluN2A target structure used in model generation.

The five homology models had molpdf values ranging from 88770 – 89802 from which the lowest relative energy model was selected for further analysis. This selected model showed a G-factor of -0.06 (values below -0.5 are unusual) suggesting a good overall stereochemistry of the model. The Ramachandran plot showed 90.0% of the residues in the most favored regions, 8.6% in additional allowed areas, 0.9% in generously allowed regions and 0.5% in disallowed regions (total of 3200 amino acids). These results give us confidence in the quality of the model generated in this study. Finally, we measured the backbone RMSD of the GluN2A model lacking the ATD from a newly released cryo-EM structure (6IRA) (Zhang et al., 2018), which gave a value of 3.7Å (across ~4700 atoms) when aligned on the entire model and had a range between 2.5 and 2.9Å (across ~1500 atoms) when aligned on each chain independently.

The results presented thus far suggest that the aromaticity of the amino acid residue at position 553 of GluN2A is critical for normal function of GluN2A-containing NMDARs. In order to explore the mechanism by which this side chain contributes to channel gating, we performed molecular dynamics simulations over a 300 ns time scale to allow residues in the model to relax to a steady-state position. Analysis revealed a complex network of aromatic residues that were coordinated around GluN2A-Phe553 and included residues Phe810 of the GluN1 pre-M4 linker, Phe641 and Tyr645 of the GluN2A M3 transmembrane helix, and Trp558

of the GluN2A M1 transmembrane helix **(Figure 3.6B)**. The simulation places Phe553 near the middle of this aromatic network within a range permissible to both edge-to-face and face-to-face pi-pi stacking. Specifically, our simulation showed that the centroids between the aromatic rings of GluN2A-Phe553 is a mean distance of 6.2, 6.5, 5.1, and 5.7 Å from GluN1-Phe810, GluN2A-Phe641, GluN2A-Tyr645, and GluN2A-Trp558, respectively. In addition, GluN1-Phe641 is within 5.9 Å of GluN2A-Phe637, which is about 6.3 Å from GluN1-Phe817**.** All of these reported distances are shorter than the "strict" pi-pi interaction distance of 6.5 Å for large biomolecules derived from a survey of the entire Protein Data Bank (Piovesan et al., 2016).

To explore how this aromatic network might be disrupted upon substitution of GluN2A-Phe553 with alanine, we repeated the 300 ns molecular dynamics simulation with the introduction of this single mutation (**Figure 3.6D**). Without the presence of the phenylalanine aromatic side chain at position 553, GluN2A-Tyr645 and GluN1-Phe810 reorient away from this central residue, thereby interfering with communication of the pre-M1 helix with both the M3 helix and the adjacent GluN1 subunit. This finding supports the electrophysiological data in that the receptor's ability to open or close is altered if interactions between the ABD-tethered pre-M1 helix and the channel pore are disrupted.

Many of these aromatic residues are conserved across NMDAR subunits (**Figure 1B**) implying that the interactions between these residues is similarly conserved. However, the GluN1 pre-M1 helix appears to participate in gating in a manner distinct from that of GluN2A, as suggested by results showing that mutations in the GluN1 pre-M1 helix do not slow receptor activation, while their GluN2 counterparts do (Gibb et al., 2018; Ogden et al., 2017). We therefore investigated the amino acid environment surrounding the GluN1-Phe558 residue (**Figure 3.6C**). We found that GluN1-Phe558 is within 4.2, 4.8, and 3.5 Å of GluN1-Tyr647,

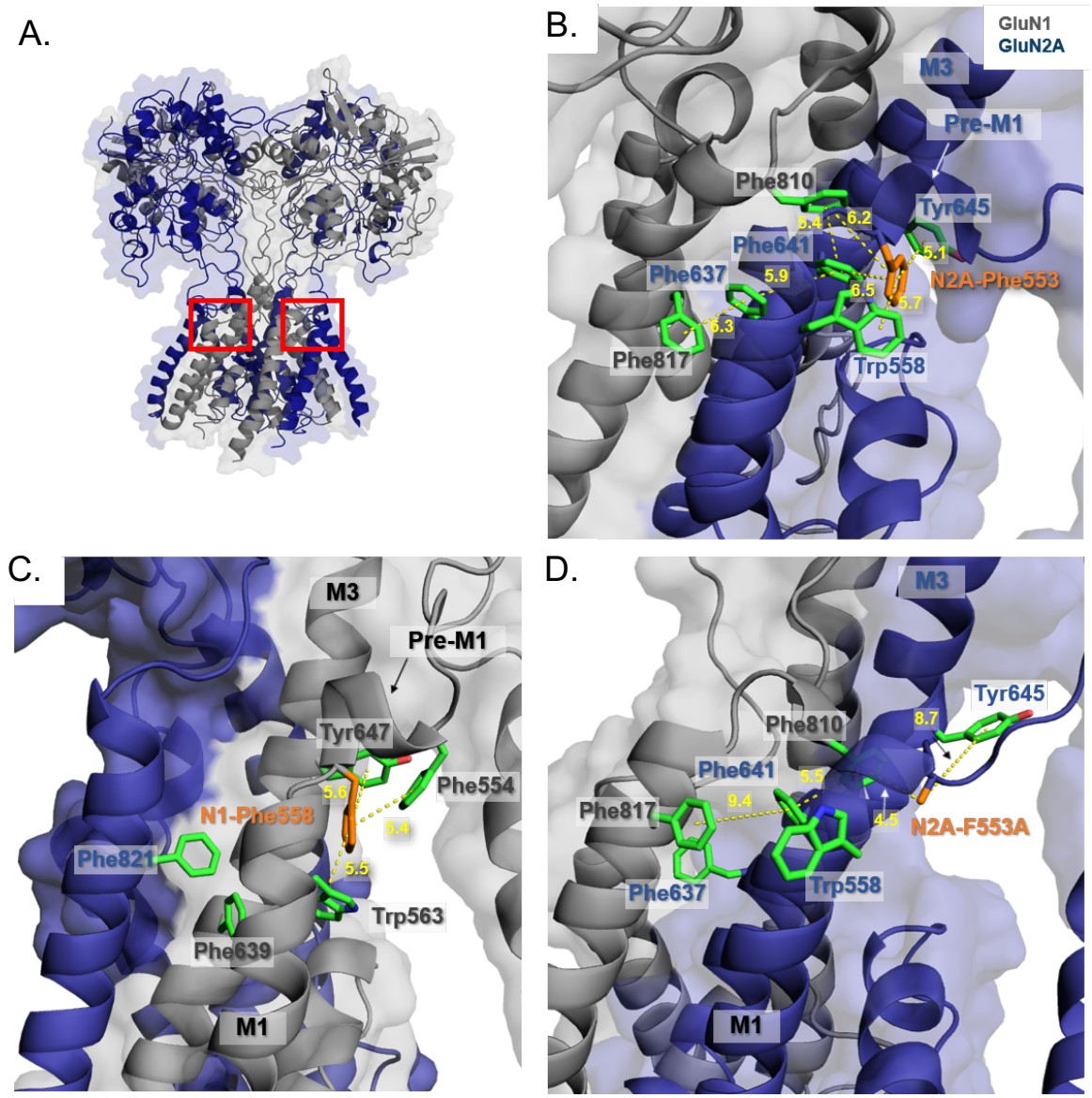

Figure 3.6: A network of aromatic residues around GluN2A-Phe553 and GluN1-Phe558
A) Homology model used for the simulations with the ATD truncated. **B**) A pose of GluN2A (blue) and GluN1 (gray) at the 152 ns time point in the MD simulation showing seven potential interactions among aromatic residues including GluN2A-Phe553; all interactions are within the range of favorable distances for π-π interactions (Piovesan et al., 2016). **C**) Wild-type GluN1 at the 152 ns time point showing a less extensive network of aromatic residues surrounding GluN1-Phe558. **D**) GluN1/GluN2A-F553A at the 155 ns time point showing that this mutation disrupts the aromatic network found in the wild-type receptor; note that the M3 helix has turned, displacing N2A-F637 and N2A-641 from their positions seen in the WT simulation. All time points shown represent the centroid structure from the largest cluster of frames over an equilibrated 235ns period for the GluN2A WT and GluN2A-F553A simulations (see Methods). Yellow dashed lines represent the average distance (in Ångstroms) between the centers of aromatic rings across this same 235ns period.

GluN1-Phe554, and GluN1-Trp563, respectively. GluN1-Tyr647 corresponds to GluN2A-Tyr645 and GluN1-Trp563 corresponds to GluN2A-Trp558. The additional residue interacting with GluN1-Phe558 is GluN1-Phe-554, another conserved aromatic residue that, although present at an analogous position in GluN2A, does not appear to participate in the aromatic network surrounding GluN2A-Phe553 based on these simulations. Additionally, the GluN1 equivalent of GluN2-Phe651 and the GluN2 equivalent of GluN1-Phe810 are both replaced by isoleucine, which are incapable of participating in the aromatic network. Comparison of the set of GluN1-Phe558 and GluN2A-Phe553 aromatic interactions might explain why disease-associated mutations in GluN2A do not have the same functional consequences when expressed in GluN1(Gibb et al., 2018; Ogden et al., 2017). Because the aromatic network that potentially dictates channel gating is less extensive in GluN1 pre-M1 helix, mutations in this region might have reduced functional consequences.

To better understand the changes in the macroscopic and single channel properties of the receptors upon the introduction of specific mutations, we used a physics-based approach to calculate the change in protein stability and the affinity between specific mutations of the GluN2A pre-M1 and the interacting residues from both the GluN2A and GluN1 subunits. This method is part of the BioLuminate package and has previously been used to study antibody modeling, protein-protein binding, protein stabilization, and enzyme design (Beard et al., 2013; Guo et al., 2010; Sirin et al., 2014). Changes in protein
stability can be calculated from a thermodynamic cycle by looking at the change in energy between the folded and unfolded state. The change in affinity is calculated similarly by determining the difference in energy of the wild-type and mutant to its binding partner or interacting residues. Our calculations use equilibrated structures captured during a molecular

dynamics simulation and give us the most realistic insight into the effects of the mutations on the channel properties, given the available structural data. Introducing the GluN2A-F553A mutation reduced protein stability (15.2 kcal/mol) and affinity (5.94 kcal/mol) of the pre-M1 region and its interacting residues. The introduction of the GluN2A-L550A mutation decreases the protein stability (29.76 kcal/mol) but showed an increase in affinity (-10.46 kcal/mol).

Discussion

In this study, we investigated the role of the GluN2A pre-M1 helix in channel gating. We found the GluN2A residue Phe553 to be particularly critical for channel function as indicated by significant changes to both macroscopic and single channel properties. Moreover, we used molecular dynamics simulations to probe the mechanism by which this residue might contribute to gating. Our analysis revealed a network of aromatic amino acids within pi-stacking range surrounding GluN2A-Phe553 that was disrupted by alanine substitution at this position.

Specifically, we conducted scanning mutagenesis of the pre-M1 helix to investigate the effects on various receptor properties. Of the mutants tested, GluN2A-F553A presented the greatest effect on glutamate and glycine EC_{50}, showing an ~11-fold and an ~18-fold increase in potency, respectively. That is, GluN2A-F553A shifted the potency of both NMDAR agonists, despite only being introduced to the GluN2A subunit. In addition, GluN2A-F553A prolonged the weighted deactivation time course by ~9-fold, reduced peak amplitude by ~16-fold, decreased open probability ~10-fold, and reduced mean open time by ~7-fold. GluN2A-L550A, situated on the same side of the pre-M1 helix as GluN2A-Phe553, also altered single channel properties, decreasing open probability by ~10-fold, increasing mean open time by ~3-fold, and increasing mean closed time by ~30-fold. Together, these results suggest that these two amino acids in

GluN2A (Leu550 and Phe553) control channel gating in a manner that is likely dependent upon their structural contacts with residues adjacent to their side of the pre-M1 helix. Additionally, these results may also provide mechanistic context for the previously characterized disease-associated mutations—GluN1-P557R, GluN2A-P552R, and GluN2B-P553L— in this region (Ogden et al., 2017).

GluN2A-Phe553 has previously been investigated for its role in desensitization. In AMPA receptors, a leucine resides at this position, perhaps suggesting that the amino acid at this position contributes to the differences in desensitization between these two families of ionotropic glutamate receptors. When GluN1-Phe558—the equivalent of GluN2A-Phe553— was substituted with leucine and expressed with wild-type GluN2A, the receptor retained its GluN2A-like desensitization phenotype. However, when GluN2A-F553L or GluN2B-F554L was expressed with wild-type GluN1, the desensitization resembled that of the AMPA receptor (Alsaloum et al., 2016). It was proposed, therefore, that the mechanism of desensitization in NMDARs differs from that of AMPARs as a result of differences between the composition of a hydrophobic box made up of aromatic residues within pre-M1 and M3. While this finding emphasizes the importance of receptor-specific hydrophobic boxes in functional divergence between the ionotropic glutamate receptors, it does not address the functional differences between GluN1 and GluN2 subunits suggested by the finding that the homologous F553L mutation in GluN1 was not sufficient to alter desensitization.

Interestingly, when GluN2A-Phe553 was substituted with tyrosine, the GluN2C and GluN2D amino acid equivalent, we found no measurable effect on desensitization as previously reported (Alsaloum et al., 2016; Krupp et al., 1998), suggesting that the pre-M1 segment cannot account for differences in desensitization between different GluN2 subunits. Our results show

that, while GluN2A-F553Y had no significant effect on macroscopic properties, this mutation significantly reduced open probability, consistent with the reduced open probability of GluN2C- and GluN2D-containing receptors. We found that GluN2D-Y578F reduced glutamate potency, reduced glycine potency, and increased open probability as determined by MTSEA relative to the wild-type GluN2D receptor. These findings suggest that, in addition to being critical for the gating mechanism, the identity of the residue at position 553 can impart subunit-specific single channel properties to the receptor. The hydroxyl group of the tyrosine in this position for GluN2C and 2D receptors may introduce a hydrogen bond that is absent from GluN2A and GluN2B receptors. One possibility for such a hydrogen bond interaction, as predicted from sidechain positions in the MD simulations, could be between the hydroxyl group of the tyrosine at this site in the pre-M1 and the tyrosine of the SYTANLAAF motif (Y645 in GluN2A, Figure 3.6B). Additionally, the GluN2A-Ala555 residue is also not conserved across the NMDA subunits. In GluN2C and GluN2D, the residue in this position is a proline, as tested in our experiments. However, as our data show, the GluN2A-A555P mutation was not sufficient on its own to produce significant changes to macroscopic or single channel properties of the receptor, suggesting that pre-M1 control of single channel properties is specific to the residue at position 553.

The side of the helix that harbors GluN2A-Leu550 and GluN2A-Phe553 appears to be oriented toward the SYTANLAAF conserved helical bundle and the pre-M4 helix of the adjacent subunit (Chen et al., 2017). That is, the residues that were of consequence during our scanning mutagenesis study are positioned toward the triad that has been proposed to control channel gating (Gibb et al., 2018). Our findings, taken with the results from Alsaloum et al., suggest that the phenylalanine of the pre-M1 helix, despite being critical for channel gating and

desensitization, differs in function among GluN subunits, likely as a result of differences in local residues with which this region can interact.

We used molecular dynamics to explore the hydrophobic network in the context of pre-M1 scanning mutagenesis to identify potential roles for pre-M1 that could account for differences in gating control between GluN1 and GluN2. Using a GluN2A homology model built from a GluN2B crystal and cryo-EM structures as well as the TMD of a closed AMPA structure, we examined the amino acid environment surrounding the pre-M1 helix. Within the GluN2A subunit, Phe553 is surrounded by a network of aromatic amino acids comprised of GluN2A-Phe641 and GluN2A-Tyr645 of the GluN2A M3 helix, and GluN2A-Trp558 of the GluN2A M1 helix, and GluN1-Phe810 of the neighboring GluN1 pre-M4 helix. When we repeated the simulation with an alanine substituted at the position of GluN2A-Phe553, we saw that GluN2A-Tyr645 and GluN2A-Trp558 are oriented away from the aromatic cluster at distances that do not permit even weak side-chain interactions. This supports the hypothesis that the aromatic network is critical for channel function and disruption of this network can perturb channel function. Finally, comparison of the GluN1 aromatic network with that observed for GluN2A revealed a reduction in the number of interacting residues in GluN1, suggesting that the network plays a unique role in the GluN2A subunit.

Lending credibility to the notion that this aromatic amino acid network is facilitating gating in the NMDA receptor are several previous findings which identify some of the residues within contacting distance to GluN2A-Phe553 also influence channel function and gating. Firstly, the disease-associated mutation GluN2A-W558S was identified in a patient with epilepsy (ClinVar, https://www.ncbi.nlm.nih.gov/clinvar). Within the M3 helix, GluN2A-Phe637 has been shown to influence agonist potency and channel gating (Ren et al., 2007) and GluN1-

Y647S has been identified in a patient with infantile spasms (Allen et al., 2013). In the M4 helix, GluN1-F817L has been identified in a patient with intellectual disability, developmental delay, and movement disorder (Lemke et al., 2016; Zhu and Paoletti, 2015). Although these disease-associated mutations have not been functionally characterized, their potential role in these neurological disorders suggest that they likely disrupt normal NMDAR function.

In 2018, 23 full-length structures of the GluN2A receptor were resolved (4.5-16.5Å) using cryo-electron microscopy, none of which had resolution covering the complete transmembrane and linker regions (Jalali-Yazdi et al., 2018; Zhang et al., 2018). Some structures showed resolution within the pre-M1 helix region; however, they showed high B-factor values (358-515). When we compared the two GluN2A chains, Phe553 and Leu550 had different positions on the chains (B and D) suggesting uncertainty within the structures and we therefore opted to use homology models and not the cryo-EM GluN2A structures for calculations. Future studies however could benefit from incorporating the cryo-EM GluN2A structures in conjunction with AMPAR structures as templates to build homology models. The homology models generated were from crystal and cryo-EM structures that had resolution within the pre-M1 and linker regions. We used the well-resolved transmembrane region of the AMPA receptor, with high sequence homology and structural similarity to the transmembrane regions of GluN1 and GluN2A. Moreover, we equilibrated our structures using molecular dynamics before using the structure in any calculations. To better conceptualize the role pre-M1 plays in gating, we calculated the changes in protein stability and the affinity of the pre-M1 region for its surrounding contact residues following the introduction of two mutations, GluN2A-F553A and GluN2A-L550A. We studied the effects on protein stability and affinity because we can reliably model the receptor in the closed state, and we know that the pre-M1 undergoes a change in the

degree of association and dissociation with the receptor allowing for ligands to bind between pre-M1 helix and the more internal pore-forming structures of the receptor, in both NMDA and AMPA receptors (Perszyk et al., 2018; Yelshanskaya et al., 2016).

The interpretation from our computational results provides a simplistic and reductionist explanation of a complex gating system. We found both mutations, GluN2A-F553A and GluN2A-L550A, to decrease the protein stability within the pre-M1 region. We interpret these results to mean that the decreased protein stability leads to a pre-M1 helix with less structural integrity, altering the gating mechanism when the GluN2A ABD-TMD linker acts on pre-M1 to open the channel upon glutamate binding. We further suggest that the reduced structural integrity produces a decrease in the open probability and reduced mean open time. However, the change in affinity of pre-M1 to its binding region (closed state) predicted the GluN2A-F553A mutant to associate more weakly than wild-type, whereas the L550A mutant had a stronger association. This result is consistent with the finding that the GluN2A-F553A mutant had a 9-fold slower deactivation time compared to a 3.5-fold faster deactivation time of the L550A mutant. Similarly, we observed a decrease in the glutamate EC_{50} for the GluN2A-F553A, but an increase for the GluN2A-L550A mutant. We hypothesize that the weaker association of pre-M1 as seen in the GluN2A-F553A mutant has two effects. First, it reduces the energy barrier needed to overcome conformational changes that allow channel opening upon glutamate binding, thereby decreasing the EC_{50} of glutamate. Second, once the conformational changes needed to open the channel have taken place, a lower affinity means a slower return to the closed state from which glutamate can dissociate, resulting in a slower deactivation time. In contrast, the GluN2A-L550A mutant displayed increased association between pre-M1 and the receptor. We hypothesize that this stronger association increases the glutamate EC_{50} value because the energy barrier for the

conformational changes to open the channel is higher, requiring a higher concentration of glutamate to produce the same effect. Moreover, the tighter association of the pre-M1 mutant with the receptor facilitates the binding of pre-M1 in the closed state, reducing the deactivation time. We propose then that the increase in affinity between pre-M1 and interacting residues drives the deactivation time course by facilitating the return of the pre-M1 helix to its position in the closed state of the channel, allowing the receptor to reach a state from which glutamate can unbind. Similar to the GluN2A-F553A mutation, the change in affinity of the pre-M1 helix for its interacting residues, although opposite in magnitude, is in agreement with this observed 2-fold increase EC_{50} (decrease in potency) of glutamate for the L550A mutant.

Overall, the results from this study emphasize the previously suggested role of the pre-M1 helix in channel gating by demonstrating how specific residues within this region are critical for channel function. In addition, these results implicate the surrounding amino acid environment in the mechanism of channel gating by revealing a network of aromatic residues that is disrupted by an alanine substitution at the central phenylalanine residue. Finally, these results suggest unique subunit-specific contributions of pre-M1 helices in GluN1 and GluN2 to channel gating due to nonequivalent gating triads.

Chapter 4: Gating Effects of Disease-Associated Mutations within the Pre-M1 Helix*

*Parts of this chapter have been published in the following two manuscripts:

Gibb AJ, Ogden KK, McDaniel MJ, Vance KM, Kell SA, Butch C, Burger P, Liotta DC and Traynelis SF (2018) A structurally derived model of subunit-dependent NMDA receptor function. *The Journal of physiology* **596**(17): 4057-4089.

Ogden KK, Chen W, Swanger SA, McDaniel MJ, Fan LZ, Hu C, Tankovic A, Kusumoto H, Kosobucki GJ and Schulien AJ (2017) Molecular mechanism of disease-associated mutations in the pre-M1 helix of NMDA receptors and potential rescue pharmacology. *PLoS genetics* **13**(1): e1006536.

Abstract

N-methyl-D-aspartate (NMDA) receptors are tetrameric ionotropic glutamate receptors comprised of two glycine-binding GluN1 and two glutamate-binding GluN2 subunits whose activity is implicated in both normal and aberrant brain function. One missense *de novo* mutation of particular interest, GluN2A-P552R, was identified in a patient with epilepsy and developmental delay. In this study, we use GluN2A-P552R in the pre-M1 helix to propel our understanding of how this region contributes to function by controlling channel gating. We evaluate the functional changes that arise from substitutions at the GluN2A-Pro552 position and analyze how one or two copies of the Pro to Arg mutation alter activation and deactivation in homomeric and heteromeric receptors. Our results show that the prolonged activation and deactivation rates of the GluN2A-P552R mutant could only be recapitulated by substitution with lysine, suggesting that residue charge is of functional importance. Additionally, we found that GluN1/GluN2A, GluN1/GluN2B, and GluN1/GluN2A/GluN2B receptors exhibit a prolonged deactivation time course with one or two mutant GluN2 subunits, but only display a slow rise time with two mutant subunits. These results suggest that rearrangement of a single GluN2 pre-M1 helix is sufficient for rapid activation. Finally, we use the structure of glutamate receptors to develop a mechanism describing both single channel and macroscopic currents. We propose that each agonist-bound subunit undergoes a rate-limiting conformational change between agonist binding and channel opening. We hypothesize that this change occurs within a triad of interactions between the pre-M1 helix, the pore forming M3 helix, and the linker preceding the M4 helix of the adjacent subunit. Overall, results from this study suggest that mutations within the pre-M1 helix are of significant functional consequence, implicate the pre-M1 region in gating, and provide mechanistic insight into how individual subunits contribute to gating.

Introduction

The N-methyl-D-aspartate (NMDA) receptor is a calcium-permeable ligand-gated ion channel protein found in nerve cells. With a role in long-term potentiation and depression (Asztély and Gustafsson, 1996; Liu et al., 2004; Maren and Baudry, 1995; Takeuchi et al., 2014), learning and memory (Hebb, 1962), and overall neural development (Ewald and Cline, 2009), appropriate function of the NMDA receptor is crucial for normal brain function. Aberrant NMDA receptor function has been associated with the development of Alzheimer's disease (Hynd et al., 2004), Huntington's disease (Zeron et al., 2002), epilepsy (Lemke et al., 2014; Rice and DeLorenzo, 1998; Yuan et al., 2015b), intellectual disabilities (XiangWei et al., 2018), schizophrenia (Coyle, 2006; Olney et al., 1999) and memory impairment (Newcomer et al., 1999). In addition, recent advances in the technologies of next-generation whole exome sequencing have led to the identification of several rare variants and *de novo* mutations associated with neuropsychiatric disorders in the *GRIN* genes encoding the NMDA receptor subunits (Burnashev and Szepetowski, 2015; Hu et al., 2016; Yuan et al., 2015a).

Interestingly, whole exome sequencing has also shown, by sub-region variation intolerance score (subRVIS), that the genes encoding the NMDA receptor subunits are highly intolerant to variation (Ogden et al., 2017; Swanger et al., 2016). These findings are further supported by data from the Exome Aggregation Consortium (ExAC) database, which includes the exomes from over 60,000 unrelated healthy individuals (http://exac.broadinstitute.org/). The agonist binding domain, the transmembrane domain, and the linker regions between these domains showed unusually low levels of missense variation in the general population despite the presence of synonymous variation (Ogden et al., 2017; Swanger et al., 2016). Additionally, these regions have been found to harbor a large number of disease-associated *de novo* mutations

(Ogden et al., 2017; Swanger et al., 2016). These data suggest that, in general, the occurrence of missense variation in these domains might be under greater negative selection than in the amino-terminal and carboxy-terminal domains. Moreover, the selection against mutations in these regions may also suggest that these regions are particularly important to channel function.

The hypothesis that these regions are of significant functional importance is further evidenced by the finding that several of the disease-associated *de novo* mutations have been found within exons encoding the pre-M1 helix (Ogden et al., 2017; Swanger et al., 2016), thought to be critical for the NMDA receptor gating mechanism. For example, a *GRIN1* mutation corresponding to GluN1-D552E and a *GRIN2A* mutation corresponding to GluN2A-A548T were identified in patients with intellectual disability and/or epilepsy (Ogden et al., 2017). Functional analysis of these mutations revealed reduced current responses and reduced glutamate and glycine potency (Ogden et al., 2017). Additionally, the GluN1-D552E mutation produced reduced surface expression when co-expressed with the GluN2B subunit (Ogden et al., 2017).

Of particular interest was a set of mutations that were identified at the proline residue towards the M1 end of the pre-M1 helix (Ogden et al., 2017). This residue is conserved across all NMDA receptor subunits (Ogden et al., 2017), suggesting that it is important for channel function. Three patients were identified to have a mutation at this site: one patient had a GluN1-P557R mutation and presented with intellectual disability (Ohba et al., 2015; Redin et al., 2014), a second patient had a GluN2A-P552R mutation and presented with epilepsy and developmental delay (De Ligt et al., 2012; Lesca et al., 2013; Ohba et al., 2015; Redin et al., 2014), and a third patient had a GluN2B-P553L mutation and presented with intellectual disability (Hu et al., 2016). Analysis of these mutation revealed severe functional consequences and, perhaps more importantly, began to shed light on the complex gating mechanism of the NMDA receptor.

When co-expressed with GluN2A or GluN2B, the GluN1-P557R mutation produced receptors with significantly reduced current amplitudes and increased potency of glutamate and glycine (Ogden et al., 2017). Although the reduced current amplitudes could be explained by the markedly reduced surface expression when co-expressed with GluN2A and reduced total expression when co-expressed with GluN2B, the prolonged deactivation time course suggests that there were also significant changes to receptor function. Reduced surface expression was also detected for receptors containing the GluN2B-P553L mutation (Ogden et al., 2017). Unlike the GluN1 mutant, however, the GluN2B-P553L receptors were rendered virtually non-functional. Perhaps the most surprising functional result from Ogden et al., 2017 came from the GluN2A-P552R mutation. Although this mutation produced no measurable change in current amplitudes or surface expression, the receptor kinetics were drastically altered. Like GluN1-P557R, GluN2A-P552R displayed increased glutamate and glycine potency and a significantly prolonged deactivation time course. However, unlike the GluN1 mutant, GluN2A-P552R also displayed a 60-fold increase in the 10-90 rise time. Even once agonist application had been terminated, the receptor-mediated current response continued to rise, suggesting that the slow rise time reflects a slowing of the conformational changes that precede channel opening rather than an altered rate of agonist binding (Ogden et al., 2017).

Firstly, to understand how the pre-M1 helix controls receptor function, we investigated the functional effects of multiple amino acid substitutions at the GluN2A-Pro552 residue. Additionally, we made use of the previously published method for controlling receptor stoichiometry using the dual retention sequence of GABA-B receptors to explore the kinetic consequences of a single copy of the GluN2A-P552R or GluN2B-P553R mutations (Hansen et al., 2014). Finally, we performed whole-cell patch clamp electrophysiology on GluN1/GluN2A,

GluN1/GluN2B, and GluN1/GluN2A/GluN2B receptors containing one or two copies of the GluN2 proline to arginine mutation to investigate how individual subunits contribute to the activation of the NMDA receptor.

To develop a mechanistic understanding of how gating is controlled by the pre-M1 helix of individual subunits, a conceptual model was developed by Alasdair Gibb (Department of Neuroscience, Physiology, and Pharmacology, University College of London) and Stephen Traynelis (Department of Pharmacology, Emory University) based on the structure of the NMDA receptor. This model design was guided by functional and structural data that emphasizes the unique contributions of individual subunits to overall receptor activation. Receptor symmetry and stoichiometry dictates the function of the NMDA receptor. As such, receptors composed of two identical GluN1 and two identical GluN2 subunits likely show equivalence in the rates of conformational change within subunit dimer pairs, while those with non-identical GluN1 or GluN2 subunits will lack this symmetry. Because some triheteromeric receptors have been shown to display kinetic activation and deactivation properties that are dominated by a single GluN2 subunit with properties distinct from either diheteromeric receptor (Hansen et al., 2014) and because the pre-M1 GluN2A-P552R mutation produced receptors with significantly altered receptor kinetics (Ogden et al., 2017), we hypothesize that the pre-M1 helix of each NMDA receptor subunit independently functions to control channel gating.

We used the structurally derived model to explore how independent subunits of the NMDA receptor— specifically the pre-M1 regions— could contribute to channel gating in a way that could account for the kinetic changes introduced by a single copy of the proline to arginine mutation. Although several models have been developed to make sense of agonist binding, desensitization, allosteric modulation, and pore dilation (Benveniste et al., 1990; Clements et al.,

1992; Dai and Zhou, 2013; Hansen et al., 2012; Mesbahi-Vasey et al., 2017; Nahum-Levy et al., 2001; Schorge et al., 2005; Talukder and Wollmuth, 2011; Yi et al., 2016; Zhou and Wollmuth, 2017), our model was developed to differentiate between the individual subunits of the receptor as guided by structural and functional data. The model was shown to accurately describe single channel data by fitting the open and closed times of previously published GluN2A single channel data using the maximum likelihood method. To verify that the model could also accurately describe macroscopic NMDA receptor currents, we fit the structure-based model to current responses measured from outside-out patches containing GluN1/GluN2A wild-type receptors. Finally, we performed a sensitivity analysis to confirm a single minimum in the least squares surface generated during fitting.

Our results indicated that the identity of the residue at position 552 of the GluN2A pre-M1 helix influences the kinetic response of the receptor to saturating agonist. Substitution of GluN2A-Pro552 with arginine and lysine produced receptors with significantly prolonged activation and deactivation rates, while substitution with alanine, glycine, isoleucine, or leucine did not prolong rise time or deactivation rate. Additionally, we found that the structurally derived model could accurately fit macroscopic data in a manner that could explain our results showing that a single copy of the GluN2 proline to arginine mutation was sufficient to prolong deactivation without altering rise time. Overall, our results suggest that the pre-gating conformational changes within each subunit required for receptor activation occur independently, that the pre-M1 helices are part of the structural correlate of these pre-gating steps, and that the structurally derived model can be used to interpret the functional properties of NMDA receptors with non-identical subunits.

Results

The GluN2 pre-M1 helix has been identified as being a critical structural component in channel gating based on functional changes in response to mutations, a strict intolerance to variation, and a collection of disease-associated *de novo* mutations within this region (Ogden et al., 2017). One particular *de novo* mutation, GluN2A-P552R, was shown to be detrimental to channel function resulting in significantly enhanced agonist potency and a drastically slowed response time course. We first explored the functional consequences of alternate amino acid substitutions at this position. We then used the GluN2A proline to arginine mutation and the equivalent mutation in GluN2B to explore the unique contributions of a single subunit to the overall gating mechanism according to a structurally derived mechanistic model.

Functional Consequences of Various Amino Acids

It has been shown that the disease-associated GluN1/GluN2A-P552R receptors exhibit prolonged glutamate response time course and a slow rise time in addition to increased glutamate and glycine potency. The amino acid side chains of arginine and proline drastically differ in size, charge, hydrogen bonding capacity, and effects on linker flexibility. To assess which features of this residue might account for the observed functional changes, the effects of different amino acids substituted at this position were evaluated. Specifically, we evaluated GluN1/GluN2A receptors with mutations that altered the hydrogen bonding properties of the side chain (Arg, Lys, and Gln) or the size of the side chain (Gly, Ala, Ile, and Leu). We expressed each mutant GluN1/GluN2A receptor in HEK293 cells and measured the rise time, desensitization, and deactivation time course in response to 1 second applications of glutamate (100 μM) in the

continued presence of glycine (100 μM). Because lysine and arginine both share an ionizable group, we hypothesized that GluN1/GluN2A-P552K would present with a kinetic profile similar to that of GluN1/GluN2-P552R.

Our results showed that the GluN2A-P552K mutation drastically prolonged rise time (1063 ms) compared to wild-type receptors (7.7 ms), consistent with that observed for GluN2A-P552R (576 ms) (**Figure 4.1, Table 4.1**). Moreover, receptors containing GluN2A-P552K deactivated with a time course that was 12-fold slower than that of wild-type receptors, again consistent with the 15-fold slower than wild-type deactivation time course of the GluN2A-P552R mutant. The GluN2A-P552Q mutant, which retained the hydrogen bonding capacity of the arginine without the charge, showed altered response amplitude and desensitization, but had no observable effect on rise time or deactivation time course. The only other mutation with an effect on rise time was GluN2A-P552G, which reduced side chain volume and increased chain flexibility. This mutation accelerated the 10-90% rise time, cutting the time to peak current in half. This Gly mutation, along with Ile and Leu, also accelerated the fast deactivation time constant. Mutations of Pro to Ala, Gly, Ile, Leu as well as Gln increased the degree of desensitization relative to wild-type (56%), achieving steady-state levels that were 20%, 29%, 29%, 1.5%, and 18% of the peak response, respectively (**Table 4.1**). Due to their slow response rise time, receptors containing Arg and Lys did not reach steady state during even prolonged (1 second) agonist application, and therefore, desensitization of these mutant receptors could not be determined.

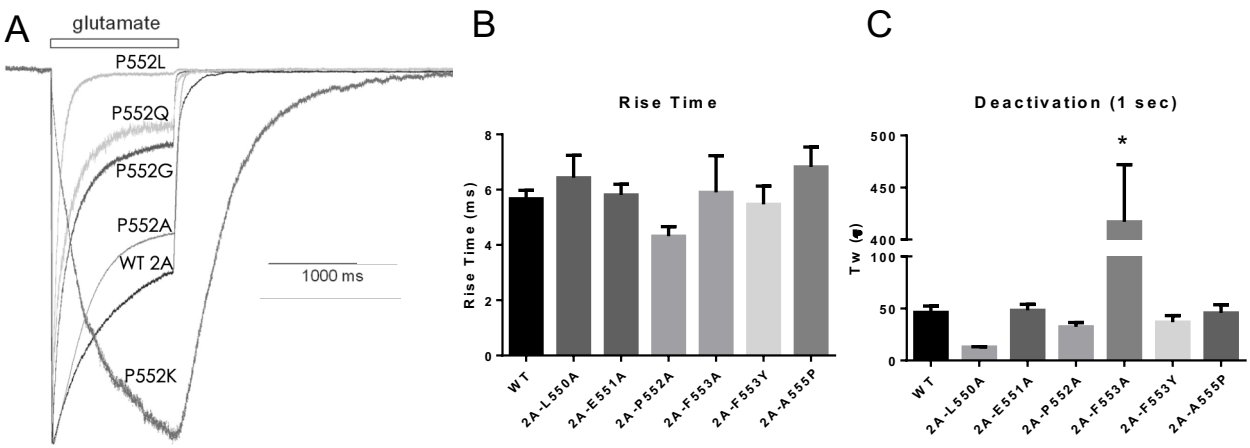

Figure 4.1: The GluN2A-P552K mutation prolongs deactivation time course of di-heteromeric GluN2A receptors

A) Whole-cell patch clamp recordings of HEK cells expressing wild-type GluN1 and wild-type or mutant GluN2A subunits following a 1 sec pulse of 1mM glutamate in the presence of 30uM glycine. Traces were normalized to peak current. **B)** Quantification of 10-90 rise time for each construct. **C)** Quantification of weighted deactivation time course for each construct determined by fitting of two exponential components. GluN2A-P552K significantly prolonged deactivation by ~13-fold.

Table 4.1: Response time course for substitution of GluN2A-ProP552 with Ala, Gly, Lys, Gln, Ile, or Leu

	WT 2A	P552Q	P552K	WT 2A	P552G	P552A	P552I	P552L
Amplitude (peak, pA/pF)	131 ± 23	35 ± 6.4*	5.8 ± 2.9*	96 ± 17	101 ± 21	115 ± 21	46 ± 13	61 ± 23
Amplitude (SS, pA/pF)	74 ± 15	5.4 ± 0.9*	--	52 ± 9.5	21 ± 5.5*	33 ± 7.7*	14 ± 3.9*	0.7 ± 0.13*
I_{SS}/I_{Peak} (%)	56 ± 5.0	18 ± 2.1*	--	58 ± 3.7	20 ± 2.3*	29 ± 4.8*	29 ± 2.7*	1.5 ± 0.1*
τ_W desensitization (ms)	735 ± 76	211 ± 21*	--	769 ± 52	235 ± 32*	374 ± 59*	742 ± 120	91 ± 4.5*
Rise Time (ms)	7.7 ± 0.51	5.7 ± 0.7	1063 ± 14*	10 ± 0.9	5.2 ± 0.4*	11 ± 1.1	8.3 ± 0.9	11 ± 1.5
τ_{Fast} (ms)	36 ± 3.3	32 ± 2.0	555 ± 47*	37 ± 2.9	16 ± 1.5*	26 ± 1.3	17 ± 1.4*	21 ± 4.4*
τ_{Slow} (ms)	271 ± 85	315 ± 60		583 ± 85	416 ± 138	705 ± 188	384 ± 118	123 ± 32*
τ_W (ms)	47 ± 5.7	65 ± 6.5	610 ± 40*	55 ± 4.2	37 ± 6.1	46 ± 5.8	25 ± 2.8*	40 ± 5.7
n	8	11	9	22	12	10	8	12

Human GluN1 and GluN2 were diheteromeric receptors and rat GluN1 and GluN2 were used for triheteromeric experiments. * $p < 0.05$ compared to GluN2A/GluN2A; one-way ANOVA, Tukey post hoc.

Effects of the Pre-M1 Proline Mutation in Triheteromeric Receptors

The patient who was determined to have GluN2A-P552R only had a single copy of the mutation. As such, it is likely that the NMDA receptors in this patient will be a mixture of those with 0, 1 or 2 copies of the mutant GluN2A subunit. It had previously been shown that, while two copies of the GluN2A-P552R subunit prolonged deactivation time course and delayed the rise time, receptors containing one mutant and one wild-type GluN2A subunit showed prolonged deactivation with a wild-type like rise time (Ogden et al., 2017). However, mounting evidence suggests that NMDA receptors often contain two different GluN2 subunits (Hansen et al., 2014; Luo et al., 1997). It has been shown that the majority of synaptic NMDA receptors in the hippocampus are GluN1/GluN2A/GluN2B triheteromeric receptors (Tovar et al., 2013). Moreover, functional analysis of these receptors revealed distinct pharmacological and kinetic profiles appearing to be dominated by the GluN2A subunit (Hansen et al., 2014). As such, we sought to explore the effects of a single copy of the GuN2A-P552R in these triheteromeric receptors.

Firstly, using the previously published technique for controlling receptor stoichiometry using the GABA-B retention sequence (Refer to Chapter 2), we expressed GluN1/GluN2A receptors that contained 0, 1 or 2 copies of GluN2A-P552R. We also expressed GluN1/GluN2B with 0, 1 or 2 copies of the analogous mutation (P553R). We then evaluated the current response time for each receptor following a 5 ms application of saturating glutamate in the continued presence of saturating glycine. We found that receptors with 0 or 1 copy of GluN2A-P552R or GluN2B-P553R can become activated at rates similar to wild type receptors, as there was no detectable difference between the 10–90% current response rise times. However, receptors with two copies of GluN2A-P552R or two copies of GluN2B-P553R respond over an order of

magnitude more slowly, with the response continuing to rise long after glutamate had been removed by the rapid perfusion system (**Figure 4.2, Table 4.2**).

We then co-expressed GluN1/GluN2A/GluN2B triheteromeric receptors with a single copy of GluN2A-P552R into the triheteromeric receptor complex and assessed the response time course. As observed with diheteromeric receptors, a single copy of the GluN2A-P552R mutation did not markedly slow the current response rise time of triheteromeric GluN1/GluN2A-P552R/GluN2B receptors to brief (5 ms) application of glutamate but did result in a significantly prolonged deactivation time course. These results suggest that a triheteromeric GluN2A/GluN2B receptor can open normally when the single wild-type GluN2B subunit has undergone pre-gating. Triheteromeric receptors where both GluN2 subunits carry the mutation also deactivate with a significantly prolonged time course but activate approximately 30-fold more slowly. Because the functional effect of the GluN2 proline residue is conserved within GluN2A and GluN2B, this result supports the hypothesis that the pre-M1 region of GluN2A and 2B subunits is an important determinant of the rate of receptor activation.

Even with the stoichiometric control imparted by the C1 and C2 peptide tags, some diheteromeric receptors could have escaped ER retention, trafficked to the surface, and contributed to the fraction of the total current response. We used the GluN2B-selective inhibitor ifenprodil in control experiments to ensure that the recorded currents reflected triheteromeric receptors and not diheteromeric receptors that had escaped ER retention. For cells transfected with GluN1/GluN2A$_{C1}$-P552R/GluN2B$_{C2}$, if appreciable GluN2B$_{C2}$ escaped the ER and formed diheteromeric GluN1/GluN2B$_{C2}$ receptors that reached the surface, then the observed peak current would be greater than that of the triheteromeric receptor alone. The GluN2B selective

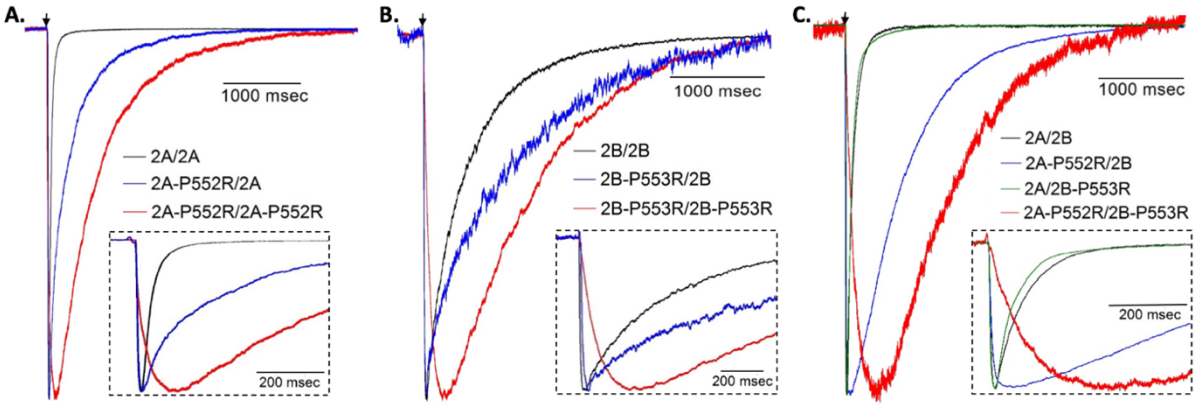

Figure 4.2: Representative current responses of GluN1/GluN2A and GluN1/GluN2B receptors
Current responses of wild-type receptors following brief (5 ms, black arrow) application of glutamate (1 mM) in the presence of glycine (30 uM). Responses show GluN1/GluN2A receptors **A)** and GluN1/GluN2B receptors **B)** containing zero (black), one (blue), or two (red) mutated GluN2 subunits. Containing a single copy of the mutation slows deactivation by 6-fold for GluN1/GluN2A and 5-fold for GluN1/GluN2B, while containing two copies of the mutation slows deactivation by 46-fold for GluN1/GluN2A and 11-fold for GluN1/GluN2B. **C)** Representative traces following fast perfusion of glutamate (1 mM) for 5 ms (black arrow) in the presence of glycine (30 uM) for GluN1/GluN2A/GluN2B (black), GluN1/GluN2A-P552R/GluN2B (blue), and GluN1/GluN2A-P552R/GluN2B-P553R (red). GluN1/GluN2A-P552R/GluN2B and GluN1/GluN2A-P552R/GluN2B-P553R slow deactivation by 7-fold and 24-fold, respectively. For all panels, the inset shows that a single copy of the mutation does not alter the rise time, but two copies of the mutations produce pronounced slowing of the deactivation time course.

Table 4.2: Di- and Triheteromeric NMDA Receptor Macroscopic Response Properties

	Rise Time (ms)	tau_1 (ms)	tau_2 (ms)	% tau_1	$tau_{weighted}$ (ms)	n
GluN2A/ GluN2A	8.3 ± 0.5	33 ± 3.0	147 ± 28	88 ± 3.5	41 ± 3.7	12
GluN2A-P552R/ GluN2A	9.5 ± 1.0	67 ± 16	367 ± 38	49 ± 8.1	260 ± 39	9
GluN2A-P552R/ GluN2A-P552R	230 ± 14*†	1200 ± 140	4040 ± 655	77 ± 19	1900 ± 180*†	8
GluN2B/ GluN2B	15 ± 1.0	210 ± 16	744 ± 31	46 ± 13	496 ± 25	16
GluN2B-P553R/ GluN2B	43 ± 3.2	310 ± 29	3990 ± 255	37 ± 4.0	2600 ± 140*	8
GluN2B-P553R/ GluN2B-P553R	960 ± 83*†	5780 ± 300	--	100 ± 0	5780 ± 300*†	8
GluN2A/ GluN2B	8.0 ± 0.3	64 ± 6.6	425 ± 101	91 ± 2.0	78 ± 5.7	14
GluN2A-P552R/ GluN2B	12 ± 1.0	440 ± 76	1790 ± 394	84 ± 8.7	540 ± 58*	9
GluN2A-P552R/ GluN2B-P553R	330 ± 21*†	1900 ± 130	--	100 ± 0	1900 ± 130*†	9

Values shown are means ± SEM to two significant figures. 'n' is the number of observations. The weighted tau was determined from the fitted tau values from two exponential functions, with the exception of 2B-P553R/2B-P553R and 2A-P552R/2B-P553R, which deactivated with a time course described by only one exponential.
∗P < 0.001 compared to wild type, one-way ANOVA, Tukey post hoc, multiple comparisons,
†P < 0.001 compared to single-copy mutants, one-way ANOVA, Tukey post hoc, multiple comparisons.
The sequential approach of Holm was used to correct familywise error.

inhibitor ifenprodil at 3 μM typically reduces the peak current of diheteromeric GluN1/GluN2B$_{C2}$ receptors by 90%, while reducing the triheteromeric peak current by 30%. We observed only partial block (38%) of the current response amplitude from GluN1/GluN2A$_{C1}$/GluN2B$_{C2}$ transfected cells, consistent with the previously reported effects of ifenprodil on GluN2A/GluN2B triheteromeric receptors (Hansen et al., 2014; Hatton and Paoletti, 2005). Additionally, when applied to GluN2A$_{C1}$-P552R/GluN2B$_{C2}$ and GluN1/GluN2A$_{C1}$-P552R/GluN2B$_{C2}$-P553R triheteromeric receptors, 3 μM ifenprodil reduced peak current by 58 ± 5.5% (n = 9) and 43 ± 6.1% (n = 9) of control, respectively. As a result, we were able to conclude that contributions to macroscopic current by diheteromeric GluN1/GluN2B$_{C2}$ receptors that escaped ER retention were minimal. The lack of effect on activation rate of one mutated GluN2 subunit in the tetrameric receptor complex supports the idea that NMDA receptor open states can be reached when either one or both GluN2 subunits have undergone some conformational change. The ability of a channel to open at the same rate as wild-type even with one impaired GluN2 subunit suggests that the receptor may reach an open state independent of the conformation of the second, mutant GluN2 subunit.

Designing a Structure Based Model to Elucidate NMDAR Gating Mechanisms

In order to gain a mechanistic understanding of NMDA receptor gating, a model was conceptualized by Steve Traynelis (Department of Pharmacology, Emory University) and Alasdair Gibb (Department of Neuroscience, Physiology, and Pharmacology, University College of London) to account for the contribution of individual subunits to overall receptor activation. Within each subunit, closing of the bi-lobed ABD clamshell is thought to proceed at least two kinetically distinct conformational changes that lead to the rapid opening of the ion channel pore.

These two kinetically distinct conformations have been inferred by the multiple components of the closed time distributions of single channel current responses and maximum likelihood fitting of these recordings with kinetic models. As such, an explicit activation mechanism was developed for a receptor containing two identical GluN1 subunits and two identical GluN2 subunits. Based on this mechanism, each agonist-bound subunit of the receptor can independently undergo a pre-gating conformational change in the GluN1 subunits (rates k_{+f} and k_{-f}) or GluN2 subunits (rates k_{+s} and k_{-s}) in any order. The two open states can interconvert (rate constants k12 and k21), and are reached by distinct opening rates, β1 and β2 (α1 and α2 are distinct closing rates). The model was constructed assuming the glycine binding site on the GluN1 subunit and the glutamate binding site on the GluN2 subunit are occupied at high concentrations of glycine (50 μM) and glutamate (1 mM) relative to their EC_{50} values. There was also assumed to be no cooperativity in these conformational changes nor in the dimer-dependent desensitization rates, such that subunit transition rates are constant and unaffected by the conformational state of the other three subunits.

The model was further modified following the identification of slow rate constants representing the GluN2 subunit pre-gating. These rate constants slowed the simulated macroscopic activation to a rate that was inconsistent with the previously established GluN2A kinetics. The model was, therefore, supplemented with additional states that could account for the receptor entering a desensitized state. The characterization of NMDA receptor desensitization as a dimer-dependent phenomenon guided modification of the model to acknowledge when GluN1 and GluN2 pre-gating steps have taken place within a dimer. That is, when one GluN1 subunit and one GluN2 subunit within a dimer have undergone a pre-gating conformational change, there was assumed to be a possibility for the receptor to enter a desensitized state.

Inclusion of the desensitized states and explicit representation of a dimer-dependent conformational change allowed the model to more accurately represent the functional data from GluN1/GluN2A receptors and accelerated the estimated rate constants for the GluN2 pre-gating steps.

The final iteration of the model included the rates of glutamate binding. We assumed that the probability of the subunit to undergo pre-gating in the absence of bound agonist was very low, while the probability of the subunit to undergo pre-gating in the presence of bound agonist was very high. Additionally, we assumed that the probability of glutamate unbinding would be very low following the pre-gating step or desensitization. Guided by synaptic agonist concentrations, we assumed that glycine is always present and bound. Therefore, the model depicts the glutamate binding steps independent of the GluN1 conformation, such that glutamate can bind a receptor that either has or has not undergone GluN1 pre-gating (**Figure 4.3**).

Predicting Macroscopic NMDA Receptor Properties with a Structure-Based Model

The structure-based model was shown to accurately account for single channel properties of the receptor. It was necessary, then, to determine whether the model could also accurately account for the macroscopic properties of the NMDA receptor. Macroscopic patches (n=9) were excised from HEK293 cells expressing wild-type GluN1/GluN2A receptors and treated with 1 second pulses of 1 mM or 3 μM glutamate in the continued presence of saturating glycine. The current responses were consistent with previously published characterization of the macroscopic properties of recombinant diheteromeric GluN21/GluN2A receptors. Specifically, the current response showed a normal activation time course, pronounced desensitization in prolonged presence of agonist, and rapid deactivation upon agonist removal. Initially, the model was fixed

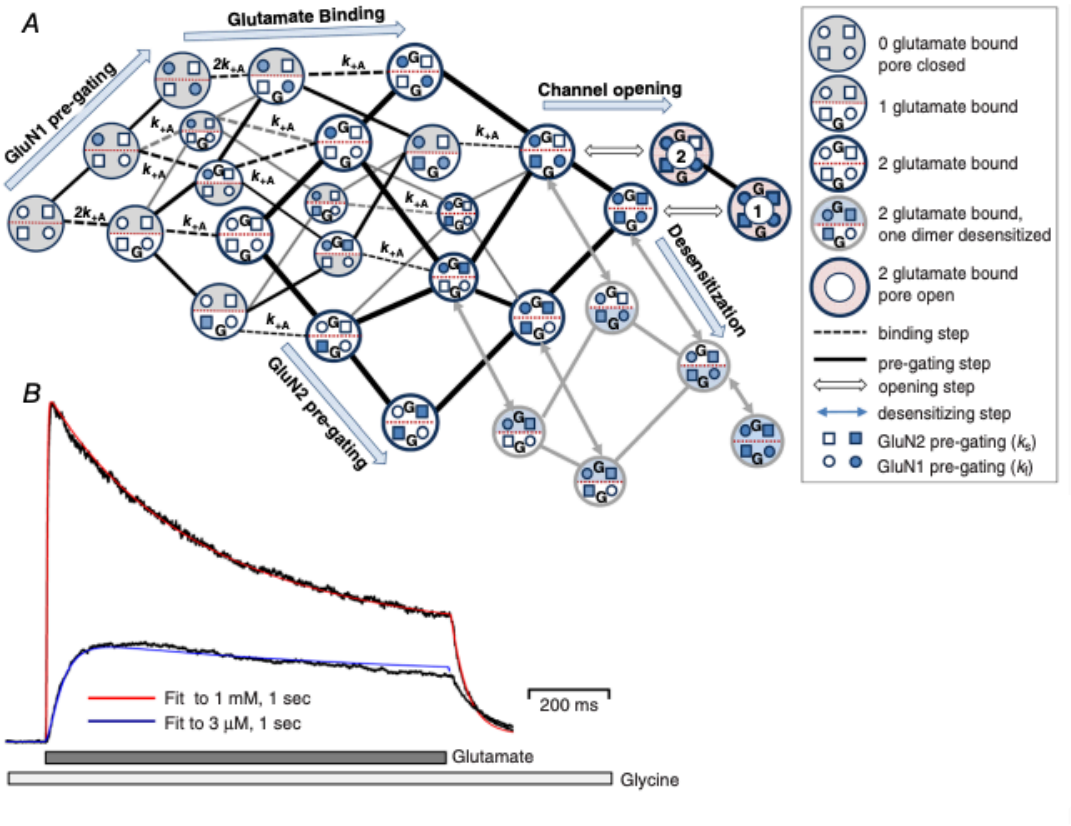

Figure 4.3: Glutamate binding to a structurally based model of receptor activation
A) Glutamate binds prior to subunit-dependent pre-gating steps (glycine is assumed to be bound at all subunits). For each binding step (dashed lines), only the association rate k_{+A} is shown for clarity; the dissociation rate k-A is not shown. **B**) Macroscopic currents from GluN1/GluN2A were recorded from excised outside-out patches in response to rapid application of 1 mM or 3 µM glutamate for 1 s. A least squares fitting algorithm was used to optimize glutamate association and dissociation rates and the rates describing the entry and exit from the desensitized state by simultaneously fitting the model in A to both waveforms. The best fit is shown superimposed onto the macroscopic currents.

with pre-gating rates corresponding to those determined by the fitting of the previously recorded single channel data. We then fit the model to the two waveforms corresponding to the low and high concentrations of glutamate to determine the microscopic glutamate association and dissociation rates and the rate of desensitization. The estimated rates were capable of reproducing the slow, complex rise time associated with submaximal glutamate and the fast rise time and deactivation time associated with brief exposure to saturating glutamate (**Figure 4.3**).

Least squares fitting was used to determine a microscopic glutamate association rate k_{+A} of 6.7×10^6 M^{-1} s^{-1} and a dissociation rate k_{-A} of 65 s^{-1}. We also determined the rates for the onset of (k_{+d}) and recovery from (k_{-d}) desensitization to be 7.41 s^{-1} and 1.54 s^{-1}, respectively. Moreover, these rates were consistent with those determined from fitting the single channel records (k_{+d} = 5.28 s^{-1}, k_{-d} = 1.78 s^{-1}). With the fitted rates, the response to a brief synaptic-like pulse of glutamate could be simulated. The simulated macroscopic response to a 1 second pulse of saturating glutamate displayed a 10-90% rise time of 5 ms and the EC_{50} values from peak and steady state concentration-effect curves were determined to be 6.5 and 2.4 μM glutamate, respectively. Finally, the response deactivated with a time course that could be best fitted by a single exponential function with a time constant of 40 ms. Simulated 2 second application of saturating glutamate produced a macroscopic response waveform that desensitized to a current level lower than the peak response with a variable time course. The mean response of nine patches to 1 mM glutamate in sustained 100 μM glycine was accurately described by a dual exponential function with a fast time constant of 119 ms (13%) and a slow time constant of 511 ms (87%). A similar dual exponential time course for desensitization in response to glutamate was seen for macroscopic responses simulated using fitted rate constants from the single channel data with a fast time constant of 151 ms (12%) and a slow time constant of 437 ms (88%).

Sensitivity Analysis

To validate the model, sensitivity analysis was performed by determining the sum of squares for normalized waveforms simulated with the agonist binding and desensitization rates varied over a range encompassing the fitted values. For single channel data, a sensitivity analysis allowed for the investigation of the sensitivity of the shape of the likelihood surface near the maximum to small changes in a single parameter. For macroscopic data, the sensitivity of the sum of squares was determined for small changes in parameter values around the best-fit value for the glutamate binding (k_{+A}) and unbinding (k_{-A}) rates, and rates for desensitization (k_{+d}, k_{-d}). The shape of the likelihood surface around the optimum values was determined and the models were statistically analyzed by a likelihood ratio test.

Specifically, the least squares fitting of the model to the macroscopic waveforms yielded a glutamate association rate constant k_{+A} of 6.7×10^6 M^{-1} s^{-1} and a dissociation rate constant k_{-A} of 65 s^{-1}, which yielded a sum of squares difference of 5.51. The sum of squares difference is unitless because it was calculated from waveforms that had been normalized to the peak current. A sensitivity analysis was conducted over a range of rate constants, with k_{+A} values ranging from 1.68×10^6 to 1.34×10^7 M^{-1} s^{-1} and k_{-A} values ranging from 16.25 to 130 s^{-1}. Each rate was varied independently while the other rates were held constant. The sum of squared differences (SSQ) was calculated from the simulated waveform and recorded mean waveform for each possible combination of rates for both waveforms. Moreover, the best fit of the model to the macroscopic waveforms yielded rate of onset of desensitization (k_{-d}) and rate of recovery from desensitization (k_{+d}) of 1.54 s^{-1} and of 7.41 s^{-1}, respectively. Rates of onset of and recovery from desensitization were also co-varied with association and dissociation held constant, and the sum of squares difference determined for all possible combinations. The rate k_{-d} was varied between

0.385 and 3.08 s^{-1} and k_{+d} was varied between 1.85 and 14.8 s^{-1}. The sum of squares for each co-varied pair of rates for association and dissociation rate constants with desensitization rates held constant to those determined from the best fit can be found in **Figure 4.4 A-B**. Similarly, **Figure 4.4 C-D** shows the onset and recovery of desensitization were co-varied, with association and dissociation held constant to those determined from the best fit. The sensitivity analysis reveals that the best-fit values for k_{+A}, k_{-A} and for k_{+d}, k_{-d} are at the minimum of a valley in the sum of squares surface.

Discussion

As we continue to gain insights into the structural and functional properties of the NMDA receptor, we can begin to elucidate the mechanisms with which these receptors can transduce agonist binding into channel opening. It has been proposed that the pre-M1 helix controls channel gating by facilitating communication between the ABD and the TMD (Gibb et al., 2018; Karakas and Furukawa, 2014; Lee et al., 2014; Schorge et al., 2005; Sobolevsky et al., 2009; Talukder et al., 2010; Talukder and Wollmuth, 2011). Moreover, genetic analysis has identified this region as a locus for disease-associated *de novo* mutations (CFERV Database-http://functionalvariants.emory.edu/database/index.html)(Ogden et al., 2017), while maintaining an absolute lack of missense variation in the healthy population (gnomad.broadinstitute.org) (Ogden et al., 2017). In this study, we present a structurally based model to identify individual subunit contributions to the gating mechanism after providing a functional analysis of the pre-M1 helix in the context of human mutations.

The proline residue in the pre-M1 helix of GluN2A is conserved across the NMDA receptor subunits, and mutation of GluN2A-Pro552 and GluN1-Pro557 to arginine or GluN2B-

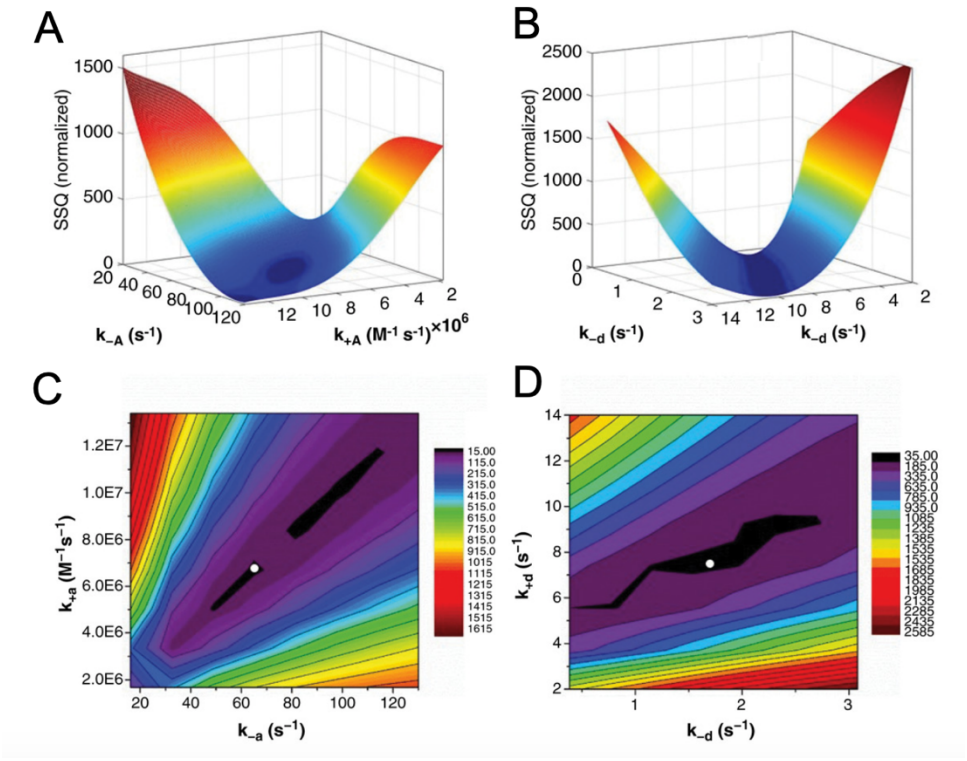

Figure 4.4: Sensitivity analysis of model rate constants
A and B) The relationship between the sum of squares (SSQ) obtained from fitting macroscopic current data, the rates of glutamate association (k_{+A}) and dissociation (k_{-A}), and the rates for the onset of (k_{+d}) and recovery from (k_{-d}) desensitization. **C and D)** The surface contour for the SSQ landscape with the minima indicated by a white dot.

Pro553 to leucine resulted in significantly altered receptor pharmacology and function. Here, GluN2A-Pro552 was substituted with amino acids of distinct charge, size, and bonding capabilities to investigate the sensitivity of this region to variation and to identify the properties of this specific residue that might alter receptor function. Results showed that substituting residues with side chains of similar volume did not enhance glutamate potency. Alternatively, only substitution of a Lys residue, predicted to possess a positive charge similar to Arg at physiological pH, could mimic the effects of GluN2A-P552R, suggesting a more important role of the charge of this side chain in the function of the receptor than flexibility or steric effects. Additionally, the substitution of GluN2A-Pro552 with glycine, which lacks a side chain, led to an increase in the speed of activation, supporting a key role for the pre-M1 helix in the steps leading to channel activation. By contrast, introduction of a leucine residue with a similar side chain size diminishes response amplitude and significantly increases desensitization, yet had no noticeable effect on response rise time or deactivation time course. Evaluation of the effect of substitution of other residues in place of this proline provides some insight into the potential nature of the actions of the Pro552Arg mutation. Moreover, the consequences of variation in the pre-M1 region is of particular functional relevance because the pre-M1 region where these mutations are located has been shown to control channel gating and, moreover, impart subunit specificity onto the gating mechanism (Ogden et al., 2017).

The GluN1/GluN2A-P552R mutation was also studied using the previously published method for controlling subunit stoichiometry using $GABA_B$ derived ER-retention tags (See Chapter 2) (Hansen et al., 2014). GluN1/GluN2A receptors containing one or two copies of GluN2A-P552R were investigated for changes in kinetic activation and deactivation properties. Our results support previously published data (Ogden et al., 2017) showing that receptors with a

single copy of GluN2A-P552R can become activated at rates similar to wild type receptors, as shown by no detectable difference between the 10–90% current response rise times. However, two copies of GluN2A-P552R produced receptors with a significantly delayed activation time course. Moreover, a single copy of the mutant subunit resulted in a prolonged deactivation time course, which was further prolonged for receptors containing two copies of the mutant subunit. This finding suggests that only three of the four subunits, presumably the two GluN1 subunits and a single GluN2 subunit, are required to undergo pre-gating before the channel can open. Or, in the case of mutant NMDA receptors, normal receptor activation can be achieved with three wild-type subunits. Alternatively, when both GluN2 subunits are mutated, receptor pre-gating steps are impaired, and activation is delayed.

Moreover, a single copy of the GluN2A-P552R mutation did not markedly slow the current response rise time of triheteromeric GluN1/GluN2A-P552R/GluN2B receptors to brief (5 ms) application of glutamate but did result in a significantly prolonged deactivation time course. Triheteromeric receptors with two mutant GluN2 subunits also show a significantly prolonged deactivation time course and activate approximately 30-fold more slowly. Together, these results support the finding that the NMDA receptor can open normally when the GluN1 subunits and a single GluN2 subunit have undergone pre-gating and provides evidence for GluN2A dominance of the GluN1/GluN2A/GluN2B triheteromeric receptor.

Not only was the rise time significantly prolonged, but the receptor activated so slowly that glutamate had already been removed from the extracellular solution before peak current was reached. That is, even after the extracellular glutamate had been washed away, the receptors that had already bound glutamate were still being activated. Because glutamate was removed from the extracellular solution before the receptor had fully activated, the rate of rise of the current

response must be dictated by conformational changes between agonist binding and channel opening. The GluN2A-P552R mutation was reported to enhance glutamate potency 10-fold (yielding a 10-fold lower glutamate EC_{50})(Ogden et al., 2017). For the wild-type GluN1/GluN2A receptor, glutamate rapidly binds and unbinds. As a result, when glutamate is removed from the extracellular solution, the agonist-bound channels rapidly close and glutamate can unbind. For the GluN1/GluN2A-P552R receptor, however, the unbinding of glutamate is much slower as glutamate remains bound to the receptor while the subunit slowly gates. In summary, the GluN2A-P552R mutant disrupts receptor gating such that, even once glutamate is removed from the extracellular solution, the receptors that have already bound glutamate will continue to open and slowly close before unbinding glutamate, leading to the observed slow rise time, prolonged deactivation time course, and reduced glutamate EC_{50}.

To investigate this complex mechanism of activation, a structure-based model was conceptualized. Guided by structural insights of the wild-type receptor (Karakas and Furukawa, 2014; Lee et al., 2014; Sobolevsky et al., 2009), and functional analysis of mutant receptors (Ogden et al., 2017), the model included independently acting subunits and open state connectivity such that channel opening could occur after both GluN1 subunits and either one or both of the GluN2 subunits had undergone pre-gating. The model was modified to include desensitization steps and glutamate binding to allow for a more accurate fit to the functional data collected for a wild-type GluN1/GluN2A receptor. After the model was demonstrated to accurately fit the functional data and verified by sensitivity analysis, we were able to reproduce the macroscopic properties of the diheteromeric wild-type GluN1/GluN2A receptor from rates derived from single channel fitting by mechanisms that included transitions that reflect unique subunit-dependent conformational changes. These conformational transitions, we predict,

represent the movement and altered interactions of linker regions that precede gating (Tajima et al., 2016).

This hypothesis is backed by a vast collection of data showing the unique role of these regions in gating (Chen et al., 2017; Kazi et al., 2013; Ogden et al., 2017; Ogden and Traynelis, 2013; Zhou and Wollmuth, 2017). It has been proposed that the pre-M1 helix is one-third of a triad also containing its intrasubunit M3 pore-forming helix and the pre-M4 region of the adjacent subunit (Chen et al., 2017; Ogden et al., 2017). This triad theory also provides an explanation for the nonequivalent contributions to gating of the GluN1 and GluN2 subunits because the pre-M1 helices of the different subunits make unique interactions with their surrounding regions (Banke and Traynelis, 2003; Tajima et al., 2016). Therefore, we propose that pre-gating conformational changes reflect two distinct sets of linker/TMD interactions that involve both subunits. Additionally, we propose a relatively slow conformational change dominated by GluN2 that involves the triad comprising the GluN2 pre-M1 helix, the GluN2 SYTANLAAF region, and the GluN1 pre-M4 linker (**Figure 4.5**). Each of these regions has conserved function and is under the strongest purifying selection demonstrated by a lack of variability within these regions in the healthy population (Ogden et al., 2017; Swanger et al., 2016).

Overall, the results presented here emphasize the role of the pre-M1 helix in channel gating and allow us to propose a mechanism of activation that requires pre-gating of only three of the four NMDA receptor subunits. Moreover, this study shows that a structurally constrained model can account for single channel and macroscopic properties of the NMDA receptor, can provide insight into how distinct subunits contribute to the gating mechanism, and can help explain some of the unique functional properties of disease-associated mutant receptors.

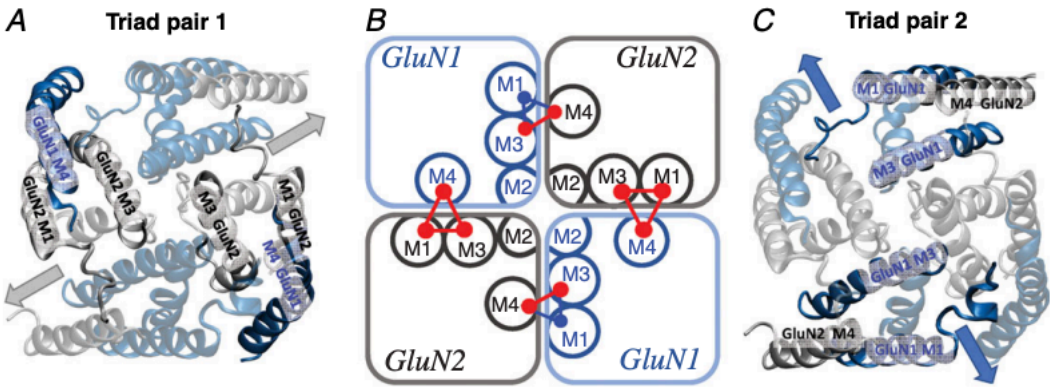

Figure 4.5: Two distinct triads that may underlie subunit-dependent pre-gating conformational changes

A) Ribbon structure of the transmembrane domains and linker regions of the NMDA receptor highlighting the GluN1 subunit pre-M4 region and GluN2 subunit pre-M1 and M3-SYTANLAAF regions that we propose interact to form a pre-gating triad. The gray arrows represent the pore dilation movement. **B)** Schematic diagram illustrating the four proposed triads, two of which are dominated by the GluN2 pre-M1 helix and two of which are dominated by the GluN1 pre-M1 helix. **C)** A second pair of triads is formed by the pre-M1 helix and the M3-SYTANLAAF regions of the GluN1 subunit and the GluN2subunit pre-M4 region. The blue arrows represent the pore dilation movement, which is thought to be less influenced by the GluN1 pre-M1 centric triad.

Chapter 5: Functional Effects of a Disease-Associated Mutation in the S1-M1 Linker

Abstract

Mounting evidence has shown that the gating mechanism of the NMDA receptor involves the pre-M1 helix in the linker between the ABD and the TMD. The functionally-critical pre-M1 helix is completely devoid of missense mutations within the healthy population, but a locus for *de novo* mutations associated with neurological disorders. One such *de novo* mutation, GluN1-L551P, was identified in a 9-year old female patient after presenting early in life with intellectual disability, developmental delay, and epilepsy. In this study, we measure the effects of GluN1-L551P on agonist potency, pharmacology, surface expression, and kinetic profile. Our results showed that GluN1-L551P significantly increased both glutamate and glycine potency, enhanced proton sensitivity 2-fold, significantly prolonged the deactivation time course, and reduced peak current and surface expression. Taken together, these results emphasize the complex functional characteristics of receptors containing the GluN1-L551P subunit. As a consequence of reduced surface expression, enhanced proton sensitivity, and reduced peak current, hypofunction of the NMDA receptor may be the most likely explanation for the abnormal neurological profile found in the GluN1-L551P patient.

Introduction

The S1-M1 linker of the NMDA receptor houses the two-turn pre-M1 helix that has been proposed to facilitate channel gating through Van der Waals interactions with the pore-forming third transmembrane (M3) helix (Gibb et al., 2018; Karakas and Furukawa, 2014; Lee et al., 2014; Schorge et al., 2005; Sobolevsky et al., 2009; Talukder et al., 2010; Talukder and Wollmuth, 2011). Characterization of a subset of missense mutations within the GluN1 S1-M1 linker has revealed significant functional consequences likely contributing to the associated neurological abnormalities (Gibb et al., 2018; Ogden et al., 2017). Specifically, GluN1-D552E and GluN1-P557R were identified in patients with intellectual disability and/or epilepsy. Characterization of these two mutations revealed reduced current responses to saturating agonist and reduced surface expression relative to total when co-expressed with GluN2A (Ogden et al., 2017). GluN1-P557R displayed reduced glutamate and glycine potency, while GluN1-D552E displayed increased agonist potency. When the Genome Aggregation Database (gnomAD) was used to assess the variation in the GluN1 S1-M1 linker, it revealed an absolute lack of missense mutations between residues 546 and 561 in a population of over 140,000 healthy individuals (gnomad.broadinstitute.org). Overall, genetic analysis would suggest that a missense mutation in the S1-M1 linker region of the GluN1 subunit could have significant effects on receptor function and, consequently, brain health.

One *de novo* mutation in this region, GluN1-L551P, has recently been identified in a 9-year old female patient after she presented early in life with intellectual disability, developmental delay, and epilepsy (Fry et al., 2018). Although her corpus callosum, lateral ventricles, and hippocampi appeared healthy, her cortex showed evidence of bilateral perisylvian polymicrogyria. Such cortical malformations, characterized by an excess of small gyri and

abnormal cortical lamination particularly in the region surrounding the sylvian fissures, are commonly associated with mild mental retardation, epilepsy, and pseudobulbar palsy (Kuzniecky et al., 1993; Villard et al., 2002).

Previously, this residue has been studied for its effects on the activity of NMDAR positive allosteric modulator GNE-9278, which binds to the extracellular surface of the TMD. When mutated to alanine, GluN1-Leu551 reduced glutamate EC_{50} by ~10% and completely abolished GluN1/GluN2A potentiation by GNE-9278 (Wang et al., 2017). Additionally, GluN1-Leu551 and a number of its surrounding residues are highly conserved across several species (Fry et al., 2018; Ohba et al., 2015), suggesting that there may exist an evolutionary advantage to retaining this specific amino acid (**Figure 5.1**). Interestingly, however, the leucine residue is not conserved among the other GluN subunits, consistent with the finding that the pre-M1 helices of different GluN subunits contribute differently to channel function and gating (McDaniel et al., 2019). When GluN1-L551P was investigated for its effect on hydrogen bonds between the glycine ligand and the glycine-binding residues of GluN1, it was predicted that the number of bonds would increase from 4 for wild-type to 9, suggesting that the mutation could contribute to altered kinetics of co-agonist binding (Fry et al., 2018). Structurally, the location of the GluN1-Leu551 residue within the S1-M1 linker suggests that it might have an effect on channel gating and function. A homology model of the GluN1/GluN2A receptor puts GluN1-Leu551 in close proximity to the GluN1 M1, M3, and M4 helices, as well as the GluN2A M3 helix. Moreover, GluN1-Leu551 is located just upstream of the pre-M1 helix that is involved in the triad between the GluN1 S1-M1 linker, the GluN1 M3 helix, and the GluN2A pre-M4 helix proposed to control gating, and several disease-associated mutations have been identified within these regions (Ogden et al., 2017; Ogden et al., 2014; Ohba et al., 2015). Moreover, modeling the

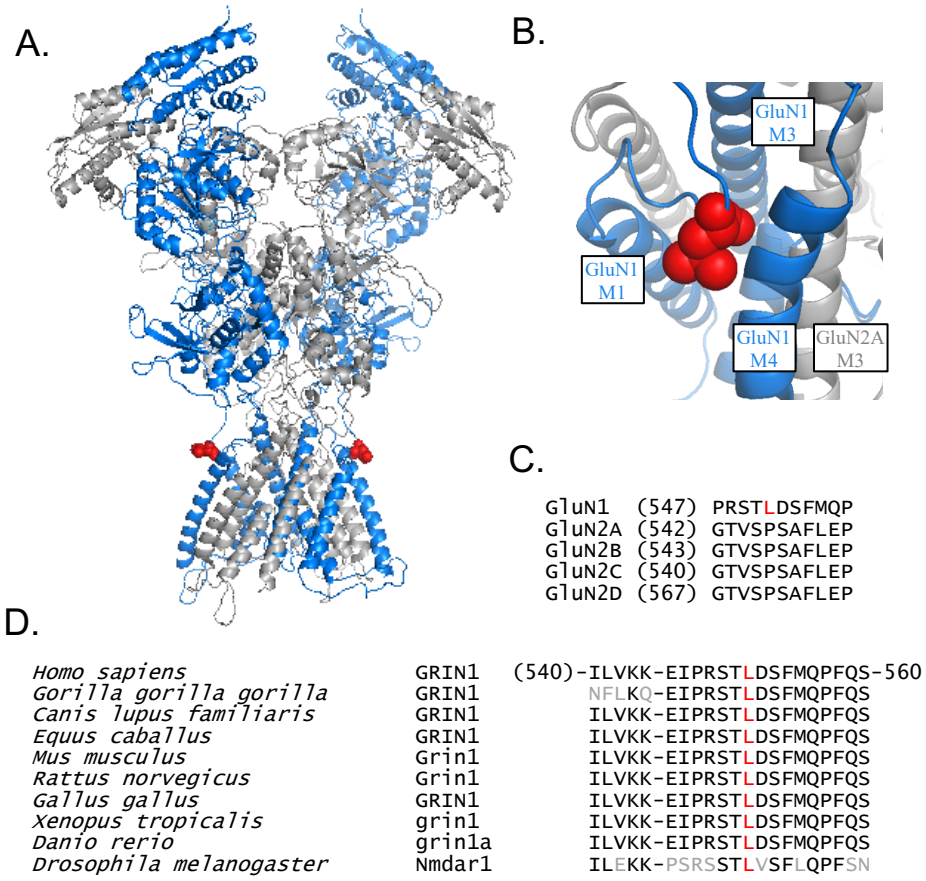

Figure 5.1: GluN1-Leu551 Location and Sequence Alignment
A) Homology model of a GluN1/GluN2A NMDA receptor. GluN1 subunits are shown in blue, and GluN2A subunits are shown in gray. GluN1-Leu551 is shown in red. **B)** Close-up view of GluN1-Leu551 showing neighboring helices: GluN1 M1 helix, GluN1 M3 helix, GluN1 M4 helix, and GluN2A M3 helix. **C)** Sequence alignment of the S1-M1 linker in the GluN subunits shows that GluN1-L551P is not conserved. **D)** Sequence alignment of the GluN1 subunit across several species reveals that this residue is conserved, along with the majority of the surrounding residues. Adapted from Fry et al., 2018.

effects of the GluN1-L551P mutation on the position of other regions of the GluN1 subunit suggested that GluN1-L551P altered the position of the extracellular gating region of the M3 helix by 6.5 Å (Fry et al., 2018).

Based on the information presented thus far, we hypothesized that GluN1-L551P would have significant functional effects that contribute to the phenotype displayed by the patient. To test this hypothesis, we co-expressed the GluN1-L551P mutation with GluN2A or GluN2B and measured the effects on pharmacology, kinetics, and trafficking using two-electrode voltage clamp, whole-cell electrophysiology, and the β-lactamase assay, respectively. We found that GluN1-L551P produced profound functional consequences, contributing to the mounting evidence that the S1-M1 linker and its individual residues 1) play an important role in channel function and 2) may explain the neuronal abnormalities identified in the patient with this specific *de novo* mutation.

Results

GluN1-L551P Increases Agonist Potency

The GluN1-L551P mutation was identified in a 9-year-old female patient displaying several neuroatypical characteristics including bilateral polymicrogyria, intellectual disability, developmental delay, and epilepsy. GluN1-Leu551 resides within the highly conserved S1-M1 linker of the GluN1 subunit suggests that it is likely functionally consequential and, therefore, disease causing. To test this hypothesis, we co-expressed the mutant subunit with either wild-type GluN2A or wild-type GluN2B using *Xenopus* oocytes. We then used two-electrode voltage clamp to measure the current in response to increasing concentrations of agonist. With glycine held at a maximally effective concentration, we applied glutamate over a range of concentrations

and measured the associated current response. The concentration-response curve was used to determine that the half-maximally effective concentration (EC_{50}) of glutamate for the GluN1-L551P/GluN2A receptor was increased approximately 17-fold from 2.98 μM for wild-type GluN1/GluN2A to 0.18 μM. When we maintained a maximally effective concentration of glutamate and varied the concentration of glycine, the concentration-response curve revealed an approximate 72-fold increase in glycine potency from 0.82 μM for wild-type GluN1/GluN2B to 0.011 μM. Similarly, when GluN1-L551P was co-expressed with GluN2B, glutamate potency increased approximately 60-fold from 1.34 μM for wild-type GluN1/GluN2B to 0.023 μM, and glycine potency increased approximately 15-fold from 0.39 μM for wild-type GluN1/GluN2B to 0.03 μM (**Figure 5.2, Table 5.1**). These data suggest that the GluN1-L551P mutation produces significantly enhanced sensitivity of NMDAR to both of their glutamate and glycine co-agonists.

GluN1-L551P Alters Receptor Pharmacology

One clinically important feature of the NMDA receptor is its ability to be regulated by a series of endogenous modulators. Specifically, magnesium ions, protons, and zinc act as negative allosteric modulators and inhibit the ability of the NMDAR to pass current. Using the same *Xenopus* oocyte expression system and voltage-clamp method, we produced a concentration-response curve for magnesium at maximally effective glutamate and glycine concentrations. Analysis of the Mg^{2+} concentration-response curve revealed that the GluN1-L551P mutation had no effect on magnesium potency when co-expressed with GluN2A, with an IC_{50} of 20 μM relative to the 21 μM of the wild-type receptor. Application of Zn^{2+} at maximally effective agonist concentrations produced an IC_{50} of 8.0 μM for the GluN1-L551P/GluN2A receptor, which matches that of the wild-type GluN1/GluN2A receptor. When we investigated inhibition

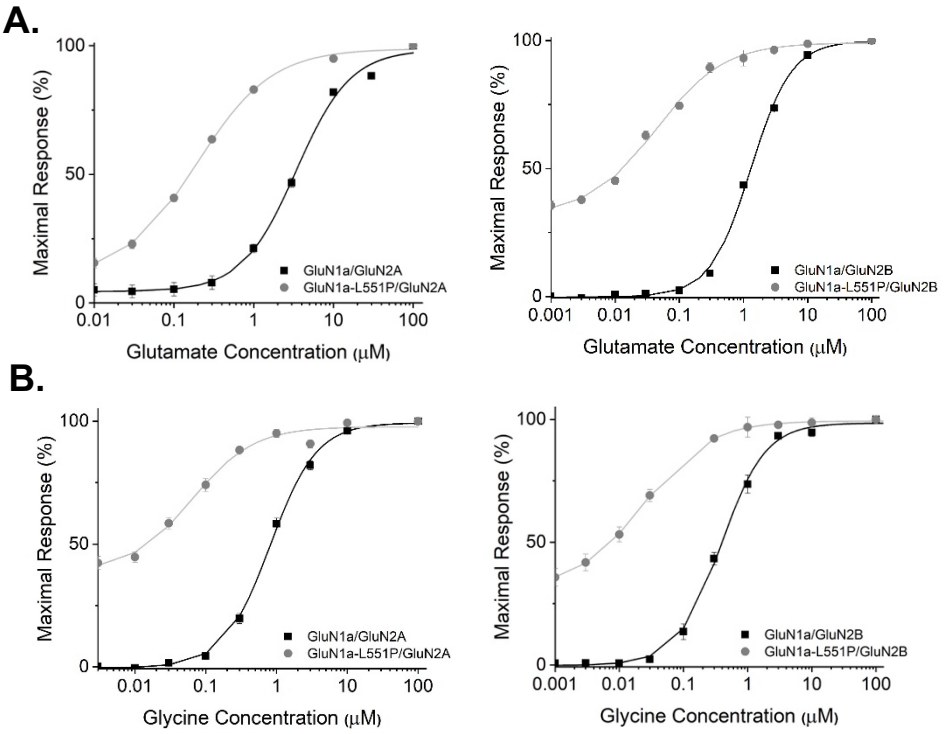

Figure 5.2: GluN1-L551P enhances glutamate and glycine potency. Steady-state concentration-response curves for glutamate in the presence of 100 μM glycine **(A)** and glycine in the presence of 100 μM glutamate **(B)**. The Hill equation was fitted to the composite data for GluN1/GluN2A wild-type, GluN1-L551P/GluN2A, GluN1/GluN2B wild-type, and GluN1-L551P/GluN2B. GluN1-L551P shifted glutamate potency approximately 17-fold (EC_{50} from 2.98 μM to 0.18 μM) and glycine potency approximately 7-fold (EC_{50} from 0.82 μM to 0.011 μM) when co-expressed with GluN2A. When co-expressed with GluN2B, GluN1-L551P shifted glutamate potency approximately 58-fold (EC_{50} from 1.34 μM to 0.023 μM) and glycine potency approximately 13-fold (EC_{50} from 0.39 μM to 0.03 μM) Fitted EC_{50} values can be found in Table 1. Data shown here collected by CFERV.

Table 5.1: Summary of GluN1-L551P Pharmacology

	GluN1/ GluN2A	N	GluN1-L551P/ GluN2A	N	GluN1/ GluN2B	N	GluN1-L551P/ GluN2B	N
Glu EC_{50} (μM)	2.98 (2.6-3.4)	12	0.18* (0.15-0.21)	12	1.34 (1.2-1.5)	14	0.023* (0.018-0.031)	11
Gly EC_{50} (μM)	0.82 (0.70-0.95)	13	0.011* (0.007- 0.017)	15	0.39 (0.33-0.46)	12	0. 030* (0.019-0.037)	12
Mg^{2+} IC_{50} (μM)	21.4 (16-28)	21	20.5 (14-29)	15	25.5 (16-34)	12	15.0* (13-17)	12
Zn^{2+} IC_{50} (μM)	0.008 (0.006-0.011)	24	0.008 (0.005-0.012)	17	--	-	--	-
Proton, $I_{pH\ 6.8}/I_{pH\ 7.6}$ (%)	49 ± 3.3	19	26 ± 1.5*	16	14 ± 1.5	20	8.4 ± 1.2*	20

All data are from GluN1 co-expressed with either GluN2A or GluN2B; the concentration response curve for each recording was fitted by the Hill equation, $Response(\%)=100/(1+(EC_{50}/concentration)^{H})$ where EC_{50} is the concentration of agonist that produces a half maximal response and *H* is the Hill slope, which remained largely unchanged among mutants. Data are mean EC_{50} with the 95% confidence interval determined from the log EC_{50} given in parentheses (two significant figures). Proton inhibition is given as percent ± SEM. N is the number of oocytes recorded. Data collected by CFERV.

* Indicates non-overlapping confidence intervals between mutant and wild-type receptor

by protons, however, the concentration-response curves revealed that the mutant receptor enhanced proton inhibition. The current recorded at pH 6.8 as a percent of that recorded at 7.6 was 49% for wild-type GluN1/GluN2A and 26% for GluN1-L551P/GluN2A (**Figure 5.3, Table 5.1**).

When co-expressed with the GluN2B subunit, GluN1-L551P produced a 1.7-fold decrease in Mg^{2+} IC_{50}, from 26 μM for the wild-type GluN1/GluN2B receptor to 15 μM. GluN1-L551P/GluN2B also resulted in enhanced proton sensitivity, with the current recorded at pH 6.8 as a percent of that recorded at 7.6 being 14% for wild-type GluN1/GluN2B and 8% for GluN1-L551P/GluN2B. Overall, the GluN1-L551P mutation resulted in enhanced proton sensitivity when co-expressed with both GluN2A and GluN2B but resulted in little to no effect on inhibition by magnesium or zinc (**Figure 5.3, Table 5.1**).

GluN1-L551P Slows Receptor Deactivation

In order to assess the effects of the GluN1-L551P mutation on receptor kinetics, we expressed the mutant and wild-type GluN1 subunits with either GluN2A or GluN2B in HEK293 cells. Cells were transferred to a recording chamber where they were perfused with maximally saturating concentrations of glycine with applications of saturating glutamate for either 5 ms or 1 sec. During the 1 second application of agonist, the mutation showed no significant effect on rise time when co-expressed with either GluN2A or GluN2B. However, co-expression of GluN1-L551P with GluN2A significantly prolonged the deactivation time course, increasing τ_{weighted} from 56 ms for wild-type GluN1/GluN2A to 470 ms. The percent of steady state current to peak current was also increased from 58% to 86%, suggesting a reduction in desensitization. These results were matched by the functional changes observed when GluN1-L551P was co-expressed

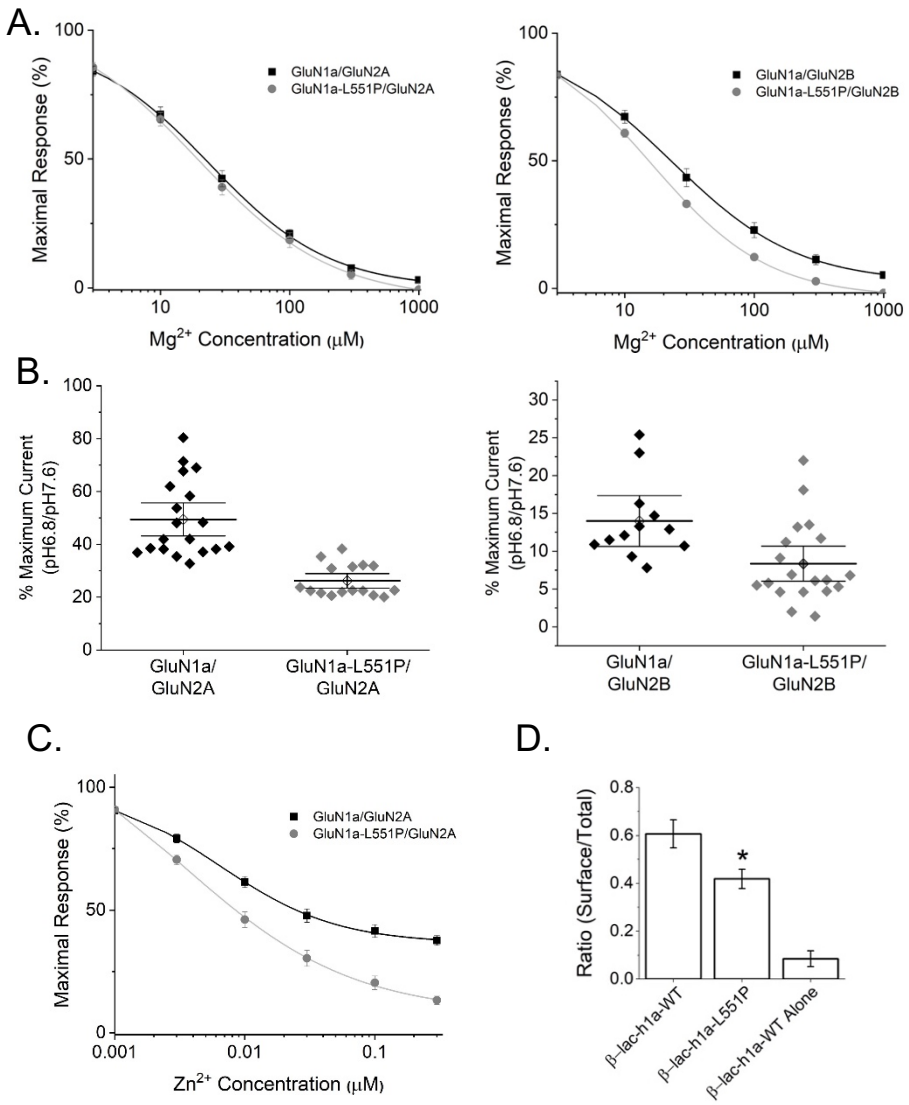

Figure 5.3: GluN1-L551P effects inhibition by antagonists and surface expression.
A) Steady-state concentration-response curves for magnesium in the presence of 100 µM glycine and 100 µM glutamate. GluN1-L551P had no effect on magnesium potency with GluN2A and shifted magnesium potency ~1.7-fold (IC_{50} from 26 µM to 15 µM) when co-expressed with GluN2B. **B)** Proton sensitivity as determined from the peak current measured at pH 6.8 relative to that measured at pH 7.6. GluN1-L551P modestly enhanced proton sensitivity about 2-fold when co-expressed with GluN2A or GluN2B. **C)** When co-expressed with GluN2A, GluN1-L551P had no observable effect on zinc IC_{50}. Quantification of the data can be found in Table 1. Two-electrode voltage clamp performed by CFERV. **D)** Ratio of surface expression to total expression for GluN2A when co-expressed with ß-lactamase tethered wild-type or mutant GluN1. GluN1-L551P reduced the surface expression of GluN2A receptors by ~30%.
* $p<0.05$ compared with WT, unpaired t-test.
Refer to Table 5.1.

with GluN2B. While rise time remained unchanged, $\tau_{weighted}$ increased from 520 ms for wild-type GluN1/GluN2B to 5900 ms, and the steady state to peak current ratio increased from 75% to 80%. Moreover, introduction of the mutant GluN1 subunit produced currents with drastically reduced peak amplitudes. GluN1-L551P reduced current amplitude 2.5-fold and 5.8-fold when expressed with GluN2A and GluN2B, respectively (**Figure 5.4, Table 5.2**).

GluN1-L551P Reduces Surface Expression

We hypothesized that GluN1-L551P would have altered receptor localization as suggested by its altered agonist potency and reduced current amplitude. That is, we predicted that at least some of the measured reduction in current amplitude was due to the inability of the receptor to effectively traffic to the surface. To quantitatively assess the effect of GluN1-L551P mutation on receptor trafficking, we implemented a β-lactamase reporter assay. We fused the β-lactamase enzyme to the extracellular region of the GluN1 subunit and expressed it with wild-type GluN2A in HEK293 cells. The enzyme cleaves the cell- impermeable chemogenic substrate nitrocefin resulting in a measurable change in absorbance (See Chapter 2). Changes in absorbance over time would suggest that the enzyme and its tethered receptor were able to traffic to the cell surface, while no change in absorbance would suggest an inability to traffic. To measure changes to total expression, cells were lysed before nitrocefin was added and absorbance was measured. The forwarding trafficking efficiency was determined by the ratio of surface-to-total protein levels. Despite an increase in agonist potency, GluN1-L551P had no effect on total receptor expression, but reduced surface-to-total ratio when co-expressed with GluN2A from 0.61 ± 0.06 to 0.42 ± 0.04 (Figure 5.3).

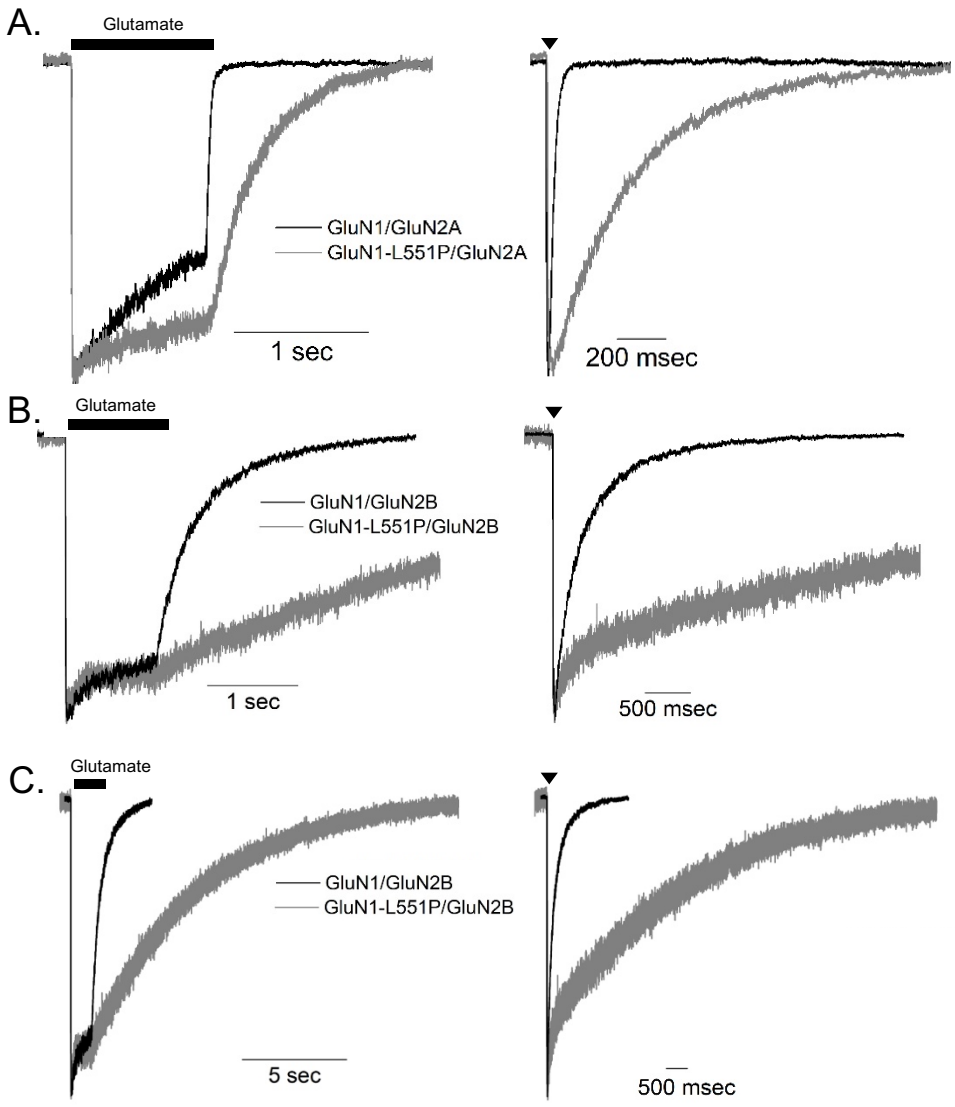

Figure 5.4: GluN1-L551P significantly prolongs the glutamate deactivation time course. Representative current response time course from whole-cell patch clamp recordings of wild-type and mutant GluN1 co-expressed with GluN2A **(A)** or GluN2B **(B)** activated by a 1 second pulse (Left panels, black bar) or 5 ms pulse (Right panels, black arrow) of 1 mM glutamate in the continuous presence of 30 µM glycine. The response time courses are normalized to the peak current levels to allow comparison of the deactivation time course. Rise times did not differ significantly for the mutant subunits when compared to wild-type. GluN1-L551P prolonged the weighted deactivation time course by approximately 8-fold from 56 ms to 470 ms when co-expressed with GluN2A and by approximately 11-fold from 520 ms to 5900 ms when co-expressed with GluN2B as determined following the 5 ms pulse of glutamate. Summary of fitted values can be found in Table 2. **C)** Representative current response time course shown in (B) on a time scale to show full deactivation of the mutant receptors.

Table 5.2: Summary of GluN1-L551P Kinetic Profile

	GluN1/GluN2A	GluN1-L551P/ GluN2A	GluN1/GluN2B	GluN1-L551P/ GluN2B
N	7	7	8	7
Rise Time (ms)	7.2 ± 0.9	6.5 ± 1.2	8.5 ± 0.4	7.2 ± 0.6
I_{Peak} (pA)	1030 ± 200	420 ± 170*	560 ± 140	97 ± 29*
τ_{Fast} (ms)	34 ± 6	320 ± 50	210 ± 21	---
τ_{Slow} (ms)	230 ± 50	640 ± 150	750 ± 47	5900 ± 400
% τ_{Fast}	78 ± 10	75 ± 8	41 ± 4	---
τ_{w} (ms)	56 ± 5	470 ± 40*	520 ± 21	5900 ± 400*
SS/I_{Peak} (%)	58 ± 3	86 ± 1	75 ± 3	80 ± 5

Data are mean ± SEM and given to two significant figures.
* $p<0.05$ compared with associated wild-type GluN2A or GluN2B, unpaired t-test. Analysis performed on rise time, peak current, and weighted τ.

Discussion

The *de novo* mutation encoded by the *GRIN1* gene, GluN1-L551P, has recently been identified in a 9-year old female patient after she presented early in life with intellectual disability, developmental delay, and epilepsy (Fry et al., 2018). This residue is of particular interest due to its location within the S1-M1 linker thought to control channel gating (Gibb et al., 2018; Ogden et al., 2017), its conservation across several species (Fry et al., 2018; Ohba et al., 2015), and its location within a sequence of amino acids that houses no missense mutations in the healthy population (gnomad.broadinstitute.org). Together, this functional and genetic information would suggest that the GluN1-Leu551 residue plays an important role in channel function, such that a mutation at this position could lead to drastic changes in receptor properties and, ultimately, changes in overall brain function. Here we provide the first analysis of the functional, pharmacological, and expression consequences of the GluN1-L551P mutant. Our data support the hypothesis that the GluN1-L551P causes aberrant receptor function which could explain the neurological abnormalities experienced by the patient.

Because GluN1 serves as the obligatory subunit for the NMDA receptor, its co-expression with GluN2A or GluN2B could be even more consequential in the developing brain during which time the GluN2B subunit reaches its peak expression and the GluN2A subunit expression begins to increase throughout the CNS. Therefore, a gain-of-function mutation could lead to overactivation of receptors whose function needs to be tightly regulated to allow for normal neuronal circuitry to develop or to neuron damage as a result of excitotoxicity (Choi, 1992; Choi, 1994). NMDA receptor hyperfunction has been linked to the development of several neurological disorders including Alzheimer's disease (Hynd et al., 2004), Huntington's disease (Zeron et al., 2002), epilepsy (Lemke et al., 2014; Rice and DeLorenzo, 1998; Yuan et al.,

2015b), and intellectual disabilities (XiangWei et al., 2018). Alternatively, NMDA receptor hypofunction associated with schizophrenia (Coyle, 2006; Olney et al., 1999) and memory impairment (Newcomer et al., 1999). As such, based on the phenotypic profile of the patient displaying intellectual disability, developmental delay, and epilepsy we would hypothesize that the GluN1-L551P results in overall hyperfunction of the NMDA receptor.

Two-electrode voltage clamp experiments revealed that the disease associated GluN1-L551P mutation leads to a significant increase in glutamate and glycine potency when co-expressed with either the GluN2A or the GluN2B subunit. As a consequence of increased agonist potency, receptors that include the mutated GluN1 subunit will be particularly sensitive to glutamate and glycine, likely leading to increased activation at concentrations of agonists that would otherwise be too low to elicit a response. Moreover, the beta-lactamase assay revealed that the GluN1-L551P mutation resulted in reduced surface expression of the receptor despite no measurable change in total expression. This result suggests that the trafficking of the functional receptor is impaired with the presence of the GluN1-L551P mutation. Such trafficking impairment could be of physiological consequence because a reduction in the number of functional receptors at the synapse could result in insufficient postsynaptic activation, reduced synaptic strength, and abnormal neurodevelopment. However, while reduced surface expression in HEK cells may account for reduced peak current, measuring the changes in receptor trafficking in neurons would be helpful to more confidently conclude that this mechanism contributes to the GluN1-L551P patient phenotype.

Electrophysiological analysis of the GluN1-L551P mutation also revealed that this subunit, when co-expressed with either GluN2A or GluN2B, resulted in a significantly prolonged deactivation time course relative to the respective wild-type. This finding is consistent with the

characterization of other disease-associated mutations within the GluN1 S1-M1 linker. Specifically, GluN1-P557R (Gibb et al., 2018; Ogden et al., 2017) and GluN1-D552E (Ogden et al., 2017) also resulted in a prolonged deactivation time course. Moreover, GluN1-L551P containing receptors displayed a significant reduction in peak current and desensitized less profoundly than their wild-type counterparts. Overall, the electrophysiological data supports the hypothesis that the S1-M1 linker contributes to the activation of the NMDA receptor in response to agonist binding. Because the S1-M1 linker is responsible for facilitating the communication between the ABD and the channel pore, it is likely that mutations in this region are of measurable functional consequence.

The mechanism by which the GluN1-L551P mutation might contribute to disease, however, remains unclear. Although the increased glutamate and glycine potency, the prolonged deactivation time course, and the reduced desensitization would suggest that the mutation results in a gain-of-function receptor, the impaired surface trafficking, reduced current amplitude, and enhanced proton sensitivity are more consistent with loss-of-function. Even without a comprehensive understanding of exactly how the GluN1-L551P mutation contributes to the disease state, its effect on the function of the NMDA receptor is apparent. Leucine has a side chain isobutyl group, making it a nonpolar aliphatic amino acid. Proline, while still considered a nonpolar aliphatic amino acid, has a side chain pyrrolidine. This cyclic structure of proline lends itself to greater conformational rigidity compared to leucine and the other amino acids. As such, if flexibility of the S1-M1 linker is required for transducing agonist binding to channel opening, then it is likely that a proline substitution in this region would disrupt this mechanism.

Overall, the GluN1-L551P mutation leads to significantly altered NMDA receptor function that might contribute to the phenotypic abnormalities displayed by the patient.

Moreover, the results from this study provide an example of a single amino acid substitution that leads to a combination of functional consequences ultimately leading to a physiologically disruptive NMDA receptor.

Chapter 6: Functional Effects of Genetic Variation within NMDA Receptor Domains

Parts of this chapter have been published:

Regan MC, Grant T, McDaniel MJ, Karakas E, Zhang J, Traynelis SF, Grigorieff N and Furukawa H (2018) Structural mechanism of functional modulation by gene splicing in NMDA receptors. *Neuron* **98**(3): 521-529. e523.

Wells G, Yuan H, McDaniel MJ, Kusumoto H, Snyder JP, Liotta DC and Traynelis SF (2018) The GluN2B-Glu413Gly NMDA receptor variant arising from a de novo GRIN2B mutation promotes ligand-unbinding and domain opening. *Proteins: Structure, Function, and Bioinformatics* **86**(12): 1265-1276.

Abstract

Excitatory neurotransmission in the brain is mediated by glutamate binding to and activating ionotropic receptors. N-methyl-D-aspartate (NMDA) receptors are thought to make up the slow component of fast excitatory neurotransmission and have been deemed critical for normal brain development, synaptic plasticity, and long-term memory formation. Aberrant NMDA receptor function has been associated with several neurological disorders, and missense *de novo* mutations have been tied to epilepsy, intellectual disabilities, and developmental delays. NMDA receptors are tetrameric proteins typically formed from the assembly of two glycine-binding GluN1 subunits and two glutamate-binding GluN2 subunits. The eight splice variants of GluN1 and the four subunits (A-D) of GluN2 endow the receptor with distinct properties. Moreover, some regions of the GluN subunits show a high degree of conservation. For example, the exon 5 motif of the GluN1 subunit can be found across several species and the glutamate binding site is identical across the GluN2 subunits, suggesting that these regions play a vital role in channel function. In this study, we mutated residues within the exon 5 motif of GluN1 and the ABD of GluN2B and measured the effects on deactivation using whole-cell patch clamp. We then correlated deactivation rate to proton sensitivity and agonist egress time for the exon 5 motif and GluN2B ABD, respectively. For exon 5, we found a direct correlation between proton IC_{50} and $\tau_{weighted}$, a direct correlation between proton IC_{50} and τ_{fast}, and an inverse correlation between proton IC_{50} and % τ_{fast}. For the GluN2B ABD, we found a direct correlation between ligand egress and $\tau_{weighted}$. Overall, this study provides evidence that the highly conserved exon 5 motif and GluN2 agonist binding site are critical for channel function, that deactivation correlates with other unique properties of the NMDA receptor, and that genetic diversity can be used as a tool to investigate the role of certain parts of the NMDA receptor in overall function.

Introduction

The function of NMDA receptors has largely been understood in the context of the GluN1 and GluN2 subunits that comprise it. The subunits make extensive contact with each other, allowing for unique and important allosteric communication that influences channel function. Furthermore, different subunits endow the receptor with distinct spatial, pharmacological, and kinetic properties making it particularly valuable to consider how these subunits interact (Akazawa et al., 1994). The functional properties of each receptor are further influenced by the domains that make up each subunit. When these domains present genetic variation in the form of splice variation or missense mutations, receptor function can be drastically impacted (Laurie and Seeburg, 1994; Paupard et al., 1997; Swanger et al., 2016; Zhong et al., 1995). Moreover, some regions within the NMDA receptor domains are highly conserved across subunits or throughout evolution, suggesting that these regions are particularly important for channel function. However, the role of the semi-autonomous domains and their interactions in NMDA receptor function remains unclear. Guided by naturally existing mechanisms of biodiversity and aberrant genetic variation, we can better understand how the function of the NMDA receptor is influenced by evolutionarily conserved functional regions.

For example, the GluN1 subunit is ubiquitously expressed in the central nervous system (CNS), serves as the obligatory subunit of the NMDA receptor, and is responsible for binding co-agonist glycine (Dingledine et al., 1999). It is encoded by a single gene (*GRIN1*), but can be alternatively spliced to produce eight different isoforms (Durand et al., 1992; Hollmann et al., 1993; Nakanishi et al., 1992; Sugihara et al., 1992), which show distinct regional, developmental, functional, and pharmacological profiles. (Laurie and Seeburg, 1994; Paupard et al., 1997; Zhong et al., 1995). Exon 5, for example, encodes a 21 amino acid sequence in the

ATD. The sequence of exon 5 is highly conserved throughout vertebrate GluN1 subunits, suggesting that this region likely serves an important evolutionary role in healthy neurological function (Hansen et al., 2018).

It has been hypothesized that the residues encoded by exon 5 might facilitate communication between the ATD of the GluN1 and the ABDs of GluN1 and GluN2 based on the reduced agonist potency and accelerated deactivation time course for receptors containing exon 5 (Cull-Candy et al., 2001; Rumbaugh et al., 2000; Traynelis et al., 1998; Traynelis et al., 1995; Vance et al., 2012). Additionally, the ATDs of NMDA receptors bind subunit-selective antagonists (i.e. ifenprodil at GluN2B), extracellular zinc, and protons. When exon 5 encoded amino acids are present, inhibition by all three of these allosteric modulators is reduced and potentiation by extracellular polyamines is eliminated (Hansen et al., 2018). Pathologically, it has been proposed that exon 5 might contribute to enhanced excitotoxity during ischemia-induced acidosis as a consequence of its effect on proton sensitivity. That is, a decrease in pH resulting from injury, stroke, or seizure could lead to enhanced NMDA receptor activity and, therefore, damage to the neurons if proton inhibition is reduced by the presence of exon 5 (Kaku et al., 1993; Rumbaugh et al., 2000; Traynelis et al., 1995). However, despite its role in both brain physiology and pathology, the mechanism by which exon 5 encoded amino acids exert their control over receptor function has remained elusive.

Like exon 5, the ABDs of the GluN2 subunits show a high degree of conservation. Not only do the GluN2 subunits share 63% sequence identity within their ABDs (Paoletti, 2011), but all ten amino acids that make contact with the glutamate ligand are strictly conserved (Paoletti and Neyton, 2007). Moreover, the identity of the GluN2 subunit endows the receptor with unique spatial, pharmacological, and functional properties despite their high degree of sequence identity

(Paoletti et al., 2013). As such, we can hypothesize that 1) the residues within the ABDs of the GluN2 subunits are particularly important for receptor function, and 2) missense mutations of the residues that comprise the ABDs of GluN2 subunits would alter channel function.

These hypotheses were supported by the discovery of the GluN2B missense *de novo* mutation of glutamate at position 413 (Adams et al., 2014) in a patient with severe neurological and developmental impairment. Exome sequencing revealed a GluN2B-E413G mutation, which is positioned within the ABD clamshell near the binding site of glutamate (Furukawa et al., 2005; Vance et al., 2011) at a residue that is conserve across all GluN2 subunits (Kinarsky et al., 2005). Characterization of this mutation revealed that GluN2B-E413G reduced the glutamate potency >50-fold compared to the wild-type GluN1/GluN2B receptor (Adams et al., 2014), accelerated the deactivation rate ~30-fold (Swanger et al., 2016), and reduced the ratio of surface-to-total expression by 50% (Swanger et al., 2016) . A molecular dynamics model predicted that the GluN2B-E413G mutation introduced a larger solvent-accessible area, suggesting that water can more readily compete for atomic contacts and that the paths that glutamate can take to exit the cleft are increased in number (Swanger et al., 2016). The characterization of this mutation is consistent with the genetic evidence that the ABD residues are highly sensitive to variation. By assessing genetic variation across GluN2 domains, it was revealed that the ABD, TMD, and domain linkers were particularly intolerant to functional variation (Swanger et al., 2016). Moreover, results indicated that the ABD of the GluN2B subunit was far less tolerant to mutation than the ABD of the GluN2A subunit (Swanger et al., 2016). It is necessary, then, to develop a more comprehensive and mechanistic understanding of how the GluN2B ABD facilitates glutamate binding and, ultimately, receptor function.

To explore the functional contributions of highly conserved regions of NMDA receptor, we used mutagenesis to investigate the functional consequences of residue changes within these regions. Specifically, we mutated residues within the exon 5 motif of GluN1 and the ABD of GluN2B and measured the effects on receptor deactivation using whole-cell patch clamp. We identified residues in each of these regions which contribute significantly to deactivation and used these residues to guide a mechanistic understanding of how the GluN1 exon 5 motif and the GluN2B ABD control channel function.

Results

In order to develop a mechanistic understanding of how highly conserved regions of the NMDA receptor contribute to function, we used site-directed mutagenesis to substitute specific residues within the GluN1 exon 5 motif and the GluN2B ABD. We then used whole-cell patch clamp to measure the effect of these mutations on receptor deactivation. Finally, we correlated deactivation data to proton sensitivity and ligand exit time to develop a mechanistic understanding of the role of the exon 5 motif and of the GluN2B ABD, respectively.

Structure of the GluN1 Exon 5 Motif Controls Deactivation Rates

Firstly, single-particle cryo-EM analysis of the GluN1/GluN2B NMDA receptor containing the exon 5 sequence was performed. The receptor was bound by glutamate and glycine agonists, ifenprodil and MK-801 antagonists, and included a functionally inert inter-GluN2B ATD disulfide bond to reduce conformational flexibility. Cryo-EM analysis of this modified receptor clearly showed the heterotetrameric assembly of the GluN1/GluN2B receptor. Moreover, the bilobed GluN2B ATD, GluN1 ABD, and GluN2B ABD domains were found to

be in the closed conformation, consistent with previous structural analysis of these ligand-bound isolated regions. The cryo-EM structure showed density for eight exon 5 encoded residues at the ATD/ABD interdomain interface (GluN1-Tyr204-Lys211), which "caps" the GluN1/GluN2B subunit interface of the ABD through interactions between GluN1-Lys190 and GluN2B-Tyr507 and between GluN1-Lys211 and GluN1-Asp786. Because the regions surrounding these interacting residues are devoid of missense mutations in the healthy population, we hypothesized that these residues are under strong selection due to their importance for receptor function.

Structural biologists Michael Regan and Hiro Furukawa (Cold Spring Harbor Laboratory) explored the architecture of the region surrounding the exon 5 motif using cryo-EM. They found that the region between GluN1-Glu186 and GluN1-Lys190 was altered in the receptor containing exon 5. With exon 5 present, this stretch of residues extends toward the ATD-ABD linker of the GluN2B subunit creating contacts that are specific only for receptors containing exon 5. These contacts include those between GluN1-Lys190 and GluN2B-Tyr507 and between GluN1-Lys211 and GluN2B-Tyr507. Moreover, Michael Regan verified the interactions of the exon 5 motif with the GluN2B subunit by disulfide crosslinking and subsequent western blotting. Possible interactions were identified between the beginning region of the exon 5 motif and the GluN2B ATD-ABD linker (GluN1-Ser191 or Lys192 and GluN2B-Gln401), the beginning region of the exon 5 motif and the GluN2B ABD (GluN1-Ser191 or Lys192 and GluN2B-Gly771), and the end region of the exon 5 motif and the GluN2B ABD (Regan et al., 2018).

Because the presence of exon 5 has been shown to accelerate the deactivation rate of NMDA receptors, we assessed whether or not the residues involved in the intrasubunit interactions within GluN1 and the intersubunit interactions between GluN1 and GluN2B also affected deactivation. Whole-cell patch clamp experiments were conducted on HEK293 cells

expressing the wild-type or mutant receptors containing point mutations which disrupted interactions between the exon 5 motif and the GluN2B ATD-ABD, the beginning region of the exon 5 motif and the GluN2B ABD, and the end region of the exon 5 motif and the GluN2B ABD. Cells were treated with a 5 ms pulse of saturating glutamate (1mM) in the continued presence of saturating glycine (30 μM), and the current response (**Figure 6.1**) was fit by two exponential components (See methods). Disruption of the exon 5/ABD interactions by point mutations at GluN1-Lys190, GluN1-Lys 211, GluN1-Asp786, and GluN2B-Tyr507 had little or no effect in slowing down the NMDA receptor deactivation time course compared to the wild-type GluN1/GluN2B NMDA receptor as monitored by a weighted average of two time constants ($\tau_{weighted}$) (**Figure 6.2A**). Furthermore, conversion of negatively charged residues (**Figure 6.2B**) or truncation of the flexible region of the exon 5 motif (**Figure 6.2C**) resulted in only minimal effects (**Table 6.1**). Together, these results show that to completely reverse the effect of exon 5, its structure and positioning need to be sufficiently altered by a combination of the Δexon5-C truncation and disruption of the exon 5/ABD interaction by the GluN1- K211A mutation (**Figure 6.2C**). Thus, the major factor controlling deactivation rate is the structural arrangement and orientation of the exon 5 motif within the ATD/ABD interface. As such, when the GluN1-GluN2B ABD interface is perturbed by the GluN2B-L781A mutation, the exon 5 mediated control of deactivation rate is abolished, and the deactivation rate becomes equivalent to the exon-5-lacking GluN1/GluN2B NMDA receptor (**Figure 6.2D**).

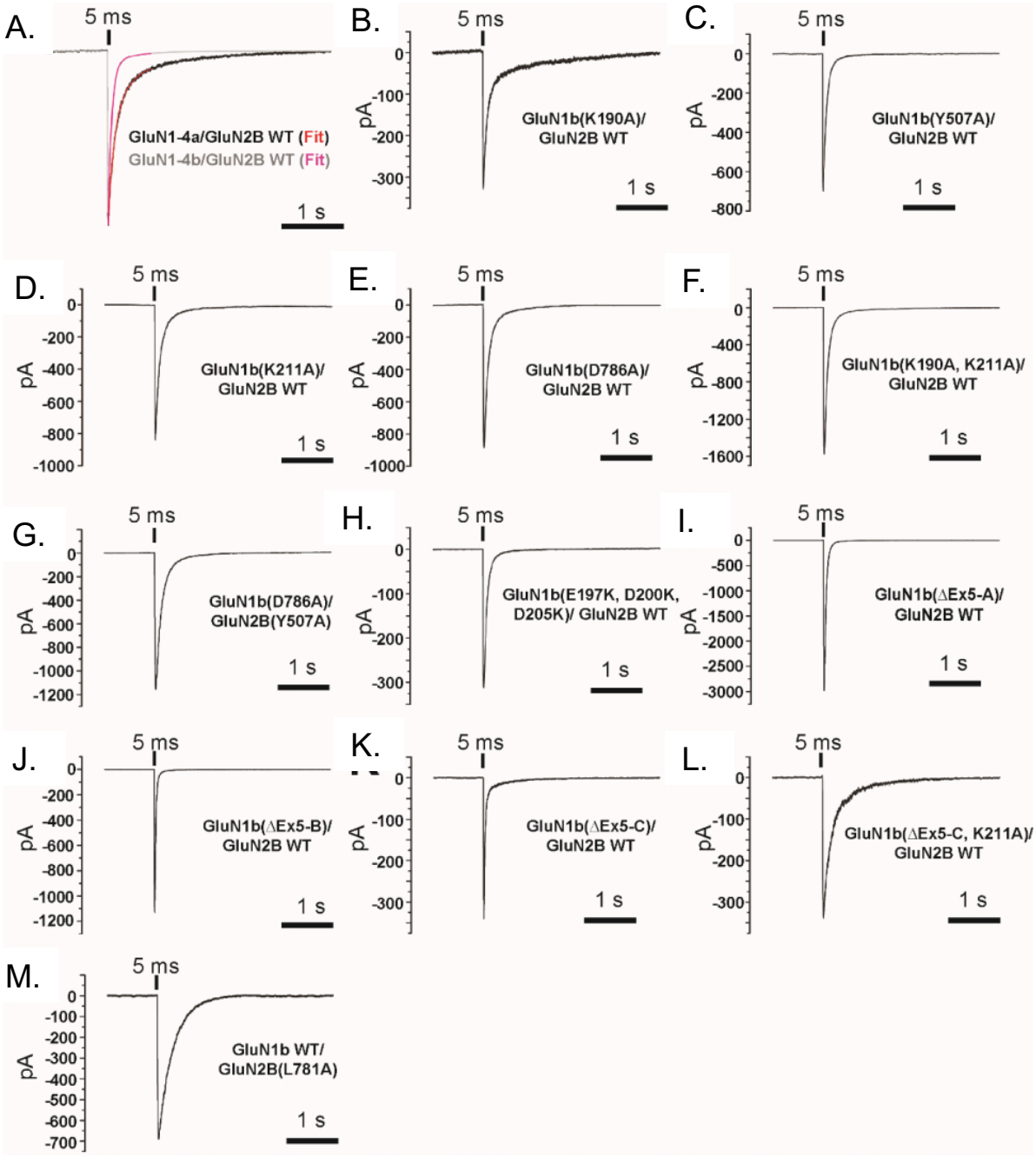

Figure 6.1: Current Responses for Exon 5 or GluN2B Mutants

A) Representative traces for whole cell patch-clamp experiments recorded from HEK cells expressing wild type GluN1-4a/GluN2B (black) and GluN1-4b/GluN2B (grey). Recordings were fit by two exponential functions (See methods) to determine the weighted deactivation rate. The fits for GluN1-4a/GluN2B and GluN1-4b/GluN2B are overlaid in red and magenta, respectively. **B-M)** Representative whole-cell patch clamp recordings from HEK cells expressing various mutants upon activation by a 5 ms application of glutamate (1 mM) in the continued presence of glycine (30 μM).

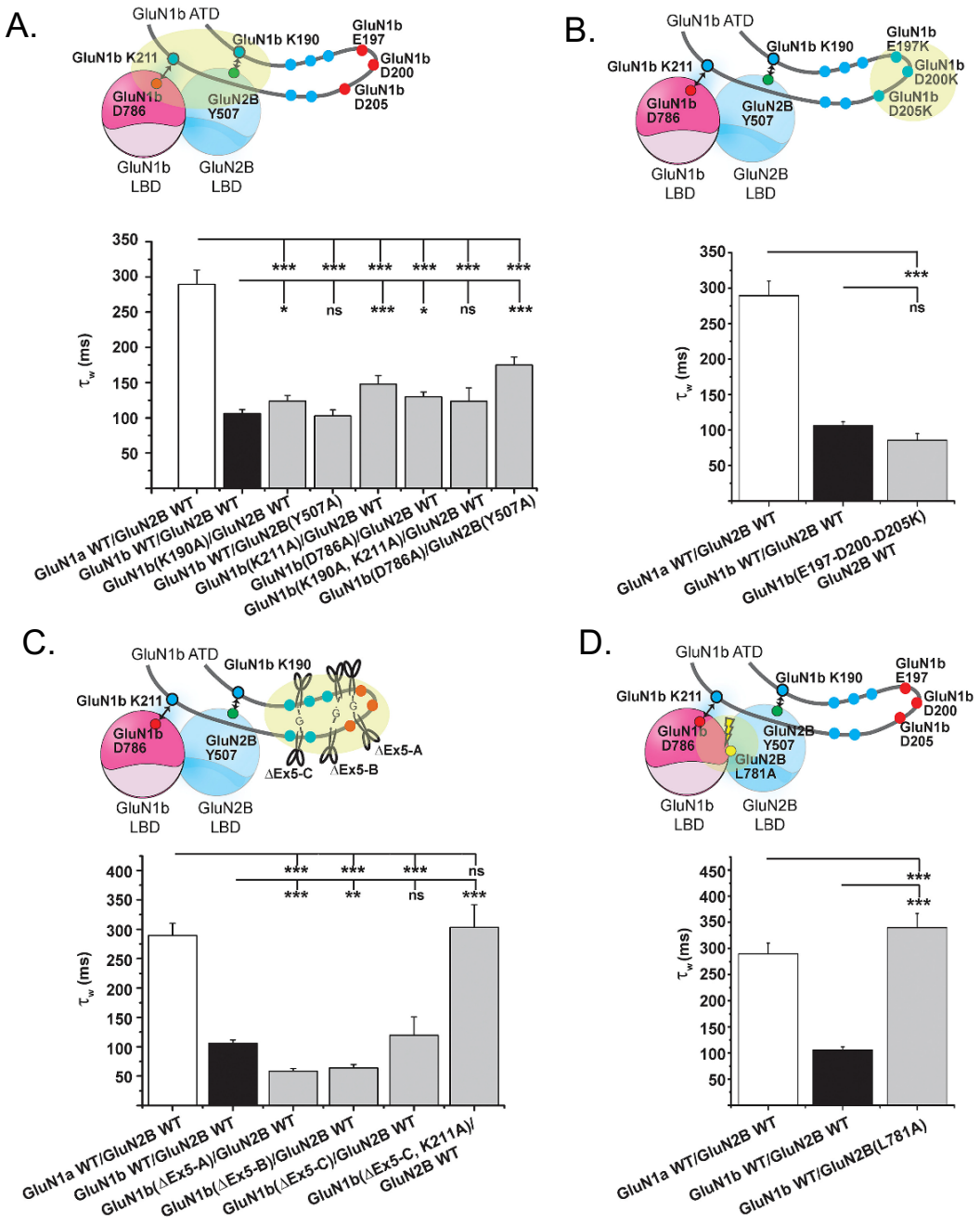

Figure 6.2: Structure and Placement of the Exon 5 Motif at the ATD-ABD Interface Are Critical for Controlling Deactivation Rates

A and B) Mutant GluN1-4b-GluN2B NMDA receptors were tested for deactivation rates in HEK293T cells by whole-cell patch clamp. No pronounced effects were observed by disrupting the exon 5/ABD interactions **(A)** or reversing residue charges **(B)**. **(C)** To reverse the effect of exon 5, a combination of truncation and disruption of the exon 5/ABD interaction (GluN1b DEx5-C/K211A) was tested. **(D)** Disruption of the GluN1b-GluN2B ABD heterodimer interface by GluN2B Leu781Ala overrode the effect of exon 5. Six or more recordings were conducted on transfected HEK293.

*p < 0.05, **p < 0.01; ***p < 0.001; ns, not significant, as determined by one-way ANOVA with Tukey's test. Bar graphs represent mean ± SEM.

Table 6.1: Electrophysiological Data for GluN1 Exon 5 and GluN2B Mutants

#	Construct	τ_{fast}	τ_{slow}	τ_{fast} (%)	$\tau_{weighted}$	n_{wcpc}	pH IC_{50}	n_{tevc}
1	GluN1a WT/ GluN2B WT	113.1 ± 12.1	741.5 ± 52.7	70 ± 2	289.2 ± 21.3	12	7.72 ± 0.02	15
2	GluN1b WT/ GluN2B WT	71.31 ± 3.83	436.5 ± 36.7	88 ± 2	106.2 ± 5.53	44	7.04 ± 0.01	17
3	GluN1b(K190A)/ GluN2B WT	73.21 ± 7.48	467.4 ± 21.6	87 ± 1	124.0 ± 7.90	10	7.33 ± 0.01	5
4	GluN1b WT/ GluN2B(Y507A)	66.59 ± 4.53	427.8 ± 80.9	86 ± 8	102.9 ± 8.50	9	7.28 ± 0.04	6
5	GluN1b(K211A)/ GluN2B WT	94.85 ± 19.5	615.6 ± 89.4	81 ± 6	147.8 ± 12.3	8	7.40 ± 0.04	7
6	GluN1b(D786A)/ GluN2B WT	73.22 ± 9.00	733.1 ± 121.8	86 ± 2	162.5 ± 33.0	8	7.35 ± 0.03	10
7	GluN1b(K190A, K211A)/ GluN2B WT	128.9 ± 47.7	391.0 ± 87.2	82 ± 11	108.8 ± 13.6	8	7.65 ± 0.02	5
8	GluN1b(D786A)/ GluN2B(Y507A)	103.3 ± 12.1	581.1 ± 60.3	84 ± 1	175.1 ± 11.2	7	7.66 ± 0.04	5
9	GluN1b(D197, D200, D205K)/ GluN2B WT	70.32 ± 8.04	249.1 ± 85.2	95 ± 2	85.6 ± 9.69	10	7.21 ± 0.09	5
10	GluN1b(ΔEx5-A)/ GluN2B WT	42.70 ± 4.15	222.7 ± 20.1	92 ± 1	57.07 ± 4.93	11	6.89 ± 0.03	12
11	GluN1b(ΔEx5-B)/ GluN2B WT	46.56 ± 4.35	502.3 ± 150.4	95 ± 1	64.19 ± 5.17	11	6.84 ± 0.06	7
12	GluN1b(ΔEx5-C)/ GluN2B WT	51.13 ± 18.0	336.2 ± 43.8	88 ± 1	87.19 ± 25.2	6	7.21 ± 0.02	8
13	GluN1b(ΔEx5-C, K211A)/ GluN2B WT	147.9 ± 46.7	921.2 ± 162.4	79 ± 5	303.4 ± 38.3	9	7.57 ± 0.02	6
14	GluN1b WT/ GluN2B(L781A)	221.6 ± 22.2	526.3 ± 91.2	51 ± 12	340.0 ± 27.1	7	8.76 ± 0.18	7

pH inhibition data were collected from TEVC experiments conducted by Mike Regan (Cold-Springs Harbor, Furukawa Lab), while τ values are from whole-cell patch clamp experiments recorded with 5 ms application of glutamate (1mM) in saturating glycine (30 μM).
The number of replicates for whole-cell patch clamp or two-electrode voltage clamp experiments is listed as n_{wcpc} and n_{tevc}, respectively. Sequential numbering refers to the specific data point labeled in Figure Z.
WT, wild-type.

Exon 5 Mediated Changes in Receptor Deactivation Correlates with Proton Sensitivity

The relatively minor but statistically significant effects on deactivation rate correlate with the proton sensitivity as assessed by a linear regression analysis. Specifically, time constants ($\tau_{weighted}$, τ_{fast}, and τ_{slow}) and proportion of τ_{fast} were plotted against pH IC_{50} to establish whether or not a correlation exists (**Figure 6.3**). Notably, $\tau_{weighted}$ and τ_{fast} increase as a function of pH IC_{50}, (**Figure 6.3 A-B**) with R values of 0.82 and 0.94, respectively. Moreover, the relative contribution to deactivation by τ_{fast} decreases with an R value of -0.94 as proton IC_{50} increases (**Figure 6.3 C**). These results suggest that the contributions of the exon 5 motif to the NMDA receptor deactivation profile and sensitivity to changes in pH are not independent phenomena.

Mutations Within GluN2B ABD Accelerate Deactivation Rate

As with the GluN1 exon 5 motif, some residues of the ABD, particularly of the GluN2B subunit, are highly conserved and remarkably intolerant to functional variation (Swanger et al., 2016). Moreover, genetic analysis of a patient with developmental delays revealed a mutation, GluN2B-E413G, located in the GluN2B ABD (Adams et al., 2014). This mutation resides in close proximity to the residues that have been shown to be in direct atomic contact with the glutamate agonist (Furukawa et al., 2005; Vance et al., 2011), and it has been shown to drastically reduce glutamate potency (Adams et al., 2014) and accelerate deactivation rate (Swanger et al., 2016). Moreover, a model of the GluN2B-E413G mutation predicts that this particular mutation increases the average glutamate solvent accessible surface area, allowing for glutamate to more easily escape the binding site. To analyze the relationship between agonist unbinding and egress, we measured the deactivation rate of several mutations at and around the

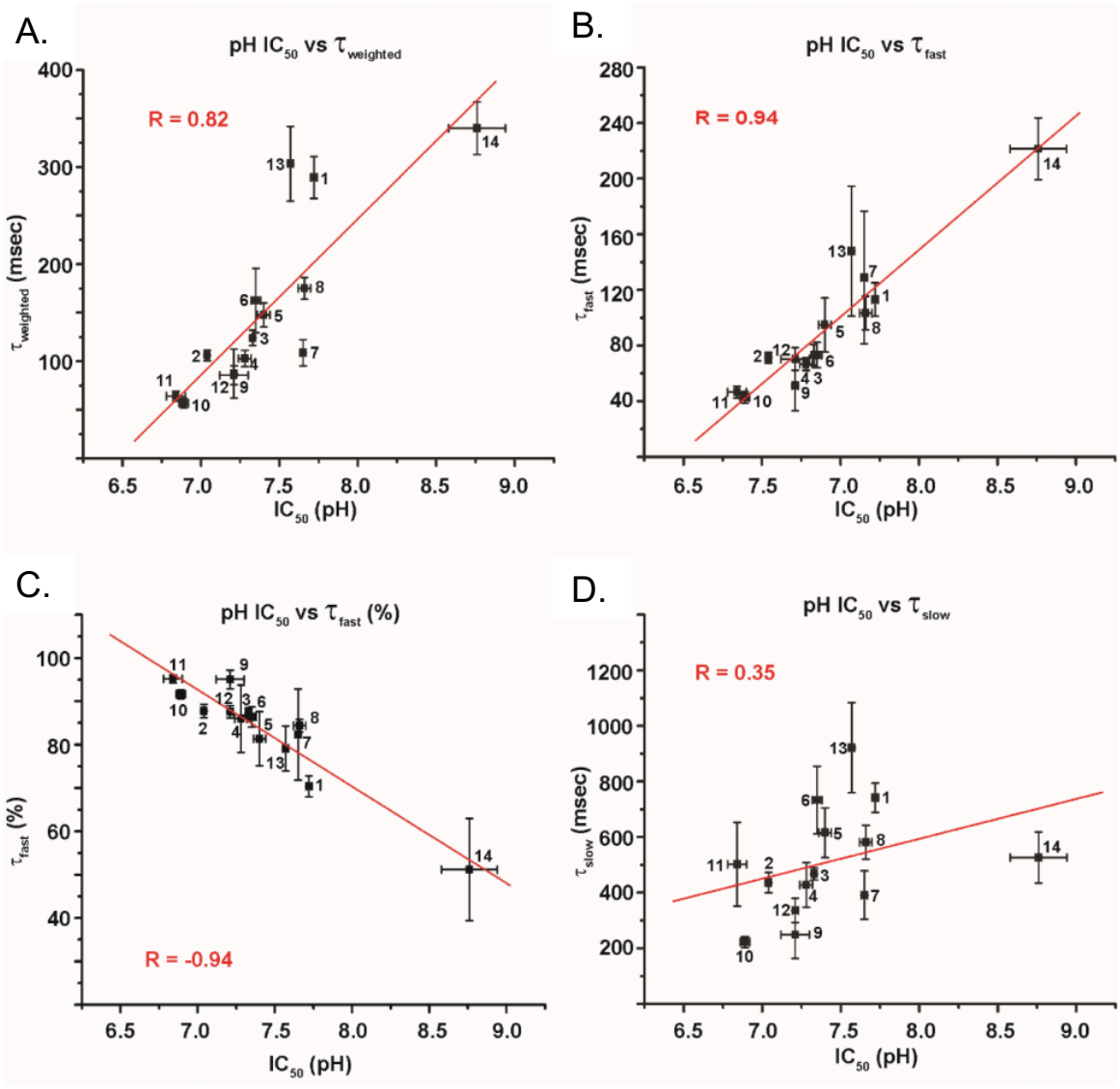

Figure 6.3: Correlation Between Kinetic Deactivation Properties and Proton IC_{50}
Figure shows plots correlating **A)** $\tau_{weighted}$ and pH IC_{50} (R=0.82), **B)** τ_{fast} and pH IC_{50} (R=0.94), **C)** τ_{fast} (%) and pH IC_{50} (R=-0.94), and **D)** τ_{slow} and pH IC_{50} (R=0.35). Red line indicates linear regression fit. Error bars represent ± SEM. Each data point is numbered as in Table 1.

GluN2B-Glu413 residue in response to a 1 second and 5 ms pulse of glutamate (1 mM) in the continued presence of glycine (30 μM).

Substitution of the GluN2B-Glu413 residue with glycine, glutamine, aspartic acid, asparagine, and alanine all led to an accelerated deactivation time course (**Figure 6.4, Table 6.2**). More specifically, all tested substitutions at this position resulted in accelerated fast and slow components of the deactivation time course, as well as an increase in the percent of the fast component contributing to the dual exponential fit. The combined effect of these changes resulted in an overall accelerated weighted deactivation τ for all tested mutations at this site. Additionally, we recorded the deactivation rates of mutations made at the position of GluN2B-His486. Modeling of the GluN2B ABD has revealed that this histidine residue is in close proximity to GluN2B-Glu413 and has effects on glutamate agonist binding according to orientation and protonation state. When GluN2B-His486 was substituted with phenylalanine or glycine, the receptors displayed accelerated τ_{fast}, an increase in the percent of τ_{fast}, and an overall acceleration of the weighted deactivation τ.

Deactivation Rate Correlates with Ligand Egress time for GluN2B ABD Mutations

Based on the proximity of GluN2B-Glu413 and GluN2B-His486 to the glutamate binding site, the mutation-induced increases in glutamate potency and acceleration in deactivation time course at these sites, and the previously predicted increase in solvent-accessible area, mutations at these two sites were modeled to evaluate their effects on ligand egress (Performed by Gordon Wells, Department of Chemistry, Emory University). RAMD simulations of ligand egress were performed

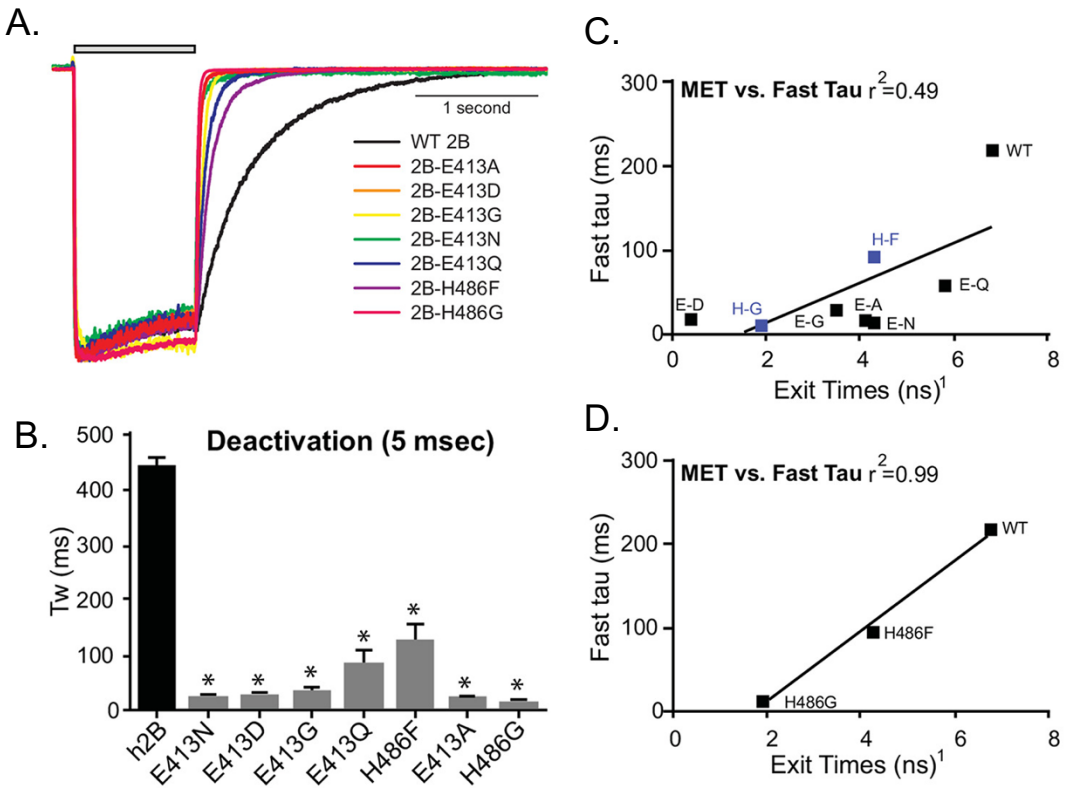

Figure 6.4: Glu413 and His486 Mutant Analysis
A) Representative whole cell current responses recorded from HEK cells expressing GluN1/GluN2B with the indicated mutations. Receptors were activated by a 1 second pulse of glutamate (1 mM, gray bar) in the continued presence of glycine (30 µM). **B)** Quantification of the current response deactivation time course following rapid removal of glutamate fitted by the sum of two exponential functions (Refer to methods). Significant difference from wild-type by one-way ANOVA ($p < 0.0001$) is indicated by an asterisk. **C and D)** The fast time constants were plotted as a function of mean exit time. Linear regression for all mutants together yielded an R^2 value of 0.49. His486 mutants analyzed independently yielded an R^2 value of 0.99.

Table 6.2: Deactivation and Simulated Egress Times for Wild-Type and ABD Mutant GluN2B

	Exit Time (ns)	τ_{Fast} (ms)	τ_{Slow} (ms)	A_{Fast} (%)	$\tau_{Weighted}$ (ms)	n
WT	6.8	220 ± 15	740 ± 34	55 ± 2.5	440 ± 17	23
H486F	4.3	95 ± 7.4	840 ± 381	94 ± 1.3	120 ± 9.9	10
E413Q	5.8	57 ± 5.4	330 ± 104	86 ± 5.5	81 ± 7.8	8
E413D	0.4	20 ± 1.8	130 ± 19	97 ± 1.2	23 ± 1.3	8
E413N	4.3	16 ± 1.6	87 ± 27	91 ± 4.6	19 ± 2.2	12
E413A	4.1	18 ± 1.6	160 ± 104	95 ± 4.8	20 ± 1.7	11
E413G	3.5	30 ± 3.6	49 ± 9.4	90 ± 6.8	34 ± 3.1	8
H486G	1.9	13 ± 1.6	164 ± 104	98 ± 4.5	14 ± 0.88	10

All values are mean ± SEM.
Weighted tau was determined as explained in the Methods.
Exit time was determined during RAMD with acceleration set to 0.225. Egress time was the minimum time taken for the ligand to be 10 Å from the protein center of mass.

and the ligand egress was plotted against the measured changes in deactivation rate. For all mutations, there was a decrease in mean exit time relative to the simulated wild-type (**Table 6.2**). Results showed a direct correlation (R^2= 0.49, P< 0.06) between ligand egress and the fastest component of the deactivation time constant, which is less likely to be influenced by entry into and exit from desensitized states. When GluN2B-His486 mutations were analyzed independently from the GluN2B-Glu413 mutations, the relationship between ligand egress and tau deactivation became even more apparent (**Figure 6.4**). The fast time constant describing deactivation (τ_{fast}) and ligand egress showed an apparent linear relationship with an R value of 0.99.

Discussion

As we continue to strive for a comprehensive understanding of the NMDA receptor, genetic information has the capacity to inform experimental design and scientific inquiry. Evolutionary biology provides insight into the critical components of receptor function by indicating specific regions that have been protected by natural selection. For example, the high degree of conservation that is observed for sequences such as those comprising the exon 5 motif of the GluN1 subunit and the glutamate binding site of the GluN2 subunits imply that these regions are particularly critical for normal receptor function and, ultimately, normal brain function. In this study, we provide functional analysis of these two highly conserved regions by investigating how these regions influence receptor deactivation time course. Moreover, we correlate deactivation rate with proton sensitivity and rate of ligand egress to 1) explore how functional changes upstream of the channel gate can influence receptor deactivation, 2) establish a better understanding of why residues in these regions might be under such strict evolutionary conservation, and 3) develop a relationship between distinct properties of channel function.

The exon 5 sequence is conserved throughout vertebrate GluN1 subunits as far back as cartilaginous fishes and hemichordates (http://consurf.tau.ac.il), suggesting that the location and composition of this region is evolutionarily advantageous for the maintenance of healthy neurological functions. Moreover, this region between residues 190 and 211 is devoid of missense variants in the human population with the exception of a single aspartate to asparagine mutation, GluN1-D200N identified in two individuals (Lek et al., 2016; Ogden et al., 2017), providing further evidence that this highly conserved sequence is under strong selection. In juxtaposition to the functional conservation of this region is the fact that it is also subject to alternative splicing. This mechanism of regulating the inclusion or exclusion of particular exons lends itself to biodiversity and is a common route of modulation that can be found among a wide variety of ion channels including potassium, voltage-gated sodium (Farmer et al., 2012) and calcium (Castiglioni et al., 2006) channels, acid-sensing sodium channels (Bässler et al., 2001), and iGluRs (Lerma et al., 2001; Palmer et al., 2005; Penn et al., 2012; Schiffer et al., 1997; Sommer et al., 1990). In the case of the exon 5 motif, its inclusion results in significantly reduced sensitivity to protons and an accelerated rate of deactivation (Adams et al., 2014; Rumbaugh et al., 2000; Traynelis et al., 1995; Vance et al., 2012), indicating that this region contributes to excitatory postsynaptic current and could alter calcium signaling in the event of an acidified environment created locally by high-frequency neuronal firing, stroke, or seizure (Kaku et al., 1993).

Structural analysis by Michael Regan and Hiro Furukawa (Cold Spring Harbor Laboratory) of exon 5 revealed that this motif lies at the interface of the GluN1 ATD, the GluN1 ABD, and the GluN2B ABD. The results presented here show that the ATD/ABD interface is an important locus for regulating ion channel function. Specifically, mutations and truncations to

the exon 5 motif that disrupt this interaction have drastic effects on deactivation rate, which we show closely correlates with proton sensitivity. The exon 5 motif acts as a tethered ligand positioned to control the GluN1/GluN2B ABD intersubunit interface, which in turn regulates ion channel activity at the TMD. Structural analysis of ionotropic glutamate receptors (iGluRs) has revealed that the interaction between the ATD and the ABD is far more extensive in NMDA receptors compared to that of the non-NMDA iGluRs (Karakas and Furukawa, 2014; Lee et al., 2014; Tajima et al., 2016). Therefore, in NMDA receptors, a relatively small structural element such as the exon 5 motif is capable of modulating the ATD/ABD interface and altering receptor functions. Alternatively, non-NMDA iGluRs have too few potential interactions between the ATD and the ABD for each to be capable of modulating the other. Consequently, there is little or no ATD-mediated modulation of functions such as proton sensitivity and deactivation rates in non-NMDA iGluRs. Based on the concept of the exon 5 motif acting as a tethered ligand, it is likely that polyamines such as spermine and spermidine similarly bind to and modulate the ATD/ABD domain interface to elicit exon-5-like effects, such as reduced proton sensitivity (Mony et al., 2011) and faster deactivation rates (Rumbaugh et al., 2000). A similar mechanism may also explain the effects of a set of subtype-specific compounds such as PYD-106 that are predicted to bind to the ATD/ABD interface (Khatri et al., 2014). This modulatory site at the ATD/ABD interface in NMDA receptors may provide an important target for context-dependent therapeutic compounds whose activity depends upon the acidified environment created by seizure and stroke (Kaku et al., 1993; Rumbaugh et al., 2000; Traynelis et al., 1995).

As opposed to the evolutionarily conserved variation that exists as a result of highly regulated alternative splicing, *de novo* mutations in specific regions of the NMDA receptor can also contribute to functional diversity. Several *de novo* mutations have been identified in highly

conserved regions of the receptor (e.g. the pre-M1 helix, the glutamate binding site, etc.) that have been attributed to the development of diverse neurodevelopmental conditions ranging from developmental delays to seizures (Ogden et al., 2017; Swanger et al., 2016). Just as evolutionary conservation points to regions of the NMDA receptor that are likely critical to normal function, disease-associated *de novo* mutations can also draw attention to regions by identifying sequences in the receptor that are intolerant to variation. By characterizing these mutations, we can develop an understanding not only of a disease mechanism, but also of how the wild-type receptor requires specific amino acids in specific positions to perform its normal function.

In this study, we exploited the disease-associated *de novo* mutation GluN2B-E413G observed in a heterozygous patient exhibiting developmental delay to investigate the functional role of residues within the glutamate binding site. The Glu413 residue is conserved across GluN2 subunits (Kinarsky et al., 2005), again suggesting functional importance. The proximity of this mutation to the glutamate binding-site suggests that mutations at Glu413 could alter agonist association and dissociation, and moreover, the synaptic NMDA receptor response time course in patients harboring this mutation. We performed functional analysis of various mutations at or near Glu413 and evaluated atomic level molecular simulations to determine the mechanism underlying the functional effects of the *de novo* GRIN2B mutation on agonist potency. We showed that mutations at GluN2B-Glu413 and GluN2B-His486 resulted in a drastically accelerated deactivation time course. Moreover, we correlated these deactivation rates with the glutamate egress time determined by random acceleration molecular dynamics (RAMD) simulations (Lüdemann et al., 2000).

Evaluation of egress time (performed by Gordon Wells, Department of Chemistry, Emory University) was consistent with the previously published prediction that substitution at

this position increases flexibility and solvent access, which contribute to agonist dissociation (Swanger et al., 2016). These results provide a mechanistic understanding of how substitutions at Glu413 and His486 influence the stability of the agonist-bound state by altering the glutamate binding pocket. Moreover, the exit time for glutamate from several GluN2B-E413 mutations was determined to be faster than from wild-type GluN2B. As such, when glutamate egress time was plotted against the fast component of the deactivation time course and fitted by linear regression, we could observe a direct, albeit weak, relationship. That is, as the glutamate egress time grew longer, so too did the fast component of the deactivation time course. Of course, this direct relationship is consistent with the understanding that the longer the agonist remains bound to the receptor, the longer the receptor will remain open. When glutamate is rapidly removed from the extracellular space, the rate at which the channel stops passing current is dependent upon the amount of time it takes for the ABD clamshell to open and release the glutamate ligand. An even stronger direct relationship between the fast component of the deactivation time course and glutamate exit time was observed with the His486 mutations were analyzed independently. And, as with Glu413, the His486 residue is conserved across the GluN2 subunits (Kinarsky et al., 2005).

Taken together, the results from this study emphasize the importance of evolutionarily conserved sequences in the function of the NMDA receptor. Evolutionary conservation of particular amino acid sequences can point us towards regions of the receptor of particular functional consequence. Moreover, by exploiting genetic variation in the context of alternative splicing or *de novo* mutations, we have the ability to ask and answer new questions pertaining to the strictly regulated function of the NMDA receptor required to appropriately facilitate excitatory neurotransmission. Discreet expression profiles and unique functional properties of

individual GluN subunits are critical to ensure that the correct response is elicited in response to synaptic glutamate release. By investigating the ways in which conserved regions of the receptor influence function by measuring the effect of mutations in these regions, we can begin to elucidate the mechanism by which the NMDA receptor responds to its agonists

Overall, this study provides evidence that the highly conserved regions of the GluN1 exon 5 motif and the GluN2 agonist binding site—namely residues Glu413 and His486—are critically important for channel function. Moreover, we show that deactivation correlates with other unique properties of the NMDA receptor. Finally, the results from this study emphasize the value of evolutionary conservation, purposeful mechanisms of biodiversity, and randomly occurring *de novo* mutations as tools to investigate how the function of the NMDA receptor is dependent upon its specific amino acid composition.

Chapter 7: Discussion

The findings presented in this dissertation contribute to our continually evolving understanding of the complex mechanisms that control NMDA receptor function and gating. Guided by structural, genetic, and functional analysis of these receptors, these findings highlight the regions of particular functional consequence within the receptor and allow for a better understanding of the role of the NMDA receptor in both the physiological and pathological brain. By investigating how particular regions of the NMDA receptor contribute to channel function, we can also expand upon our knowledge of how disease occurs, how these receptors facilitate excitatory neurotransmission, and how to more effectively modulate these receptors in the event of aberrant activity. This work highlights the importance of highly conserved regions within the different domains of the NMDA receptor: the exon 5 motif of the GluN1 subunit, the glutamate binding site in the ABD of the GluN2 subunits, and the S1-M1 linker of both GluN1 and GluN2. Moreover, the work presented here provides a mechanistic understanding of how these regions might exert their control over the unique properties of the NMDA receptor.

In addition to a better understanding of the NMDA receptor, the results presented in this dissertation have implications for the broader ionotropic glutamate receptor family. Because the regions explored in this study are found across several iGluR members, the functional influence of these regions can likely be extrapolated to explain some of the functional characteristics of other glutamate-binding ion channels. Finally, the findings presented here demonstrate the value of genetic evaluation in guiding research efforts. By taking advantage of the information afforded to us by evolutionary biology, we are able to circumvent some of the obstacles we might otherwise face while investigating the function of receptors and other important proteins. Instead of blindly guessing which regions of the receptor may be important for function, we can

use highly conserved sequences to guide our research. Highly conserved regions tend to experience strong selection against variation because these regions contribute the most significantly to maintaining normal receptor function (Ogden et al., 2017; Swanger et al., 2016; Veltman and Brunner, 2012). Consequently, when missense mutations do occur in these regions, they tend to be associated with functional abnormalities and, moreover, neurological disorders (Ogden et al., 2017; Poduri et al., 2013; Swanger et al., 2016). Overall, the findings presented in this dissertation contribute to the expanding functional profile of highly conserved regions of the NMDA receptor and provide evidence for the effectiveness of genetic information in guiding the functional exploration of mechanistically complex receptors such as the NMDA receptor.

The Pre-M1 Helix Controls Channel Gating

The pre-M1 helix has recently received a lot of attention for the mounting evidence suggesting its role in the gating mechanism of the NMDA receptor. First, mutations of individual residues within this region to cysteine produce receptors with small currents and abnormal kinetic profiles (Beck et al., 1999; Kashiwagi et al., 2002; Thomas et al., 2006). Second, MTS modification of cysteine residues substituted into this region lead to significant changes in leak current (Sobolevsky et al., 2007). Third, alanine substitution of select pre-M1 residues can result in spontaneously active receptors (Chang and Kuo, 2008). Fourth, the pre-M1 helix and adjacent regions have been shown to harbor structural determinants for subunit-selective positive allosteric modulators of the GluN2C- and GluN2D-containing NMDARs (Mullasseril et al., 2010). Fifth, mutations in and near pre-M1 can alter NMDAR function (Alsaloum et al., 2016; Talukder et al., 2010). And finally, structural investigation of the S1-M1 linker puts the pre-M1 helix within van der Waals contact with the M3 gate, allowing it to facilitate communication

between the ABD and the TMD (Karakas and Furukawa, 2014; Lee et al., 2014; Sobolevsky et al., 2009).

In this study, we investigated the role of the GluN2A pre-M1 helix in channel gating by systematically substituting residues and measuring the functional consequences. We showed that, of the residues within the GluN2A pre-M1 helix, the Phe553 residue made the most substantial contribution to channel function, as indicated by significant changes to both macroscopic and single channel properties. Furthermore, molecular dynamics simulations provided a mechanistic understanding of how this residue might contribute to gating by participating in a network of aromatic amino acids. These amino acids, which are within pi-stacking range of each other, reside within the pre-M1 helix, the M3 helix, and the pre-M4 linker of the adjacent subunit. More specifically, the GluN2 pre-M1 helix makes contact with the GluN2 M3 helix and the GluN1 pre-M4 linker, while the GluN1 pre-M1 helix makes contact with the GluN1 M3 helix and the GluN2 pre-M4 linker.

The Residues of the Pre-M1 Helix Contribute to Normal NMDA Receptor Function

This aromatic network and the amino acids therein have been previously implicated in the gating mechanism of the NMDA receptor. Relative to the entire receptor, the pre-M1 regions of the GluN2 subunits are significantly less variable (Ogden et al., 2017), and characterization of disease-associated mutations in pre-M1 region has contributed to the hypothesis that these regions play an important functional role. Of the most profound pre-M1 disease-associated mutations studied was GluN2A-P552R, which was identified in a patient displaying seizure disorders and intellectual disability (De Ligt et al., 2012). This proline residue is conserved across GluN subunits in multiple species (Alsaloum et al., 2016), and was determined to be a

gain-of-function variant based on its increased glutamate and glycine potency and prolonged deactivation time course (Ogden et al., 2017). Interestingly, however, substitution of GluN2-Pro552 with alanine did not produce the same functional effects, resulting in minimal effects on glutamate and glycine potency, and virtually no effect on activation and deactivation kinetics or the single channel profile. Together, these results may support the hypothesis that GluN2A-Phe553 participates in a functionally critical aromatic network such that the mutation of the neighboring proline residue, GluN2A-Pro552, to a large, charged residue disrupts the network leading to profound functional abnormalities.

The Pre-M1 Helix Contributes to Subunit Specific Contributions to Receptor Function

GluN2A-Phe553 has been investigated for its role in desensitization because sequence alignment of NMDA receptors and AMPA receptors revealed that the equivalent position in the AMPA receptor is occupied by a leucine residue. Because the NMDA and AMPA receptors differ so drastically in desensitization (Dingledine et al., 1999; Traynelis et al., 2010), it was thought that this amino acid difference between the two receptors might be responsible for the functional difference. Interestingly, when the GluN1 equivalent of GluN2A-Phe553, GluN1-Phe558, was substituted with leucine and expressed with wild-type GluN2A, the receptor retained its GluN2A-like desensitization phenotype. However, when GluN2A-F553L or GluN2B-F554L was expressed with wild-type GluN1, the desensitization resembled that of the AMPA receptor (Alsaloum et al., 2016). It was proposed, therefore, that the mechanism of desensitization in NMDARs differs from that of AMPARs as a result of differences between the composition of a “hydrophobic box” made up of aromatic residues within pre-M1 region and the M3 helix. This finding supports our hypothesis of aromatic interactions between the pre-M1

helix, the M3 helix, and the pre-M4 helix of the adjacent subunit. The functional discrepancies between the receptors with the GluN1-F558L mutation and those with the GluN2A-F553L or GluN2B-F554L mutations are consistent with the idea that the GluN1 and GluN2 subunits each participate in unique aromatic networks, each with its own functional role. This hypothesis is further supported by the discovery that, while the pre-M1 GluN2A-P552R mutation drastically prolonged receptor activation, the homologous mutation in GluN1, GluN1-P558R, had no effect on receptor activation (Ogden et al., 2017).

This, of course, raises the question as to whether or not the functional differences between GluN2 subunits (Dingledine et al., 1999; Paoletti et al., 2013) can be explained by their unique aromatic networks because the equivalent residue to GluN2A-Phe553 that we propose is central to the aromatic network is a tyrosine in the GluN2C and GluN2D subunits. However, when we substituted GluN2A-Phe553 with tyrosine, we were unable to detect a measurable effect on desensitization, as consistent with previous findings showing that swapping the residue at this position in GluN2A (phenylalanine) for that of GluN2C (tyrosine), which displays no desensitization, does not result in a concomitant swapping of desensitization phenotypes (Alsaloum et al., 2016; Krupp et al., 1998). This result suggests that the pre-M1 helix cannot singularly account for functional differences in desensitization between different GluN2 subunits. However, despite having no significant effect on macroscopic properties, GluN2A-F553Y significantly reduced open probability, consistent with the reduced open probability of GluN2C- and GluN2D-containing receptors. Moreover, the inverse mutation, GluN2D-Y578F, reduced glutamate potency, reduced glycine potency, and increased open probability as determined by MTSEA relative to the wild-type GluN2D receptor. Taken together, these results suggest that, in addition to being central for the gating mechanism, the residue at position 553 is

at least in some part responsible for the subunit-specific single channel properties of the NMDA receptor. Moreover, the hydroxyl group of the tyrosine in this position for GluN2C and GluN2D receptors may introduce a hydrogen bond with the tyrosine of the SYTANLAAF, as suggested by the molecular dynamics simulations and supported evidence showing that the side of the helix that harbors GluN2A-Phe553 appears to be oriented toward the SYTANLAAF conserved helical bundle and the pre-M4 helix of the adjacent subunit (Chen et al., 2017). Because the strength of a hydrogen bond (enthalpy ~0-4 kcal/mol) may be greater than that of a pi-stacking interaction (enthalpy ~2 kcal/mol), it is possible that the introduction of such a bond would alter the aromatic network and, ultimately, the gating mechanism.

The Pre-M1 Helix is Part of an Aromatic Gating Network

To further validate the presence and functional importance of the aromatic network, we used molecular dynamics to explore its interactions in the context of our scanning mutagenesis to identify potential interactions that could account for differences in gating control between GluN1 and GluN2. Using a GluN2A homology model built from a GluN2B crystal and cryo-EM structures as well as the TMD of a closed AMPA structure, we examined the amino acid environment surrounding the pre-M1 helix. We identified four residues surrounding GluN2A-Phe553 that could participate in a pi-stacked aromatic network. However, when we substituted alanine for phenylalanine in our simulation, of this residue with an alanine in GluN2A, we found that two of the residues that were previously implicated in the aromatic network were oriented away from the aromatic cluster at distances that do not permit even weak side-chain interactions. Moreover, repeating this simulation for the GluN1 pre-M1 region also revealed fewer possible interacting residues, suggesting that the network plays a unique role in the GluN2A subunit. This

inequity might explain why the GluN2 subunits dictate the functional properties of the receptor (Paoletti et al., 2013), why the GluN1 pre-M1 mutations have less severe functional consequences than GluN2 (Ogden et al., 2017), and why the GluN2 pre-M1 helix is less tolerant to variation than GluN1 (Ogden et al., 2017).

Evaluation of residues within the aromatic network lends credibility to the proposal that this network facilitates NMDA receptor gating. Several of the residues implicated in the aromatic network have been associated with receptor dysfunction or disease. For example, the mutation GluN2A-W558S in the M1 helix was identified in a patient with epilepsy (ClinVar, https://www.ncbi.nlm.nih.gov/clinvar). Within the M3 helix, GluN2A-Phe637 has been shown to influence agonist potency and channel gating (Ren et al., 2007) and GluN1-Y647S has been identified in a patient with infantile spasms (Allen et al., 2013). In the M4 helix, GluN1-F817L has been identified in a patient with intellectual disability, developmental delay, and movement disorder (Lemke et al., 2016; Zhu and Paoletti, 2015). Functional analysis of these residues would provide a clearer understanding of how these specific amino acids contribute to channel function and, more specifically, the aromatic network. However, despite the lack of functional data, their association with neurological disorders supports the hypothesis that these residues are of notable functional importance.

Despite the substantial revolution that has taken place in the realm of structural biology, comprehensive structural analysis of the S1-M1 linker region of the NMDA receptor has remained elusive as a result of its flexibility. In our study, we used homology models generated from crystal and cryo-EM structures that had resolution within the pre-M1 and linker regions. We used the well-resolved transmembrane region of the AMPA receptor, with high sequence homology and structural similarity to the transmembrane regions of GluN1 and GluN2A. As a

consequence, we cannot state with absolute certainty that the structure we are using in our molecular dynamics simulations accurately represents the structure of the NMDA receptor. While cryo-EM structures are improving, the structures are not high enough resolution to accurately place side chains within the dynamic regions, such as the linkers. Additionally, the structural analysis of proteins, particularly by x-ray crystallography, requires the proteins to be kept at cryogenic temperatures (Weik and Colletier, 2010). Our homology model was constructed from the crystal structures of an agonist-bound GluN1/GluN2B receptor, a non-active (apo) GluN1/GluN2B receptor, and the TMD of the GluA2 receptor. In addition to the fact that the cryogenic temperatures provide only structural information for one distinct and stationary conformation, the molecular dynamics simulations were conducted at 310 K. As such, side chain positions predicted by the simulation are estimated from the orientation of the amino acids at the stationary cryogenic state. In 2018, 23 full-length structures of the GluN2A receptor were resolved (4.5-16.5Å) using cryo-electron microscopy, none of which had resolution covering the complete transmembrane and linker regions (Jalali-Yazdi et al., 2018; Zhang et al., 2018). Future studies could benefit from incorporating the recently published higher resolution cryo-EM GluN2A structures in conjunction with AMPAR structures as templates to build homology models.

To better conceptualize the role pre-M1 plays in gating, we calculated the changes in protein stability and the affinity of the pre-M1 region for its surrounding contact residues following the introduction of two mutations, GluN2A-F553A and GluN2A-L550A. We are able to reliably model the receptor in the closed state, and we know that the pre-M1 helix undergoes a conformation change— consistent with association and dissociation with the receptor— that can introduce a binding site for allosteric modulators between pre-M1 helix and the pore-forming

structures of the receptor, in both NMDA and AMPA receptors (Perszyk et al., 2018; Yelshanskaya et al., 2016).

Our computational results, accompanied by functional analysis, allows for a simplistic and reductionist interpretation of a complex gating system. We found that alanine substitution of GluN2A-Phe553 and GluN2A-Leu550 decreases the protein stability within the pre-M1 region. As a consequence, the pre-M1 helix likely experiences reduced structural integrity, ultimately leading to an impaired gating mechanism. With reduced structural integrity, the conformational changes required for the GluN2A ABD-TMD linker to act upon the pre-M1 helix to promote channel opening are likely compromised. Alternatively, while the GluN2A-F553A mutant was predicted to associate more weakly to its binding region, the L550A mutant was predicted to have a stronger association, consistent with the finding that L550A mutant accelerated the deactivation time course. We also observed an increase in glutamate EC_{50} for the GluN2A-L550A mutant.

Mechanism of Pre-M1 Control of Gating

The hypothesis for the role of pre-M1 in gating is as follows. The pre-M1 helix facilitates channel opening in response to the ABD clamshell closure induced by agonist binding (Armstrong and Gouaux, 2000; Furukawa et al., 2005; Inanobe et al., 2005; Jin et al., 2003; Karakas and Furukawa, 2014; Lee et al., 2014; Mayer, 2011; Sun et al., 2002; Vance et al., 2011). Specifically, this motion within the ABD pulls on the three ABD-TMD linkers: the S1-M1 linker containing the pre-M1 helix, the M3-S2 linker, and the S2-M4 linker. Perhaps, while the M3-S2 linker pulls upward on the M3 helix, the S1-M1 linker and the pre-M1 helix therein, pull outward on the extracellular ends of the M3 helices resulting in the M3 helices bending

away from the central axis of the pore (Refer to **Figure 1.2**) (Wollmuth and Sobolevsky, 2004). Therefore, when the interactions between the S1-M1 linker and the M3 helix are disrupted by amino acid substitutions, the receptor displays a prolonged activation rate because pulling on the S1-M1 linker does not lead to the M3 bending away from the channel pore as rapidly or efficiently. Moreover, the intersubunit triads suggest that the S2-M4 linker of the adjacent subunit also interacts with the M3 helix and S1-M1 linker, such that the conformational changes facilitating channel opening in one subunit may be influenced by the conformational state of the adjacent subunit (Chen et al., 2017; Gibb et al., 2018; Ogden et al., 2017).

We hypothesize that the weaker association of pre-M1 as seen in the GluN2A-F553A mutant has two primary functional effects: 1) it reduces the energy barrier needed to overcome conformational changes that allow channel opening upon glutamate binding, leading to a decrease in the EC_{50} of glutamate, and 2) the lower affinity results in a slower return to the closed state from which glutamate can dissociate, leading to a prolonged deactivation time course. We also hypothesize the inverse of this to be true for the GluN2A-L550A mutant. That is, the stronger association of GluN1-L550A results in 1) a higher energy barrier for the conformational changes to open the channel, requiring a higher concentration of glutamate, and 2) rapid binding of pre-M1 in the closed state, reducing the deactivation time. We propose then that the increase in affinity between pre-M1 and interacting residues drives the deactivation time course by facilitating the return of the pre-M1 helix to its position in the closed state of the channel, allowing the receptor to reach a state from which glutamate can unbind.

Overall, the results presented here emphasize and provide substantial evidence for the previously suggested role of the pre-M1 helix in channel gating. We show here a functional evaluation of residues within this region of the NMDA receptor and implicate the surrounding

amino acid environment in the mechanism of channel gating. Moreover, we present a model showing a network of aromatic residues that offers unique subunit-specific contributions of pre-M1 helices in GluN1 and GluN2 to channel gating and propose a mechanism whereby the residues of the pre-M1 helix control channel gating by interacting closely with the pore-forming helices and local linker regions.

Modeling the NMDA Receptor Gating Mechanism

With more information regarding the structural and functional properties of the NMDA receptor, particularly guided by sequence conservation and genetic variation, we can begin to piece together the complex mechanisms that allow these receptors to transduce agonist binding into channel opening. Genetic analysis has identified the pre-M1 helix as a locus for disease-associated *de novo* mutations (CFERV Database-http://functionalvariants.emory.edu/database/index.html)(Ogden et al., 2017), while maintaining an absolute lack of missense variation in the healthy population (gnomad.broadinstitute.org) (Ogden et al., 2017). In this study, we have provided functional analysis of a disease-associated residue by systematic amino acid substitution, we have characterized receptors with non-equivalent GluN2 subunits, and we have proposed a structurally based model that can account for macroscopic and single channel data to provide mechanistic insight into the gating mechanism of the NMDA receptor.

Pre-Gating of Only Three Subunits is Required for Channel Opening

The disease-associate mutation responsible for guiding the investigation of the role of pre-M1 in the gating mechanism is GluN2A-P552R. The functional consequences of the

GluN2A-P552R mutation in the pre-M1 region is of particular importance because the pre-M1 region where this mutation is located controls channel gating and, moreover, imparts subunit specificity onto the gating mechanism (McDaniel et al., 2019). To elucidate the mechanism with which the GluN1/GluN2A-P552R mutation interferes with channel gating, we employed the previously published method for controlling subunit stoichiometry using GABA ER-retention tags (Hansen et al., 2014). GluN1/GluN2A, GluN1/GluN2B, and GluN1/GluN2A/GluN2B receptors containing one or two copies of the GluN2 proline to arginine mutation were investigated for changes in kinetic activation and deactivation properties. Our results showed that receptors with a single copy of the mutation could become activated at rates similar to wild type receptors, but deactivate much more slowly, while, two copies of the mutation produced receptors with a significantly delayed activation time course and an even slower rate of deactivation.

These results led to the hypothesis that the NMDA receptor does not require activation of all four subunits for the channel to open. Generally, it has been thought that NMDA receptors require co-activation by glutamate binding to the two GluN2 subunits and glycine binding to the two GluN1 subunits in order to promote channel opening. This hypothesis predicts that the subunits move in a coordinated fashion such that channel opening is achieved when all the subunits work in concert. The results presented here, however, suggest that the receptor can open normally when only a single GluN2 subunit has undergone its pre-gating steps following agonist binding. Not only does this additional open state present an alternative route to channel opening, but it also draws into question the validity of the previously established conditions that were thought to be required for NMDA receptor activation. Instead of subunit cooperativity facilitating channel opening, this alternative route to channel opening might support the

hypothesis that each subunit is a free moving entity, with gating occurring the moment that some specific combination of conformations among the subunits is achieved.

In addition, this finding also provides insight into the activation mechanism of the other ionotropic glutamate receptors. Because the NMDA receptor shares a majority of its structural features with the AMPA and kainate receptors (Armstrong and Gouaux, 2000; Dingledine et al., 1999; Furukawa et al., 2005; Lee et al., 2014; Mayer, 2011) and because the proline residue is conserved across all members of the iGluR family (Klippenstein et al., 2017), it stands to reason that this additional open state also exists for non-NMDA iGluRs as well.

A Structure-Based Model Can Predict Conformational Transitions in Individual Subunits

To make sense of this complex mechanism of activation, a structure-based model was conceptualized by Alasdair Gibb and Stephen Traynelis (Department of Pharmacology, Emory University), guided by structural insights of the wild-type receptor and functional analysis of mutant receptors. The model included independently acting subunits and open state connectivity such that channel opening could occur after both GluN1 subunits and either one or both of the GluN2 subunits had undergone pre-gating, as suggested by the functional analysis of the GluN1/GluN2A/GluN2A-P552R mutant triheteromeric receptor. The model was shown to accurately fit macroscopic and single channel data (Recorded by Kevin Ogden) for the wild-type GluN1/GluN2A receptor and was verified by sensitivity analysis. We then used the model to derive transition rates between the multiple pre-gating states that reflect unique subunit-dependent conformational changes. These conformational transitions, we predict, represent the movement and altered interactions of linker regions that precede gating (Tajima et al., 2016).

This hypothesis is backed by a vast collection of data showing the unique role of these regions in gating (Chen et al., 2017; Kazi et al., 2013; Ogden et al., 2017; Ogden and Traynelis, 2013; Zhou and Wollmuth, 2017). Several lines of evidence have suggested that the pre-M1 helix participates in an aromatic network as one-third of a triad also containing its intrasubunit M3 pore-forming helix and the pre-M4 region of the adjacent subunit (Gibb et al., 2018; Ogden et al., 2017). Because the triads surrounding the GluN1 and GluN2 pre-M1 helices are unique, we propose that pre-gating conformational changes reflect two distinct sets of linker/TMD interactions that involve both subunits.

Overall, our findings provide further evidence for the role of the pre-M1 helix in channel gating. By exploiting the functionally-consequential GluN2A-P552R mutation, we were able to propose a mechanism of activation that requires pre-gating of only three of the four NMDA receptor subunits, challenging the convention that the NMDA receptor requires co-activation by two glycine and two glutamate molecules. Moreover, this study provides a structurally constrained model that can account for single channel and macroscopic properties of the NMDA receptor, can provide insight into how individual subunits contribute to the complex gating mechanism, and can help explain some of the unique functional properties of disease-associated mutant receptors.

A Disease-Associated Mutation in the S1-M1 Linker Impairs Receptor Function

As previously explained, characterization of disease-associated variants allows not only for a better understanding of how the NMDA receptor contributes to a diseased state, but also provides information regarding the role of particular residues in maintaining appropriate receptor function. Slightly upstream of the GluN1 pre-M1 helix lies a leucine residue, Leu551, shown to be conserved across several species (Fry et al., 2018; Ohba et al., 2015) and located within a

sequence of amino acids that houses no missense mutations in the healthy population (gnomad.broadinstitute.org). Interestingly, despite its conservation across the *GRIN1* genes of several species, it is not found in the GluN2 subunits (Ogden et al., 2017). This distinction, whereby a residue in the S1-M1 linker of the GluN1 subunit likely to be of functional consequence based on evolutionary conservation is absent in the GluN2 subunit, is consistent with the data presented here suggesting that the S1-M1 linker regions of different GluN subunits play distinct roles in the gating mechanism (McDaniel et al., 2019).

GluN1-L551P Alters Receptor Pharmacology, Kinetics, and Surface Expression

This leucine residue is also the site of a *de novo* mutation, GluN1-L551P, which has recently been identified in a 9-year old female patient after she presented early in life with intellectual disability, developmental delay, and epilepsy (Fry et al., 2018). We provide the first analysis of the functional, pharmacological, and expression consequences of the GluN1-L551P mutant. Our data support the hypothesis that the GluN1-L551P causes aberrant receptor function which could explain the neurological abnormalities experienced by the patient.

Functional analysis revealed that the disease associated GluN1-L551P mutation resulted in a significant increase in glutamate and glycine potency, a prolonged deactivation time course, and reduced desensitization when co-expressed with either the GluN2A or the GluN2B subunit consistent with a gain-of-function mutation. However, GluN1-L551P also resulted in enhanced proton sensitivity, reduced surface expression, and reduced peak current, consistent with a loss-of-function mutation. It is challenging, then, to predict whether or not this mutation leads NMDA receptor hyperfunction or hypofunction when present in the human brain. Either way, because the GluN1 subunit is an obligate subunit for the NMDA receptor (Cull-Candy et al., 2001;

Monyer et al., 1992; Paoletti et al., 2013; Traynelis et al., 2010), the functional abnormalities displayed during its co-expression with GluN2A or GluN2B could be particularly consequential in the developing brain during which time the GluN2B subunit reaches its peak expression and the GluN2A subunit expression begins to increase throughout the CNS (Paoletti, 2011). An overall gain-of-function could lead to overactivation of receptors whose function needs to be tightly regulated to allow for normal neuronal circuitry to develop or to neuron damage as a result of excitotoxicity (Choi, 1992; Choi, 1994). Moreover, NMDA receptor hyperfunction has been linked to the development of several neurological disorders including Alzheimer's disease (Hynd et al., 2004), Huntington's disease (Zeron et al., 2002), epilepsy (Lemke et al., 2014; Rice and DeLorenzo, 1998; Yuan et al., 2015b), and intellectual disabilities (XiangWei et al., 2018). Alternatively, an overall loss-of-function could lead to hypofunction associated with schizophrenia (Coyle, 2006; Olney et al., 1999) and memory impairment (Newcomer et al., 1999). As such, the phenotypic profile of the patient displaying intellectual disability, developmental delay, and epilepsy would suggest that the GluN1-L551P results in overall hyperfunction of the NMDA receptor.

The functional consequences of the GluN1-L551P mutation are consistent with the characterization of other disease-associated mutations within the GluN1 S1-M1 linker. Specifically, GluN1-P557R (Gibb et al., 2018; Ogden et al., 2017) and GluN1-D552E (Ogden et al., 2017) found in patients with intellectual disability and/or epilepsy also resulted in a prolonged deactivation time course, reduced current response, and reduced surface expression,. Additionally, analysis of the GluN1-L551P mutant supports the hypothesis that the S1-M1 linker contributes to the activation of the NMDA receptor in response to agonist binding. Because the

S1-M1 linker is responsible for facilitating communication between the ABD and the channel pore, it is likely that mutations in this region are of significant functional consequence.

The Functional Consequences of Glun1-L551P are Consistent with an Abnormal Phenotype

The mechanism by which the GluN1-L551P mutation might contribute to disease, however, remains unclear. Although the increased glutamate and glycine potency, the prolonged deactivation time course, and the reduced desensitization would suggest that the mutation results in a gain-of-function receptor, the impaired surface trafficking, reduced current amplitude, and enhanced proton sensitivity are more consistent with loss-of-function. We can predict, though, that the composite effect of the GluN1-L551P mutation is that of gain-of-function, as suggested by the comparison of the GluN1-L551P patient's phenotype with those associated with both gain and loss of function mutations. Even without a comprehensive understanding of exactly how the GluN1-L551P mutation contributes to the disease state, its effect on the function of the NMDA receptor is apparent. By substituting the nonpolar, aliphatic leucine residue with a side chain isobutyl group with a nonpolar, aliphatic proline residue with a side chain pyrrolidine, we are essentially replacing a structurally flexible amino acid with one of substantial conformational rigidity. If flexibility of the S1-M1 linker is required to facilitate the communication between the ABD and the TMD, then it is likely that a proline substitution in this region would interfere with this mechanism.

Overall, the GluN1-L551P mutation leads to significantly altered NMDA receptor function with both gain-of-function and loss-of-function properties that can likely account for the phenotypic abnormalities displayed by the patient. Moreover, the results from this study support the hypothesis that the residues of the S1-M1 helix—particularly those with a high degree of

conservation—are critical for normal NMDA receptor function. Finally, our results provide an example of a single amino acid substitution that leads to a complex collection of functional consequences that ultimately lead to a physiologically disruptive or pathologically implicated NMDA receptor.

The Effects on Deactivation Rate of Highly Conserved Regions of the NMDA Receptor

The results discussed thus far primarily center around developing a comprehensive understanding of how the S1-M1 linker, specifically the pre-M1 helix, contributes to the function of the NMDA receptor by directly influencing the gating mechanism. Just as we used disease-associated *de novo* mutations to guide the investigation of the functional role of the S1-M1 linker, we also used *de novo* mutations, or the absolute lack thereof, to guide the study of other highly conserved regions of the NMDA receptor subunits. Specifically, we provided functional analysis of two highly conserved regions by investigating how these regions influence receptor deactivation time course and correlating the changes in deactivation rate to other functional properties of the receptor.

Exon 5: Deactivation Rate Correlates with pH Sensitivity

The first region of interest was the exon 5 motif of the GluN1 subunit, which is conserved throughout vertebrate GluN1 subunits as far back as cartilaginous fishes and hemichordates (http://consurf.tau.ac.il) (Hansen et al., 2018), but is absolutely devoid of missense mutations in the human population (Lek et al., 2016; Ogden et al., 2017). Together, these genetic features of the exon 5 motif would suggest that this region is critical for receptor function. However, a large portion of the GluN1 subunits in the mammalian brain lack exon 5

due to the highly regulated process of alternative splicing (Cull-Candy et al., 2001; Traynelis et al., 2010). This biologically intentional mechanism for selectively expressing receptors with or without the exon 5 motif suggests that, although the NMDA receptor can function without this region, its presence endows the receptor with unique functional properties that are required at specific temporal or spatial sites or under certain conditions. Functionally, exon 5 reduces sensitivity to protons and accelerates the rate of deactivation (Adams et al., 2014; Rumbaugh et al., 2000; Traynelis et al., 1995; Vance et al., 2012), indicating that this region contributes to excitatory postsynaptic current and could alter calcium signaling in the event of an acidified environment due to high-frequency neuronal firing, stroke, or seizure (Kaku et al., 1993).

Structural analysis of exon 5 reveals that this motif lies at the interface of the GluN1 ATD, the GluN1 ABD, and the GluN2B ABD (Regan et al., 2018). By introducing mutations and truncations to the exon 5 motif that disrupt the ATD/ABD interaction, we measured drastic effects on deactivation rate, indicating that the ATD/ABD interface is an important locus for regulating ion channel function. The exon 5 motif acts as a tethered ligand positioned to control the GluN1/GluN2B ABD intersubunit interface near the site of proton modulation, leading to the changes in proton sensitivity (Cull-Candy, 2001). Moreover, because the ABD and ATD undergo significant conformational changes during the process of channel gating (Tajima et al., 2016; Wollmuth and Sobolevsky, 2004), a structure such as exon 5 that alters the interaction between these two domains may interfere with this motion, ultimately disrupting the ability of the receptor to transduce agonist binding into channel opening. We investigated the relationship between channel gating and proton sensitivity by correlating the proton IC_{50} to features of the deactivation rate in response to a brief application of glutamate and found a strong correlation between pH sensitivity and $\tau_{weighted}$, τ_{fast}, and % τ_{fast}.

The mechanism by which exon 5 exerts its functional control of the NMDA receptor may also underlie the activity of other modulators as well. For example, polyamines such as spermine and spermidine likely bind to and modulate the ATD/ABD domain interface (Ogden and Traynelis, 2011) to elicit exon-5-like effects, such as reduced proton sensitivity (Mony et al., 2011) and faster deactivation rates (Rumbaugh et al., 2000). Additionally, subtype-specific compounds such as PYD-106 are also predicted to bind to the ATD/ABD interface (Khatri et al., 2014). As such, modulatory sites at the ATD/ABD interface in NMDA receptors may provide an important target for therapeutic compounds and, perhaps more importantly, context-dependent compounds whose activity depends upon the acidified environment created by seizure and stroke (Kaku et al., 1993; Regan et al., 2015; Rumbaugh et al., 2000; Traynelis et al., 1995). Moreover, targeting the ATD/ABD interface with allosteric modulators offers the potential for subunit-specific modulation. Unlike the exon 5 motif, these regions show a much greater degree of sequence variation, thereby providing a means to target a specific NMDA receptor subtype (Zhu and Paoletti, 2015).

Agonist Binding Domain: Deactivation Rate Correlates with Glutamate Egress

Another region of the receptor that displays a high degree of conservation similar to that of the pre-M1 helix and the GluN1 exon 5 motif is the GluN2 glutamate binding site (Kinarsky et al., 2005). However, unlike the biologically intentional genetic variation awarded by the alternative splicing of exon 5, variation at the glutamate binding site occurs instead as a result of *de novo* mutations. One such *de novo* mutation, GluN2B-E413G, occurs at a conserved residue (Kinarsky et al., 2005) and was observed in a heterozygous patient exhibiting developmental delay (Adams et al., 2014). This mutation and other substitutions at GluN2B-Glu413 and

GluN2B-His486 resulted in drastically accelerated deactivation time courses. Moreover, when the fast component of the deactivation time course was plotted against glutamate egress time determined by random acceleration molecular dynamics (RAMD) simulations (Gordon Wells African Health Research Institute), a direct correlation was identified— prolonged deactivation rate corresponded with a slower egress time. By reducing the stability of the agonist-bound state and increasing the solvent accessibility of the binding pocket, mutations at Glu413 and His486 have a substantial impact on the amount of time that glutamate remains bound and, moreover, the amount of time it takes for the channel to close following agonist removal.

Again, guided by genetic variation—both intentional and accidental— we were able to develop a mechanistic understanding of how highly conserved regions of the NMDA receptor impart their functional effects. By correlating receptor deactivation rate with proton sensitivity or rate of ligand egress, we were able to 1) explore how functional changes upstream of the channel gate can influence receptor deactivation, 2) establish a better understanding of why residues in these regions might be under such strict evolutionary conservation, and 3) develop a relationship between distinct properties of channel function.

Future Directions

As we continue to gather more information about the NMDA receptor structure, function, and gating mechanism, we can design more informed and deliberate experiments to address even more complex questions regarding the receptor. Firstly, because arginine might be capable of forming cation-pi interactions, further exploration into how the GluN2A-P552R mutation disrupts the gating triad could be done by introducing this mutation in addition to the GluN2A-F553A mutation and other aromatic residues that modelling suggests are within appropriate

distance to interact with the arginine residue. Complementary experiments testing lysine, leucine, and other appropriate amino acids would validate the hypothesis that effects observed with double mutants are dependent on the charge of the residue. Additionally, with the proposal that the GluN1 and GluN2 subunits make different contributions to this mechanism, it would be interesting to explore whether or not these regions singularly control gating by engineering receptors with the GluN1 subunits containing the GluN2 pre-M1 helix and, alternately GluN2 subunits containing the GluN1 pre-M1 helix. If the inequal contributions of the subunits is important for the gating mechanism, then receptors with four identical pre-M1 helices would gate differently than the wild-type receptors. Is it required that the NMDA receptor have two different pre-M1 triads to function? If the four triads were the same, would the NMDA receptor behave like an AMPA receptor? How might these hybrid receptors change the gating rates in the structurally-based gating model? Overall, the results presented in this dissertation help set the stage for future studies to investigate how different modifications to the gating triad can influence receptor function.

Conclusion

The NMDA receptor is of indisputable importance for excitatory neurotransmission. Deemed critical for normal neuronal function, yet implicated in several neurological and psychiatric disorders, the NMDA receptor has become the focus of several lines of scientific inquiry. As we continue to gather information about the structural, functional, and genetic features of the NMDA receptor, we are becoming more and more equipped to address previously impossible questions about the mechanisms that facilitate its function. The work presented in this dissertation contributes to our understanding of the NMDA receptor by providing a mechanistic framework for the functional influence of highly conserved regions of the receptor, such as the pre-M1 helix, the GluN2 glutamate binding site, and the GluN1 exon 5 motif. Moreover, the results presented here lend credence to the value of genetic information in guiding the functional evaluation of such complex proteins as the NMDA receptor.

Chapter 8: References

Adams DR, Yuan H, Holyoak T, Arajs KH, Hakimi P, Markello TC, Wolfe LA, Vilboux T, Burton BK and Fajardo KF (2014) Three rare diseases in one sib pair: RAI1, PCK1, GRIN2B mutations associated with Smith–Magenis syndrome, cytosolic PEPCK deficiency and NMDA receptor glutamate insensitivity. *Molecular genetics and metabolism* **113**(3): 161-170.

Akazawa C, Shigemoto R, Bessho Y, Nakanishi S and Mizuno N (1994) Differential expression of five N-methyl-D-aspartate receptor subunit mRNAs in the cerebellum of developing and adult rats. *Journal of Comparative Neurology* **347**(1): 150-160.

Alberts B, Johnson A, Lewis J, Raff M, Roberts K and Walter P (2002) Ion channels and the electrical properties of membranes, in *Molecular Biology of the Cell 4th edition*, Garland Science.

Allen AS, Berkovic SF, Cossette P, Delanty N, Dlugos D, Eichler EE, Epstein MP, Glauser T, Goldstein DB and Han Y (2013) De novo mutations in epileptic encephalopathies. *Nature* **501**(7466): 217.

Allison DW, Gelfand VI, Spector I and Craig AM (1998) Role of actin in anchoring postsynaptic receptors in cultured hippocampal neurons: differential attachment of NMDA versus AMPA receptors. *Journal of Neuroscience* **18**(7): 2423-2436.

Alsaloum M, Kazi R, Gan Q, Amin J and Wollmuth LP (2016) A molecular determinant of subtype-specific desensitization in ionotropic glutamate receptors. *Journal of Neuroscience* **36**(9): 2617-2622.

Armstrong N and Gouaux E (2000) Mechanisms for activation and antagonism of an AMPA-sensitive glutamate receptor: crystal structures of the GluR2 ligand binding core. *Neuron* **28**(1): 165-181.

Asztély F and Gustafsson B (1996) Ionotropic glutamate receptors. *Molecular neurobiology* **12**(1): 1.

Auerbach A and Zhou Y (2005) Gating reaction mechanisms for NMDA receptor channels. *Journal of Neuroscience* **25**(35): 7914-7923.

Banke TG and Traynelis SF (2003) Activation of NR1/NR2b NMDA Receptors. *Nature neuroscience* **6**(2): 144.

Bässler E-L, Ngo-Anh TJ, Geisler H-S, Ruppersberg JP and Gründer S (2001) Molecular and functional characterization of acid-sensing ion channel (ASIC) 1b. *Journal of Biological Chemistry* **276**(36): 33782-33787.

Beard H, Cholleti A, Pearlman D, Sherman W and Loving KA (2013) Applying physics-based scoring to calculate free energies of binding for single amino acid mutations in protein-protein complexes. *PloS one* **8**(12): e82849.

Beck C, Wollmuth LP, Seeburg PH, Sakmann B and Kuner T (1999) NMDAR channel segments forming the extracellular vestibule inferred from the accessibility of substituted cysteines. *Neuron* **22**(3): 559-570.

Benveniste M, Clements J, Vyklický Jr L and Mayer M (1990) A kinetic analysis of the modulation of N-methyl-D-aspartic acid receptors by glycine in mouse cultured hippocampal neurones. *The Journal of Physiology* **428**(1): 333-357.

Bettler B and Mulle C (1995) AMPA and kainate receptors. *Neuropharmacology* **34**(2): 123-139.

Bouhamdan M, Yan H-D, Yan X-H, Bannon MJ and Andrade R (2006) Brain-specific regulator of G-protein signaling 9-2 selectively interacts with α-actinin-2 to regulate calcium-dependent inactivation of NMDA receptors. *Journal of Neuroscience* **26**(9): 2522-2530.

Buisson A and Choi D (1995) The inhibitory mGluR agonist, S-4-carboxy-3-hydroxy-phenylglycine selectively attenuates NMDA neurotoxicity and oxygen-glucose deprivation-induced neuronal death. *Neuropharmacology* **34**(8): 1081-1087.

Burnashev N, Monyer H, Seeburg PH and Sakmann B (1992a) Divalent ion permeability of AMPA receptor channels is dominated by the edited form of a single subunit. *Neuron* **8**(1): 189-198.

Burnashev N, Schoepfer R, Monyer H, Ruppersberg JP, Gunther W, Seeburg PH and Sakmann B (1992b) Control by asparagine residues of calcium permeability and magnesium blockade in the NMDA receptor. *Science* **257**(5075): 1415-1419.

Burnashev N and Szepetowski P (2015) NMDA receptor subunit mutations in neurodevelopmental disorders. *Current opinion in pharmacology* **20**: 73-82.

Cain DP (1997) LTP, NMDA, genes and learning. *Current opinion in neurobiology* **7**(2): 235-242.

Carroll RC, Beattie EC, von Zastrow M and Malenka RC (2001) Role of AMPA receptor endocytosis in synaptic plasticity. *Nature Reviews Neuroscience* **2**(5): 315.

Carroll RC and Zukin RS (2002) NMDA-receptor trafficking and targeting: implications for synaptic transmission and plasticity. *Trends in neurosciences* **25**(11): 571-577.

Castiglioni AJ, Raingo J and Lipscombe D (2006) Alternative splicing in the C-terminus of CaV2. 2 controls expression and gating of N-type calcium channels. *The Journal of physiology* **576**(1): 119-134.

Chang H-R and Kuo C-C (2008) The activation gate and gating mechanism of the NMDA receptor. *Journal of Neuroscience* **28**(7): 1546-1556.

Chen C and Okayama H (1987) High-efficiency transformation of mammalian cells by plasmid DNA. *Molecular and cellular biology* **7**(8): 2745-2752.

Chen G-Q, Cui C, Mayer ML and Gouaux E (1999) Functional characterization of a potassium-selective prokaryotic glutamate receptor. *Nature* **402**(6763): 817.

Chen PE, Geballe MT, Katz E, Erreger K, Livesey MR, O'toole KK, Le P, Lee CJ, Snyder JP and Traynelis SF (2008) Modulation of glycine potency in rat recombinant NMDA receptors containing chimeric NR2A/2D subunits expressed in Xenopus laevis oocytes. *The Journal of physiology* **586**(1): 227-245.

Chen W, Shieh C, Swanger SA, Tankovic A, Au M, McGuire M, Tagliati M, Graham JM, Madan-Khetarpal S and Traynelis SF (2017) GRIN1 mutation associated with intellectual disability alters NMDA receptor trafficking and function. *Journal of human genetics* **62**(6): 589.

Chiu J, DeSalle R, Lam H-M, Meisel L and Coruzzi G (1999) Molecular evolution of glutamate receptors: a primitive signaling mechanism that existed before plants and animals diverged. *Molecular biology and evolution* **16**(6): 826-838.

Choi DW (1992) Excitotoxic cell death. *Journal of neurobiology* **23**(9): 1261-1276.

Choi DW (1994) Calcium and excitotoxic neuronal injury. *Annals of the New York Academy of Sciences* **747**(1): 162-171.

Christensen ST, Leick V, Rasmussen L and Wheatley DN (1997) Signaling in unicellular eukaryotes, in *International review of cytology* pp 181-253, Elsevier.

Clements J (1996) Transmitter timecourse in the synaptic cleft: its role in central synaptic function. *Trends in neurosciences* **19**(5): 163-171.

Clements JD, Lester R, Tong G, Jahr CE and Westbrook GL (1992) The time course of glutamate in the synaptic cleft. *Science* **258**(5087): 1498-1501.

Coan E and Collingridge G (1985) Magnesium ions block an N-methyl-D-aspartate receptor-mediated component of synaptic transmission in rat hippocampus. *Neuroscience letters* **53**(1): 21-26.

Collingridge G, Herron C and Lester R (1988) Synaptic activation of N-methyl-D-aspartate receptors in the Schaffer collateral-commissural pathway of rat hippocampus. *The Journal of physiology* **399**(1): 283-300.

Colquhoun D and Hawkes A (1990) Stochastic properties of ion channel openings and bursts in a membrane patch that contains two channels: evidence concerning the number of channels present when a record containing only single openings is observed. *Proceedings of the Royal Society of London B Biological Sciences* **240**(1299): 453-477.

Coyle JT (2006) Substance use disorders and schizophrenia: a question of shared glutamatergic mechanisms. *Neurotoxicity research* **10**(3-4): 221-233.

Cull-Candy S, Brickley S and Farrant M (2001) NMDA receptor subunits: diversity, development and disease. *Current opinion in neurobiology* **11**(3): 327-335.

Cull-Candy SG (2001) NMDA receptors. *e LS*.

Dai J and Zhou H-X (2013) An NMDA receptor gating mechanism developed from MD simulations reveals molecular details underlying subunit-specific contributions. *Biophysical journal* **104**(10): 2170-2181.

De Ligt J, Willemsen MH, Van Bon BW, Kleefstra T, Yntema HG, Kroes T, Vulto-van Silfhout AT, Koolen DA, De Vries P and Gilissen C (2012) Diagnostic exome sequencing in persons with severe intellectual disability. *New England Journal of Medicine* **367**(20): 1921-1929.

Dingledine R, Borges K, Bowie D and Traynelis SF (1999) The glutamate receptor ion channels. *Pharmacological reviews* **51**(1): 7-62.

Durand GM, Bennett M and Zukin RS (1993) Splice variants of the N-methyl-D-aspartate receptor NR1 identify domains involved in regulation by polyamines and protein kinase C. *Proceedings of the National Academy of Sciences* **90**(14): 6731-6735.

Durand GM, Gregor P, Zheng X, Bennett M, Uhl GR and Zukin RS (1992) Cloning of an apparent splice variant of the rat N-methyl-D-aspartate receptor NMDAR1 with altered sensitivity to polyamines and activators of protein kinase C. *Proceedings of the National Academy of Sciences* **89**(19): 9359-9363.

Eccles JC and Jaeger JC (1958) The relationship between the mode of operation and the dimensions of the junctional regions at synapses and motor end-organs. *Proceedings of the Royal Society of London Series B-Biological Sciences* **148**(930): 38-56.

Edgar RC (2004) MUSCLE: multiple sequence alignment with high accuracy and high throughput. *Nucleic acids research* **32**(5): 1792-1797.

Edman S, McKay S, Macdonald L, Samadi M, Livesey M, Hardingham G and Wyllie D (2012) TCN 201 selectively blocks GluN2A-containing NMDARs in a GluN1 co-agonist dependent but non-competitive manner. *Neuropharmacology* **63**(3): 441-449.

Egebjerg J and Heinemann SF (1993) Ca2+ permeability of unedited and edited versions of the kainate selective glutamate receptor GluR6. *Proceedings of the National Academy of Sciences* **90**(2): 755-759.

Ehlers MD, Fung ET, O'brien RJ and Huganir RL (1998) Splice variant-specific interaction of the NMDA receptor subunit NR1 with neuronal intermediate filaments. *Journal of Neuroscience* **18**(2): 720-730.

Ehlers MD, Zhang S, Bernhardt JP and Huganir RL (1996) Inactivation of NMDA receptors by direct interaction of calmodulin with the NR1 subunit. *Cell* **84**(5): 745-755.

Erreger K, Dravid SM, Banke TG, Wyllie DJ and Traynelis SF (2005) Subunit-specific gating controls rat NR1/NR2A and NR1/NR2B NMDA channel kinetics and synaptic signalling profiles. *The Journal of physiology* **563**(2): 345-358.

Erreger K, Geballe MT, Kristensen A, Chen PE, Hansen KB, Lee CJ, Yuan H, Le P, Lyuboslavsky PN and Micale N (2007) Subunit-specific agonist activity at NR2A-, NR2B-, NR2C-, and NR2D-containing N-methyl-D-aspartate glutamate receptors. *Molecular pharmacology* **72**(4): 907-920.

Esmenjaud JB, Stroebel D, Chan K, Grand T, David M, Wollmuth LP, Taly A and Paoletti P (2019) An inter-dimer allosteric switch controls NMDA receptor activity. *The EMBO journal* **38**(2).

Ewald RC and Cline HT (2009) NMDA receptors and brain development. *Biology of the NMDA Receptor*: 1-15.

Farmer C, Cox JJ, Fletcher E, Woods CG, Wood JN and Schorge S (2012) Splice variants of Nav1. 7 sodium channels have distinct β subunit-dependent biophysical properties. *PLoS One* **7**(7): e41750.

Fitzjohna SM, Irving AJ, Palmer MJ, Harvey J, Lodge D and Collingridge GL (1996) Activation of group I mG1uRs potentiates NMDA responses in rat hippocampal slices. *Neuroscience letters* **203**(3): 211-213.

Forrest D, Yuzaki M, Soares HD, Ng L, Luk DC, Sheng M, Stewart CL, Morgan JI, Connor JA and Curran T (1994) Targeted disruption of NMDA receptor 1 gene abolishes NMDA response and results in neonatal death. *Neuron* **13**(2): 325-338.

Forsythe ID and Westbrook GL (1988) Slow excitatory postsynaptic currents mediated by N-methyl-D-aspartate receptors on cultured mouse central neurones. *The Journal of Physiology* **396**(1): 515-533.

Frerking M and Nicoll RA (2000) Synaptic kainate receptors. *Current opinion in neurobiology* **10**(3): 342-351.

Fry AE, Fawcett KA, Zelnik N, Yuan H, Thompson BA, Shemer-Meiri L, Cushion TD, Mugalaasi H, Sims D and Stoodley N (2018) De novo mutations in GRIN1 cause extensive bilateral polymicrogyria. *Brain* **141**(3): 698-712.

Furukawa H and Gouaux E (2003) Mechanisms of activation, inhibition and specificity: crystal structures of the NMDA receptor NR1 ligand-binding core. *The EMBO journal* **22**(12): 2873-2885.

Furukawa H, Singh SK, Mancusso R and Gouaux E (2005) Subunit arrangement and function in NMDA receptors. *Nature* **438**(7065): 185.

Galizia CG and Lledo P-M (2013) *Neurosciences: from molecule to behavior: a university textbook*. Springer.

Gibb AJ, Ogden KK, McDaniel MJ, Vance KM, Kell SA, Butch C, Burger P, Liotta DC and Traynelis SF (2018) A structurally derived model of subunit-dependent NMDA receptor function. *The Journal of physiology* **596**(17): 4057-4089.

Guo Z, Mohanty U, Noehre J, Sawyer TK, Sherman W and Krilov G (2010) Probing the α-helical structural stability of stapled p53 peptides: molecular dynamics simulations and analysis. *Chemical biology & drug design* **75**(4): 348-359.

Hansen KB, Ogden KK and Traynelis SF (2012) Subunit-selective allosteric inhibition of glycine binding to NMDA receptors. *Journal of Neuroscience* **32**(18): 6197-6208.

Hansen KB, Ogden KK, Yuan H and Traynelis SF (2014) Distinct functional and pharmacological properties of Triheteromeric GluN1/GluN2A/GluN2B NMDA receptors. *Neuron* **81**(5): 1084-1096.

Hansen KB, Tajima N, Risgaard R, Perszyk RE, Jørgensen L, Vance KM, Ogden KK, Clausen RP, Furukawa H and Traynelis SF (2013) Structural determinants of agonist efficacy at the glutamate binding site of N-methyl-D-aspartate receptors. *Molecular pharmacology* **84**(1): 114-127.

Hansen KB, Yi F, Perszyk RE, Furukawa H, Wollmuth LP, Gibb AJ and Traynelis SF (2018) Structure, function, and allosteric modulation of NMDA receptors. *The Journal of general physiology* **150**(8): 1081-1105.

Hatton CJ and Paoletti P (2005) Modulation of triheteromeric NMDA receptors by N-terminal domain ligands. *Neuron* **46**(2): 261-274.

Hebb DO (1962) *The organization of behavior: a neuropsychological theory*. Science Editions.

Henley JM and Wilkinson KA (2016) Synaptic AMPA receptor composition in development, plasticity and disease. *Nature Reviews Neuroscience* **17**(6): 337.

Herin GA and Aizenman E (2004) Amino terminal domain regulation of NMDA receptor function. *European journal of pharmacology* **500**(1-3): 101-111.

Hollmann M, Boulter J, Maron C, Beasley L, Sullivan J, Pecht G and Heinemann S (1993) Zinc potentiates agonist-lnduced currents at certain splice variants of the NMDA receptor. *Neuron* **10**(5): 943-954.

Horak M, Petralia RS, Kaniakova M and Sans N (2014) ER to synapse trafficking of NMDA receptors. *Frontiers in cellular neuroscience* **8**: 394.

Hu C, Chen W, Myers SJ, Yuan H and Traynelis SF (2016) Human GRIN2B variants in neurodevelopmental disorders. *Journal of pharmacological sciences* **132**(2): 115-121.

Humphrey W, Dalke A and Schulten K (1996) VMD: visual molecular dynamics. *Journal of molecular graphics* **14**(1): 33-38.

Hynd MR, Scott HL and Dodd PR (2004) Glutamate-mediated excitotoxicity and neurodegeneration in Alzheimer's disease. *Neurochemistry international* **45**(5): 583-595.

Inanobe A, Furukawa H and Gouaux E (2005) Mechanism of partial agonist action at the NR1 subunit of NMDA receptors. *Neuron* **47**(1): 71-84.

Jackson MB, Wong BS, Morris CE, Lecar H and Christian CN (1983) Successive openings of the same acetylcholine receptor channel are correlated in open time. *Biophysical journal* **42**(1): 109-114.

Jahr CE and Stevens CF (1993) Calcium permeability of the N-methyl-D-aspartate receptor channel in hippocampal neurons in culture. *Proceedings of the National Academy of Sciences* **90**(24): 11573-11577.

Jalali-Yazdi F, Chowdhury S, Yoshioka C and Gouaux E (2018) Mechanisms for zinc and proton inhibition of the GluN1/GluN2A NMDA receptor. *Cell* **175**(6): 1520-1532. e1515.

Jin R, Banke TG, Mayer ML, Traynelis SF and Gouaux E (2003) Structural basis for partial agonist action at ionotropic glutamate receptors. *Nature neuroscience* **6**(8): 803.

Jones KS, VanDongen HM and VanDongen AM (2002) The NMDA receptor M3 segment is a conserved transduction element coupling ligand binding to channel opening. *Journal of Neuroscience* **22**(6): 2044-2053.

Jones MV and Westbrook GL (1996) The impact of receptor desensitization on fast synaptic transmission. *Trends in neurosciences* **19**(3): 96-101.

Kaku DA, Giffard RG and Choi DW (1993) Neuroprotective effects of glutamate antagonists and extracellular acidity. *Science* **260**(5113): 1516-1518.

Karakas E and Furukawa H (2014) Crystal structure of a heterotetrameric NMDA receptor ion channel. *Science* **344**(6187): 992-997.

Karakas E, Regan MC and Furukawa H (2015) Emerging structural insights into the function of ionotropic glutamate receptors. *Trends in biochemical sciences* **40**(6): 328-337.

Karakas E, Simorowski N and Furukawa H (2009) Structure of the zinc-bound amino-terminal domain of the NMDA receptor NR2B subunit. *The EMBO journal* **28**(24): 3910-3920.

Kashiwagi K, Masuko T, Nguyen CD, Kuno T, Tanaka I, Igarashi K and Williams K (2002) Channel Blockers Acting atN-Methyl-D-aspartate Receptors: Differential Effects of Mutations in the Vestibule and Ion Channel Pore. *Molecular pharmacology* **61**(3): 533-545.

Kazi R, Dai J, Sweeney C, Zhou H-X and Wollmuth LP (2014) Mechanical coupling maintains the fidelity of NMDA receptor–mediated currents. *Nature neuroscience* **17**(7): 914.

Kazi R, Gan Q, Talukder I, Markowitz M, Salussolia CL and Wollmuth LP (2013) Asynchronous movements prior to pore opening in NMDA receptors. *Journal of Neuroscience* **33**(29): 12052-12066.

Khatri A, Burger PB, Swanger SA, Hansen KB, Zimmerman S, Karakas E, Liotta DC, Furukawa H, Snyder JP and Traynelis SF (2014) Structural determinants and mechanism of action of a GluN2C-selective NMDA receptor positive allosteric modulator. *Molecular pharmacology* **86**(5): 548-560.

Kinarsky L, Feng B, Skifter DA, Morley RM, Sherman S, Jane DE and Monaghan D (2005) Identification of subunit-specific and antagonist-specific amino acid residues in the NMDA receptor glutamate binding pocket. *Journal of Pharmacology and Experimental Therapeutics*.

Klippenstein V, Hoppmann C, Ye S, Wang L and Paoletti P (2017) Optocontrol of glutamate receptor activity by single side-chain photoisomerization. *Elife* **6**: e25808.

Köhr G and Seeburg PH (1996) Subtype-specific regulation of recombinant NMDA receptor-channels by protein tyrosine kinases of the src family. *The Journal of physiology* **492**(2): 445-452.

Kornau H-C, Schenker LT, Kennedy MB and Seeburg PH (1995) Domain interaction between NMDA receptor subunits and the postsynaptic density protein PSD-95. *Science* **269**(5231): 1737-1740.

Krupp JJ, Vissel B, Heinemann SF and Westbrook GL (1996) Calcium-dependent inactivation of recombinant N-methyl-D-aspartate receptors is NR2 subunit specific. *Molecular pharmacology* **50**(6): 1680-1688.

Krupp JJ, Vissel B, Heinemann SF and Westbrook GL (1998) N-terminal domains in the NR2 subunit control desensitization of NMDA receptors. *Neuron* **20**(2): 317-327.

Kuzniecky R, Andermann F, Guerrini R and Study TCMC (1993) Congenital bilateral perisylvian syndrome: study of 31 patients. *The Lancet* **341**(8845): 608-612.

Lam H-M, Chiu J, Hsieh M-H, Meisel L, Oliveira IC, Shin M and Coruzzi G (1998) Glutamate-receptor genes in plants. *Nature* **396**(6707): 125.

Lam VM, Beerepoot P, Angers S and Salahpour A (2013) A Novel Assay for Measurement of Membrane-Protein Surface Expression using a β-lactamase Reporter. *Traffic* **14**(7): 778-784.

Laskowski RA, Jabłońska J, Pravda L, Vařeková RS and Thornton JM (2018) PDBsum: Structural summaries of PDB entries. *Protein Science* **27**(1): 129-134.

Laurie DJ and Seeburg PH (1994) Ligand affinities at recombinant N-methyl-D-aspartate receptors depend on subunit composition. *European Journal of Pharmacology: Molecular Pharmacology* **268**(3): 335-345.

Lee C-H, Lü W, Michel JC, Goehring A, Du J, Song X and Gouaux E (2014) NMDA receptor structures reveal subunit arrangement and pore architecture. *Nature* **511**(7508): 191.

Lek M, Karczewski KJ, Minikel EV, Samocha KE, Banks E, Fennell T, O'Donnell-Luria AH, Ware JS, Hill AJ and Cummings BB (2016) Analysis of protein-coding genetic variation in 60,706 humans. *Nature* **536**(7616): 285.

Lemke JR, Geider K, Helbig KL, Heyne HO, Schütz H, Hentschel J, Courage C, Depienne C, Nava C and Heron D (2016) Delineating the GRIN1 phenotypic spectrum: a distinct genetic NMDA receptor encephalopathy. *Neurology* **86**(23): 2171-2178.

Lemke JR, Hendrickx R, Geider K, Laube B, Schwake M, Harvey RJ, James VM, Pepler A, Steiner I and Hörtnagel K (2014) GRIN2B mutations in West syndrome and intellectual disability with focal epilepsy. *Annals of neurology* **75**(1): 147-154.

Lerma J, Paternain AV, Rodríguez-Moreno A and López-García JC (2001) Molecular physiology of kainate receptors. *Physiological reviews* **81**(3): 971-998.

Lesca G, Rudolf G, Bruneau N, Lozovaya N, Labalme A, Boutry-Kryza N, Salmi M, Tsintsadze T, Addis L and Motte J (2013) GRIN2A mutations in acquired epileptic aphasia and related childhood focal epilepsies and encephalopathies with speech and language dysfunction. *Nature genetics* **45**(9): 1061.

Lester R and Jahr CE (1992) NMDA channel behavior depends on agonist affinity. *Journal of Neuroscience* **12**(2): 635-643.

Lester RA, Clements JD, Westbrook GL and Jahr CE (1990) Channel kinetics determine the time course of NMDA receptor-mediated synaptic currents. *Nature* **346**(6284): 565.

Leys SP (2015) Elements of a 'nervous system'in sponges. *Journal of Experimental Biology* **218**(4): 581-591.

Liman ER, Tytgat J and Hess P (1992) Subunit stoichiometry of a mammalian K+ channel determined by construction of multimeric cDNAs. *Neuron* **9**(5): 861-871.

Liu L, Wong TP, Pozza MF, Lingenhoehl K, Wang Y, Sheng M, Auberson YP and Wang YT (2004) Role of NMDA receptor subtypes in governing the direction of hippocampal synaptic plasticity. *Science* **304**(5673): 1021-1024.

Lomeli H, Mosbacher J, Melcher T, Hoger T, Kuner T, Monyer H, Higuchi M, Bach A and Seeburg PH (1994) Control of kinetic properties of AMPA receptor channels by nuclear RNA editing. *Science* **266**(5191): 1709-1713.

Lu W-Y, Man H-Y, Ju W, Trimble WS, MacDonald JF and Wang YT (2001) Activation of synaptic NMDA receptors induces membrane insertion of new AMPA receptors and LTP in cultured hippocampal neurons. *Neuron* **29**(1): 243-254.

Lüdemann SK, Lounnas V and Wade RC (2000) How do substrates enter and products exit the buried active site of cytochrome P450cam? 1. Random expulsion molecular dynamics

investigation of ligand access channels and mechanisms. *Journal of molecular biology* **303**(5): 797-811.
Luo J, Wang Y, Yasuda RP, Dunah AW and Wolfe BB (1997) The majority of N-methyl-D-aspartate receptor complexes in adult rat cerebral cortex contain at least three different subunits (NR1/NR2A/NR2B). *Molecular pharmacology* **51**(1): 79-86.
Lüscher C and Malenka RC (2012) NMDA receptor-dependent long-term potentiation and long-term depression (LTP/LTD). *Cold Spring Harbor perspectives in biology* **4**(6): a005710.
MacKinnon R (2003) Potassium channels. *FEBS letters* **555**(1): 62-65.
Magleby K and Pallotta B (1983) Burst kinetics of single calcium-activated potassium channels in cultured rat muscle. *The Journal of Physiology* **344**(1): 605-623.
Malenka RC and Bear MF (2004) LTP and LTD: an embarrassment of riches. *Neuron* **44**(1): 5-21.
Mannaioni G, Marino MJ, Valenti O, Traynelis SF and Conn PJ (2001) Metabotropic glutamate receptors 1 and 5 differentially regulate CA1 pyramidal cell function. *Journal of Neuroscience* **21**(16): 5925-5934.
Maren S and Baudry M (1995) Properties and mechanisms of long-term synaptic plasticity in the mammalian brain: relationships to learning and memory. *Neurobiology of learning and memory* **63**(1): 1-18.
Margeta-Mitrovic M, Jan YN and Jan LY (2000) A trafficking checkpoint controls GABAB receptor heterodimerization. *Neuron* **27**(1): 97-106.
Mayer ML (2011) Emerging models of glutamate receptor ion channel structure and function. *Structure* **19**(10): 1370-1380.
Mayer ML, Olson R and Gouaux E (2001) Mechanisms for ligand binding to GluR0 ion channels: crystal structures of the glutamate and serine complexes and a closed apo state. *Journal of molecular biology* **311**(4): 815-836.
McBain C and Mayer M (1994) N-methyl-D-aspartic acid receptor structure and function. *Physiological reviews* **74**(3): 723-760.
Meldrum BS (2000) Glutamate as a neurotransmitter in the brain: review of physiology and pathology. *The Journal of nutrition* **130**(4): 1007S-1015S.
Mesbahi-Vasey S, Veras L, Yonkunas M, Johnson JW and Kurnikova MG (2017) All atom NMDA receptor transmembrane domain model development and simulations in lipid bilayers and water. *PloS one* **12**(6): e0177686.
Miller G (2009) On the origin of the nervous system, American Association for the Advancement of Science.
Mony L, Zhu S, Carvalho S and Paoletti P (2011) Molecular basis of positive allosteric modulation of GluN2B NMDA receptors by polyamines. *The EMBO journal* **30**(15): 3134-3146.
Monyer H, Burnashev N, Laurie DJ, Sakmann B and Seeburg PH (1994) Developmental and regional expression in the rat brain and functional properties of four NMDA receptors. *Neuron* **12**(3): 529-540.
Monyer H, Sprengel R, Schoepfer R, Herb A, Higuchi M, Lomeli H, Burnashev N, Sakmann B and Seeburg PH (1992) Heteromeric NMDA receptors: molecular and functional distinction of subtypes. *Science* **256**(5060): 1217-1221.
Mosbacher J, Schöpfer R, Monyer H, Burnashev N, Seeburg PH and Ruppersberg JP (1994) A molecular determinant for submillisecond desensitization in glutamate receptors. *Science* **266**(5187): 1059-1062.

Moy SS, Perez A, Koller BH and Duncan GE (2006) Amphetamine-induced disruption of prepulse inhibition in mice with reduced NMDA receptor function. *Brain research* **1089**(1): 186-194.

Mu Y, Otsuka T, Horton AC, Scott DB and Ehlers MD (2003) Activity-dependent mRNA splicing controls ER export and synaptic delivery of NMDA receptors. *Neuron* **40**(3): 581-594.

Mullasseril P, Hansen KB, Vance KM, Ogden KK, Yuan H, Kurtkaya NL, Santangelo R, Orr AG, Le P and Vellano KM (2010) A subunit-selective potentiator of NR2C-and NR2D-containing NMDA receptors. *Nature communications* **1**: 90.

Nahum-Levy R, Lipinski D, Shavit S and Benveniste M (2001) Desensitization of NMDA receptor channels is modulated by glutamate agonists. *Biophysical Journal* **80**(5): 2152-2166.

Nakanishi N, Axel R and Shneider NA (1992) Alternative splicing generates functionally distinct N-methyl-D-aspartate receptors. *Proceedings of the National Academy of Sciences* **89**(18): 8552-8556.

Nakanishi N, Shneider NA and Axel R (1990) A family of glutamate receptor genes: evidence for the formation of heteromultimeric receptors with distinct channel properties. *Neuron* **5**(5): 569-581.

Newcomer JW, Farber NB, Jevtovic-Todorovic V, Selke G, Melson AK, Hershey T, Craft S and Olney JW (1999) Ketamine-induced NMDA receptor hypofunction as a model of memory impairment and psychosis. *Neuropsychopharmacology* **20**(2): 106.

Ogden KK, Chen W, Swanger SA, McDaniel MJ, Fan LZ, Hu C, Tankovic A, Kusumoto H, Kosobucki GJ and Schulien AJ (2017) Molecular mechanism of disease-associated mutations in the pre-M1 helix of NMDA receptors and potential rescue pharmacology. *PLoS genetics* **13**(1): e1006536.

Ogden KK and Traynelis SF (2011) New advances in NMDA receptor pharmacology. *Trends in pharmacological sciences* **32**(12): 726-733.

Ogden KK and Traynelis SF (2013) Contribution of the M1 transmembrane helix and pre-M1 region to positive allosteric modulation and gating of N-methyl-D-aspartate receptors. *Molecular pharmacology* **83**(5): 1045-1056.

Ogden KK, Yuan H, Hansen KB, Zhang J, Gibb AJ and Traynelis SF (2014) A Human Mutation in the M4 Helix of GluN2A Accelerates Forward Gating Transitions in NMDA Receptors. *Biophysical Journal* **106**(2): 150a.

Ohba C, Shiina M, Tohyama J, Haginoya K, Lerman-Sagie T, Okamoto N, Blumkin L, Lev D, Mukaida S and Nozaki F (2015) GRIN 1 mutations cause encephalopathy with infantile-onset epilepsy, and hyperkinetic and stereotyped movement disorders. *Epilepsia* **56**(6): 841-848.

Olney JW, Newcomer JW and Farber NB (1999) NMDA receptor hypofunction model of schizophrenia. *Journal of psychiatric research* **33**(6): 523-533.

Palmer CL, Cotton L and Henley JM (2005) The molecular pharmacology and cell biology of α-amino-3-hydroxy-5-methyl-4-isoxazolepropionic acid receptors. *Pharmacological reviews* **57**(2): 253-277.

Paoletti P (2011) Molecular basis of NMDA receptor functional diversity. *European Journal of Neuroscience* **33**(8): 1351-1365.

Paoletti P, Bellone C and Zhou Q (2013) NMDA receptor subunit diversity: impact on receptor properties, synaptic plasticity and disease. *Nature Reviews Neuroscience* **14**(6): 383.

Paoletti P and Neyton J (2007) NMDA receptor subunits: function and pharmacology. *Current opinion in pharmacology* **7**(1): 39-47.

Paoletti P, Perin-Dureau F, Fayyazuddin A, Le Goff A, Callebaut I and Neyton J (2000) Molecular organization of a zinc binding N-terminal modulatory domain in a NMDA receptor subunit. *Neuron* **28**(3): 911-925.

Paupard M-C, Friedman L and Zukin RS (1997) Developmental regulation and cell-specific expression of N-methyl-D-aspartate receptor splice variants in rat hippocampus. *Neuroscience* **79**(2): 399-409.

Penn AC, Balik A, Wozny C, Cais O and Greger IH (2012) Activity-mediated AMPA receptor remodeling, driven by alternative splicing in the ligand-binding domain. *Neuron* **76**(3): 503-510.

Perin-Dureau F, Rachline J, Neyton J and Paoletti P (2002) Mapping the binding site of the neuroprotectant ifenprodil on NMDA receptors. *Journal of Neuroscience* **22**(14): 5955-5965.

Perszyk R, Katzman BM, Kusumoto H, Kell SA, Epplin MP, Tahirovic YA, Moore RL, Menaldino D, Burger P and Liotta DC (2018) An NMDAR positive and negative allosteric modulator series share a binding site and are interconverted by methyl groups. *Elife* **7**: e34711.

Piovesan D, Minervini G and Tosatto SC (2016) The RING 2.0 web server for high quality residue interaction networks. *Nucleic acids research* **44**(W1): W367-W374.

Poduri A, Evrony GD, Cai X and Walsh CA (2013) Somatic mutation, genomic variation, and neurological disease. *Science* **341**(6141): 1237758.

Popescu G and Auerbach A (2004) The NMDA receptor gating machine: lessons from single channels. *The Neuroscientist* **10**(3): 192-198.

Price MB, Jelesko J and Okumoto S (2012) Glutamate receptor homologs in plants: functions and evolutionary origins. *Frontiers in plant science* **3**: 235.

Redin C, Gérard B, Lauer J, Herenger Y, Muller J, Quartier A, Masurel-Paulet A, Willems M, Lesca G and El-Chehadeh S (2014) Efficient strategy for the molecular diagnosis of intellectual disability using targeted high-throughput sequencing. *Journal of medical genetics* **51**(11): 724-736.

Regalado MP, Villarroel A and Lerma J (2001) Intersubunit cooperativity in the NMDA receptor. *Neuron* **32**(6): 1085-1096.

Regan MC, Grant T, McDaniel MJ, Karakas E, Zhang J, Traynelis SF, Grigorieff N and Furukawa H (2018) Structural mechanism of functional modulation by gene splicing in NMDA receptors. *Neuron* **98**(3): 521-529. e523.

Regan MC, Romero-Hernandez A and Furukawa H (2015) A structural biology perspective on NMDA receptor pharmacology and function. *Current opinion in structural biology* **33**: 68-75.

Ren H, Salous A, Paul J, Lipsky R and Peoples RW (2007) Mutations at F637 in the NMDA receptor NR2A subunit M3 domain influence agonist potency, ion channel gating and alcohol action. *British journal of pharmacology* **151**(6): 749-757.

Rice AC and DeLorenzo RJ (1998) NMDA receptor activation during status epilepticus is required for the development of epilepsy. *Brain research* **782**(1-2): 240-247.

Rose CR and Konnerth A (2001) Stores not just for storage: intracellular calcium release and synaptic plasticity. *Neuron* **31**(4): 519-522.

Rosenmund C and Westbrook G (1993) Calcium-induced actin depolymerization reduces NMDA channel activity. *Neuron* **10**(5): 805-814.

Rumbaugh G, Prybylowski K, Wang JF and Vicini S (2000) Exon 5 and spermine regulate deactivation of NMDA receptor subtypes. *Journal of neurophysiology* **83**(3): 1300-1306.

Ryan TJ and Grant SG (2009) The origin and evolution of synapses. *Nature Reviews Neuroscience* **10**(10): 701.

Šali A and Blundell TL (1993) Comparative protein modelling by satisfaction of spatial restraints. *Journal of molecular biology* **234**(3): 779-815.

Sans N, Prybylowski K, Petralia RS, Chang K, Wang Y-X, Racca C, Vicini S and Wenthold RJ (2003) NMDA receptor trafficking through an interaction between PDZ proteins and the exocyst complex. *Nature cell biology* **5**(6): 520.

Sapkota K, Dore K, Tang K, Irvine M, Fang G, Burnell ES, Malinow R, Jane DE and Monaghan DT (2019) The NMDA receptor intracellular C-terminal domains reciprocally interact with allosteric modulators. *Biochemical pharmacology* **159**: 140-153.

Schiffer HH, Swanson GT and Heinemann SF (1997) Rat GluR7 and a carboxy-terminal splice variant, GluR7b, are functional kainate receptor subunits with a low sensitivity to glutamate. *Neuron* **19**(5): 1141-1146.

Schorge S, Elenes S and Colquhoun D (2005) Maximum likelihood fitting of single channel NMDA activity with a mechanism composed of independent dimers of subunits. *The Journal of physiology* **569**(2): 395-418.

Scott DB, Blanpied TA, Swanson GT, Zhang C and Ehlers MD (2001) An NMDA receptor ER retention signal regulated by phosphorylation and alternative splicing. *Journal of Neuroscience* **21**(9): 3063-3072.

Shigemoto R, Abe T, Nomura S, Nakanishi S and Hirano T (1994) Antibodies inactivating mGluR1 metabotropic glutamate receptor block long-term depression in cultured Purkinje cells. *Neuron* **12**(6): 1245-1255.

Single FN, Rozov A, Burnashev N, Zimmermann F, Hanley DF, Forrest D, Curran T, Jensen V, Hvalby Ø and Sprengel R (2000) Dysfunctions in mice by NMDA receptor point mutations NR1 (N598Q) and NR1 (N598R). *Journal of Neuroscience* **20**(7): 2558-2566.

Sirin S, Kumar R, Martinez C, Karmilowicz MJ, Ghosh P, Abramov YA, Martin V and Sherman W (2014) A computational approach to enzyme design: predicting ω-aminotransferase catalytic activity using docking and MM-GBSA scoring. *Journal of chemical information and modeling* **54**(8): 2334-2346.

Sirrieh RE, MacLean DM and Jayaraman V (2015) Subtype-dependent N-methyl-D-aspartate receptor amino-terminal domain conformations and modulation by spermine. *Journal of Biological Chemistry* **290**(20): 12812-12820.

Sobolevsky AI, Prodromou ML, Yelshansky MV and Wollmuth LP (2007) Subunit-specific contribution of pore-forming domains to NMDA receptor channel structure and gating. *The Journal of general physiology* **129**(6): 509-525.

Sobolevsky AI, Rosconi MP and Gouaux E (2009) X-ray structure, symmetry and mechanism of an AMPA-subtype glutamate receptor. *Nature* **462**(7274): 745.

Sommer B, Keinanen K, Verdoorn TA, Wisden W, Burnashev N, Herb A, Kohler M, Takagi T, Sakmann B and Seeburg PH (1990) Flip and flop: a cell-specific functional switch in glutamate-operated channels of the CNS. *Science* **249**(4976): 1580-1585.

Song I and Huganir RL (2002) Regulation of AMPA receptors during synaptic plasticity. *Trends in neurosciences* **25**(11): 578-588.

Sprengel R and Single FN (1999) Mice with genetically modified NMDA and AMPA receptors. *Annals of the New York Academy of Sciences* **868**(1): 494-501.

Standley S, Roche KW, McCallum J, Sans N and Wenthold RJ (2000) PDZ domain suppression of an ER retention signal in NMDA receptor NR1 splice variants. *Neuron* **28**(3): 887-898.

Stavrovskaya IG and Kristal BS (2005) The powerhouse takes control of the cell: is the mitochondrial permeability transition a viable therapeutic target against neuronal dysfunction and death? *Free Radical Biology and Medicine* **38**(6): 687-697.

Stroebel D, Carvalho S, Grand T, Zhu S and Paoletti P (2014) Controlling NMDA receptor subunit composition using ectopic retention signals. *Journal of Neuroscience* **34**(50): 16630-16636.

Sugihara H, Moriyoshi K, Ishii T, Masu M and Nakanishi S (1992) Structures and properties of seven isoforms of the NMDA receptor generated by alternative splicing. *Biochemical and biophysical research communications* **185**(3): 826-832.

Sun Y, Olson R, Horning M, Armstrong N, Mayer M and Gouaux E (2002) Mechanism of glutamate receptor desensitization. *Nature* **417**(6886): 245.

Swanger SA, Chen W, Wells G, Burger PB, Tankovic A, Bhattacharya S, Strong KL, Hu C, Kusumoto H and Zhang J (2016) Mechanistic insight into NMDA receptor dysregulation by rare variants in the GluN2A and GluN2B agonist binding domains. *The American Journal of Human Genetics* **99**(6): 1261-1280.

Swanson CJ, Bures M, Johnson MP, Linden A-M, Monn JA and Schoepp DD (2005) Metabotropic glutamate receptors as novel targets for anxiety and stress disorders. *Nature reviews Drug discovery* **4**(2): 131.

Tajima N, Karakas E, Grant T, Simorowski N, Diaz-Avalos R, Grigorieff N and Furukawa H (2016) Activation of NMDA receptors and the mechanism of inhibition by ifenprodil. *Nature* **534**(7605): 63.

Takeuchi T, Duszkiewicz AJ and Morris RG (2014) The synaptic plasticity and memory hypothesis: encoding, storage and persistence. *Philosophical Transactions of the Royal Society B: Biological Sciences* **369**(1633): 20130288.

Talukder I, Borker P and Wollmuth LP (2010) Specific sites within the ligand-binding domain and ion channel linkers modulate NMDA receptor gating. *Journal of Neuroscience* **30**(35): 11792-11804.

Talukder I and Wollmuth LP (2011) Local constraints in either the GluN1 or GluN2 subunit equally impair NMDA receptor pore opening. *The Journal of general physiology* **138**(2): 179-194.

Thomas CG, Krupp JJ, Bagley EE, Bauzon R, Heinemann SF, Vissel B and Westbrook GL (2006) Probing N-methyl-D-aspartate receptor desensitization with the substituted-cysteine accessibility method. *Molecular pharmacology* **69**(4): 1296-1303.

Tong G, Shepherd D and Jahr CE (1995) Synaptic desensitization of NMDA receptors by calcineurin. *Science* **267**(5203): 1510-1512.

Tovar KR, McGinley MJ and Westbrook GL (2013) Triheteromeric NMDA receptors at hippocampal synapses. *Journal of Neuroscience* **33**(21): 9150-9160.

Traynelis J, Silk M, Wang Q, Berkovic SF, Liu L, Ascher DB, Balding DJ and Petrovski S (2017) Optimizing genomic medicine in epilepsy through a gene-customized approach to missense variant interpretation. *Genome research* **27**(10): 1715-1729.

Traynelis SF, Burgess MF, Zheng F, Lyuboslavsky P and Powers JL (1998) Control of voltage-independent zinc inhibition of NMDA receptors by the NR1 subunit. *Journal of Neuroscience* **18**(16): 6163-6175.

Traynelis SF, Hartley M and Heinemann SF (1995) Control of proton sensitivity of the NMDA receptor by RNA splicing and polyamines. *Science* **268**(5212): 873-876.

Traynelis SF, Wollmuth LP, McBain CJ, Menniti FS, Vance KM, Ogden KK, Hansen KB, Yuan H, Myers SJ and Dingledine R (2010) Glutamate receptor ion channels: structure, regulation, and function. *Pharmacological reviews* **62**(3): 405-496.

Tsien JZ, Huerta PT and Tonegawa S (1996) The essential role of hippocampal CA1 NMDA receptor–dependent synaptic plasticity in spatial memory. *Cell* **87**(7): 1327-1338.

Twomey EC and Sobolevsky AI (2017) Structural mechanisms of gating in ionotropic glutamate receptors. *Biochemistry* **57**(3): 267-276.

Twomey EC, Yelshanskaya MV, Grassucci RA, Frank J and Sobolevsky AI (2017) Channel opening and gating mechanism in AMPA-subtype glutamate receptors. *Nature* **549**(7670): 60.

Ugolini A, Corsi M and Bordi F (1997) Potentiation of NMDA and AMPA responses by group I mGluR in spinal cord motoneurons. *Neuropharmacology* **36**(8): 1047-1055.

Vance KM, Hansen KB and Traynelis SF (2012) GluN1 splice variant control of GluN1/GluN2D NMDA receptors. *The Journal of physiology* **590**(16): 3857-3875.

Vance KM, Simorowski N, Traynelis SF and Furukawa H (2011) Ligand-specific deactivation time course of GluN1/GluN2D NMDA receptors. *Nature communications* **2**: 294.

Veltman JA and Brunner HG (2012) De novo mutations in human genetic disease. *Nature Reviews Genetics* **13**(8): 565.

Villard L, Nguyen K, Cardoso C, Martin CL, Weiss AM, Sifry-Platt M, Grix AW, Graham Jr JM, Winter RM and Leventer RJ (2002) A locus for bilateral perisylvian polymicrogyria maps to Xq28. *The American Journal of Human Genetics* **70**(4): 1003-1008.

Vissel B, Krupp JJ, Heinemann SF and Westbrook GL (2001) A use-dependent tyrosine dephosphorylation of NMDA receptors is independent of ion flux. *Nature neuroscience* **4**(6): 587.

Wang T-M, Brown BM, Deng L, Sellers BD, Lupardus PJ, Wallweber HJ, Gustafson A, Wong E, Volgraf M and Schwarz JB (2017) A novel NMDA receptor positive allosteric modulator that acts via the transmembrane domain. *Neuropharmacology* **121**: 204-218.

Watanabe M, Inoue Y, Sakimura K and Mishina M (1992) Developmental changes in distribution of NMDA receptor channel subunit mRNAs. *Neuroreport* **3**(12): 1138-1140.

Weik M and Colletier J-P (2010) Temperature-dependent macromolecular X-ray crystallography. *Acta Crystallographica Section D: Biological Crystallography* **66**(4): 437-446.

Wells G, Yuan H, McDaniel MJ, Kusumoto H, Snyder JP, Liotta DC and Traynelis SF (2018) The GluN2B-Glu413Gly NMDA receptor variant arising from a de novo GRIN2B mutation promotes ligand-unbinding and domain opening. *Proteins: Structure, Function, and Bioinformatics* **86**(12): 1265-1276.

Wenthold RJ, Prybylowski K, Standley S, Sans N and Petralia RS (2003) Trafficking of NMDA receptors. *Annual review of pharmacology and toxicology* **43**(1): 335-358.

Willard SS and Koochekpour S (2013) Glutamate, glutamate receptors, and downstream signaling pathways. *International journal of biological sciences* **9**(9): 948.

Williams K (2001) Ifenprodil, a novel NMDA receptor antagonist: site and mechanism of action. *Current drug targets* **2**(3): 285-298.

Wollmuth LP and Sobolevsky AI (2004) Structure and gating of the glutamate receptor ion channel. *Trends in neurosciences* **27**(6): 321-328.

Wyllie D, Livesey M and Hardingham G (2013) Influence of GluN2 subunit identity on NMDA receptor function. *Neuropharmacology* **74**: 4-17.

Wyllie DJ, Behe P and Colquhoun D (1998) Single-channel activations and concentration jumps: comparison of recombinant NR1a/NR2A and NR1a/NR2D NMDA receptors. *The Journal of physiology* **510**(1): 1-18.

XiangWei W, Jiang Y and Yuan H (2018) De novo mutations and rare variants occurring in NMDA receptors. *Current opinion in physiology* **2**: 27-35.

Yaka R, Thornton C, Vagts AJ, Phamluong K, Bonci A and Ron D (2002) NMDA receptor function is regulated by the inhibitory scaffolding protein, RACK1. *Proceedings of the National Academy of Sciences* **99**(8): 5710-5715.

Yelshanskaya MV, Saotome K, Singh AK and Sobolevsky AI (2016) Probing intersubunit interfaces in AMPA-subtype ionotropic glutamate receptors. *Scientific reports* **6**: 19082.

Yi F, Mou T-C, Dorsett KN, Volkmann RA, Menniti FS, Sprang SR and Hansen KB (2016) Structural basis for negative allosteric modulation of GluN2A-containing NMDA receptors. *Neuron* **91**(6): 1316-1329.

Yuan H, Erreger K, Dravid SM and Traynelis SF (2005) Conserved structural and functional control of N-methyl-D-aspartate receptor gating by transmembrane domain M3. *Journal of Biological Chemistry* **280**(33): 29708-29716.

Yuan H, Low C-M, Moody OA, Jenkins A and Traynelis SF (2015a) Ionotropic GABA and glutamate receptor mutations and human neurologic diseases. *Molecular pharmacology* **88**(1): 203-217.

Yuan H, Myers SJ, Wells G, Nicholson KL, Swanger SA, Lyuboslavsky P, Tahirovic YA, Menaldino DS, Ganesh T and Wilson LJ (2015b) Context-dependent GluN2B-selective inhibitors of NMDA receptor function are neuroprotective with minimal side effects. *Neuron* **85**(6): 1305-1318.

Zeron MM, Hansson O, Chen N, Wellington CL, Leavitt BR, Brundin P, Hayden MR and Raymond LA (2002) Increased sensitivity to N-methyl-D-aspartate receptor-mediated excitotoxicity in a mouse model of Huntington's disease. *Neuron* **33**(6): 849-860.

Zhang J-B, Chang S, Xu P, Miao M, Wu H, Zhang Y, Zhang T, Wang H, Zhang J and Xie C (2018) Structural Basis of the Proton Sensitivity of Human GluN1-GluN2A NMDA Receptors. *Cell reports* **25**(13): 3582-3590. e3584.

Zhang W, Howe JR and Popescu GK (2008) Distinct gating modes determine the biphasic relaxation of NMDA receptor currents. *Nature neuroscience* **11**(12): 1373.

Zhong J, Carrozza DP, Williams K, Pritchett DB and Molinoff PB (1995) Expression of mRNAs encoding subunits of the NMDA receptor in developing rat brain. *Journal of neurochemistry* **64**(2): 531-539.

Zhou H-X and Wollmuth LP (2017) Advancing NMDA receptor physiology by integrating multiple approaches. *Trends in neurosciences* **40**(3): 129-137.

Zhu S and Paoletti P (2015) Allosteric modulators of NMDA receptors: multiple sites and mechanisms. *Current opinion in pharmacology* **20**: 14-23.

Zhu S, Stroebel D, Yao CA, Taly A and Paoletti P (2013) Allosteric signaling and dynamics of the clamshell-like NMDA receptor GluN1 N-terminal domain. *Nature structural & molecular biology* **20**(4): 477.